Table of contents

List of figures

List of Abbreviation

2D	Two-dimensional
3D	Three-dimensional
Acta2	Actin Alpha 2
ADM	Acinar-to-ductal metaplasia
Agr2	Anterior Gradient 2
ALK	Anaplastic lymphoma kinase
Ank	Ankyrin 1
Arf	Alternate reading frame
ARID1A	AT-Rich Interaction Domain 1A
ATF6	Activating transcription factor 6
ATP	Adenosine triphosphate
BET	The Bromodomain and Extra-Terminal Domain
bHLH	Basic helix-loop-helix
BiP	Binding immunoglobulin protein
BOP	N-nitroso-bis(2-oxopropyl)amine
CAF	Cancer associated fibroblasts
CC3	Cleaved caspase
CCL2	C-C Motif Chemokine Ligand 2
CCL5	C-C Motif Chemokine Ligand 5
CCL9	C-C Motif Chemokine Ligand 9
CDKN2A	Cyclin Dependent Kinase Inhibitor 2A
ChIP	Combining chromatin immunoprecipitation
CHOP	C/EBP homologous protein

CpG	Cytosine Phosphoguanine
Crabp2	Cellular Retinoic Acid-Binding Protein II
CSF1	Colony Stimulating Factor 1
CSFR1	Colony Stimulating Factor 1 Receptor
CSHL	Cold Spring Harbor Laboratory
CXCL12	C-X-C motif chemokine 12
DD	Degron domain
Ddit3	DNA Damage Inducible Transcript 3
DMEM	Dulbecco's Modified Eagle Medium
DNA	Deoxyribonucleic acid
Dnajb9	DnaJ Heat Shock Protein Family (Hsp40) Member B9
Ebox	Enhancer box
ECM	Extracellular matrix
EGF	Epidermal growth factor
Egfr	Epidermal growth factor receptor
ER	Endoplasmic Reticulum
ERAD	Endoplasmic-reticulum-associated protein degradation
Erbb2	Erb-B2 Receptor Tyrosine Kinase 2
Erk	Extracellular Signal-Regulated Kinase
Ern1	Endoplasmic Reticulum to Nucleus Signaling 1
Ern2	Endoplasmic Reticulum to Nucleus Signaling 2
ETS	E26 transformation-specific
EZH2	Enhancer of Zeste 2 Polycomb Repressive Complex 2 Subunit
Fas	Tumor necrosis factor receptor superfamily member 6

FBS	Fetal bovine serum
FFPE	Formalin-Fixed Paraffin-Embedded
FGF	Fibroblast growth factor
FGF10	Fibroblast Growth Factor 10
FlpO	Flippase
FOS	Finkel–Biskis–Jinkins murine osteogenic sarcoma
FoxA	Forkhead box
FPC	Frt-Kras$^{LSL\text{-}G12V/+}$-Frt; Trp53$^{LSLR172H/+}$; Pdx1-Cre
G12D	Glycine aspartic acid position 12
G12V	Glycine valine position 12
Gcnt3	Glucosaminyl (N-Acetyl) Transferase 3, Mucin Type
GEMM	Genetically engineered mouse models
Gpx8	Glutathione peroxidase 8
gRNA	Guide ribonucleic acid
GTP	Guanosine triphosphate
HA	hemagglutinin
HGF	Hepatocyte growth factor
Hif1a	Hypoxia inducible factor 1 subunit alpha
Hspa5	Heat Shock Protein Family A (Hsp70) Member 5
IFN	Interferons
IHC	Immunohistochemistry
IL-23	Interleukin-23
IL6	Interleukin 6
IL8	Interleukin 8

Inhba	Inhibin beta A chain
Ink4a	cyclin-dependent kinase inhibitor 2A
IPMNs	Intraductal Papillary Mucosal Neoplasms
IRE1α	Inositol-requiring transmembrane kinase
IRE1β	inositol requiring enzyme-1beta
JUNB	AP-1 Transcription Factor Subunit
KC	$Kras^{LSL\text{-}G12D/+}$;Pdx1-Cre
KO	Knockout
KPC	$Kras^{LSL\text{-}G12D/+}$; $Trp53^{LSLR172H/+}$; Pdx1-Cre
KRAS	Kirsten rat sarcoma viral oncogene homolog
lncRNA	Long non-coding RNAs
LSL	Lox-stop-lox
MALAT-1	Metastasis Associated Lung Adenocarcinoma Transcript 1
MAPK	Mitogen-activated protein kinase
MCNs	Mucinous cystic neoplasia
MLL3	Histone-lysine N-methyltransferase 2C
mM	Murine metastatic organoid
MMP2	Matrix metallopeptidase 2
MMP9	Matrix metallopeptidase 9
mN	Murine normal organoid
mP	Murine Pancreatic intraepithelial neoplasia organoids
MSCV	Murine stem csell virus
mT	Murine tumor organoid
Muc2	Mucin 2

Muc5ac	Mucin 5AC
Muc6	Mucin 6
Mxd	MAD-MAX Dimerization Protein
MYB	myeloblastosis viral oncogene homolog
MYC	Avian Myelocytomatosis Viral Oncogene Homolog
Nefl	Neurofilament Light
NIH	National Institute of Health
PanINs	Pancreatic Intraepithelial Neoplasia
PBRM1	Polybromo 1
PDAC	Pancreatic ductal adenocarcinoma
Pdx1	Pancreatic and Duodenal Homeobox 1
PGE2	Prostaglandin E2
PI3K	Phosphoinositide 3-kinases
PNT	Pointed domain
PP	Prepropancreatic Polypeptide
PSA	Prostate specific antigen
Raf	Rapidly Accelerated Fibrosarcoma
RIDD	Regulated IRE1-dependent decay of mRNA
RNA	Ribonucleic acid
ROS	Reactive oxygen species
RRE	Ras response element
RTK	Receptor tyrosine kinase
RT-qPCR	Real time quantitative polymerase chain reaction
SERCA	sarco/endoplasmic reticulum Ca^{2+}-ATPase

SMAD4	Mothers against decapentaplegic homolog 4
SMARCA4	SWI/SNF Related, Matrix Associated, Actin Dependent Regulator of Chromatin, Subfamily A, Member 4
Stat1	Signal transducer and activator of transcription 1
SUMO	Small Ubiquitin-like Modifier
SWI/SNF	SWItch/Sucrose Non-Fermentable
TAL1	Erythroid Differentiation Factor
TAMs	Tumor associated microphages
TCF	T-cell factor
TF	Transcription factor
TG	Thapsigargin
TGFb	Transcription growth factor beta
TGFBR1	Transcription growth factor beta receptor 1
TGFBR2	Transcription growth factor beta receptor 2
TIMP2	Tissue inhibitor of metalloproteinases 2
TP53	Tumor protein 53
Trp53	Tumor receptor protein 53
Tspan9	Tetraspanin 9
TSS	Transcription start site
UPR	Unfolded protein response
Wnt	Wingless-related integration site
Wnt3a	Wingless-related integration site 3 alpha
WT	Wild type
Xbp1	X-box binding protein 1

Xbp1s	X-box binding protein 1 spliced
Xbp1u	X-box binding protein 1 unspliced

Acknowledgements

I would like to acknowledge all the people who made this journey possible. First, I'd like to thank my thesis advisor, Dr. David Tuveson. Dave's infectious enthusiasm and undeterred energy to advance our understanding of pancreatic cancer have been truly inspiring. I thank him for taking the chance on me, giving me the freedom to pursue any of crazy projects that I would get excited about, and for creating an excellent learning environment in the lab. I would also like to thank my thesis committee members, Drs. Doug Fearon, Leemor Joshua-Tor and Adrian Krainer, for their critical feedback on my work and for making sure that I stay on track throughout the years. I would also like to thank Dr Gerard Evan for agreeing to serve as an external examiner on my committee. His work on elucidating the oncogenic function of Myc in solid tumors was what inspired me to study Myc in my PhD and I would like to acknowledge him for his contributions.

None of this would have been possible without all the people that I met and worked with in the Tuveson lab. First, I would like to thank all the students who I had the pleasure to work with and mentor over the years who have contributed directly to the work presented in this thesis: Kaitlin Williams, Emily Ashkin and Mathias Bigger. I was always impressed by their striking brilliance and admirable work ethic and I wish them success in their current and future endeavors. I would also like to thank the research technicians from our lab, particularly, Melissa and Matthew who helped me with my organoid transplantation experiments and who took care of my animals at different times throughout the project. I would also like to thank the postdocs in our lab who have been a constant source of knowledge and scientific discussions throughout the years. I'd, particularly, like to thank Dr Youngkyu Park whose guidance throughout my PhD has been instrumental and who taught me a lot (everything I know) about cloning, molecular biology and mouse

modeling. Most of all, I'd like to thank the graduate students in our lab and especially Tobi and Brinda who made this experience a blast. Their scientific curiosity has always made discussing my results or new studies with them an enjoyable experience and I have also benefited a lot from their willingness to help. They have been a source of constant support inside and outside the lab and I am very grateful for everything they've done for me. I would also like to thank Carl for helping me with some of the last-minute experiments for the Spdef project.

Cold Spring Harbor Lab is a unique place filled with unique people. I would like to thank Anqi whose friendship has helped me get through many tough moments during my PhD and who has also been an amazing source of scientific discussions. I'd also like to thank my class who made the first year of the Watson School bearable. In particular, I'd like to thank Michael, Laura and Giorgia for their support and the amazing trips we've been on together!

We, sometimes, also, get to meet unique people *outside* the lab, who change our lives. I'd like to thank Peter for going through all of this with me, for his constant support and grammar lessons, and making sure that I never disappoint myself!

Last but not least, I'd like to thank my family for everything they have done that allowed me to be here today. My parents, and, in particular, mom made great financial and personal sacrifices to support me during my undergraduate studies. Taking up multiple jobs so that she can afford my studying abroad, my mom has made both personal and financial sacrifices and I will be forever grateful (even if I am not usually explicit about it). I would also like to thank my grandparents for believing in me and inspiring me to be the best version of myself. My interest and passion for science stemmed directly from them and they have been one of the strongest moral supporters I have had. THANK YOU!

Summary

Pancreatic cancer is an almost universally lethal disease with a 5-year survival rate of just 9%. While extensive efforts have been focused on defining the genetic alterations that are present in tumors of patients with pancreatic ductal adenocarcinoma (PDAC), less is known about the transcriptional regulatory pathways that promote the progression of the disease. The c-Myc transcription factor features prominently in human cancers, being overexpressed or activated in more than 70% of malignancies. Recent studies, using a genetic dominant negative protein (Omomyc), have demonstrated that Myc inhibition causes rapid eradication of mutant Kras-driven lung adenocarcinomas in vivo. The effects on normal tissue were mild and fully reversible. Similarly, it has been shown that Myc is important for the initiation and progression of PDAC. To address this question, our lab previously generated 3D organoid cultures of pancreatic epithelium and neoplastic tissues from a genetically engineered mouse model (GEMM) of PDAC. Analysis of RNA-seq data comparing normal (WT), pre-neoplastic (KrasG12V) and tumor organoids (KrasG12V; Trp53R172H) showed a clear signature of upregulated Myc target genes in tumor organoids that was not significant when normal organoids were compared to PanIN-derived organoids. However, there was no difference in the mRNA or protein levels of Myc between the normal and tumor organoids. Comparison of Myc occupancy by ChIP-seq revealed a significant overall enrichment of Myc at promoters in tumor organoids. In addition, we identified 841 tumor-specific Myc peaks suggesting differences in the transcriptional regulation by Myc between proliferating normal and tumor cells and propose a model of cooperation between Myc and other transcription factors in PDAC.

Additionally, a global transcriptomic comparison of normal duct-derived and tumor-derived organoids identified Spdef, an ETS family member, as the most upregulated

transcription factor in tumor organoids. Here, we show that Spdef is upregulated in murine tumor organoids in a mutant-Kras dependent manner *in vitro* and is overexpressed in human PDAC and patient-derived tumor organoids. In tumor organoids, we find that Spdef directly regulates the expression of the GI-specific kinase/endonuclease Ern2/Ire1β. Additionally, Spdef promotes the orthotopic growth of tumor organoids *in vivo* and the non-canonical splicing of Xbp1 – a central arm of the unfolded protein response pathway. Together, these results reveal a previously unappreciated role of Spdef in pancreatic cancer and nominate its downstream target, Ern2/Ire1β, as a potential therapeutic target for intractable PDAC.

CHAPTER 1. INTRODUCTION

1.1 Epidemiology and risk factors for PDAC

Pancreatic ductal adenocarcinoma (PDAC) is a uniformly lethal disease that is projected to become the second leading cause of cancer-associated mortality by 2030 (Rahib et al. 2014). Despite extensive efforts in preclinical and clinical science, survival has not improved substantially over the past 40 years, and the current 5-year survival rate is merely 9% (Bray et al. 2018). There are at least 4 factors that influence the dismal prognosis of patients with pancreatic cancer: 1) initial diagnosis usually occurs at an advanced stage with minimal and often non-specific symptoms; 2) pancreatic cancer is an aggressive disease with early distant metastases and perineural and vascular growth preventing surgical removal; 3) pancreatic cancer is refractory to most conventional treatment options; and 4) pancreatic tumors harbor multiple genetic and epigenetic alterations that have proven to be difficult to target in the clinic (Bray et al. 2018).

In 2018, it was estimated that 458,918 new cases of pancreatic cancer will be diagnosed worldwide and 432,242 deaths will result from this disease (Bray et al. 2018). Most of these diagnoses (>50%) would come from countries with high human development index (HDI) reflecting the difficulties with diagnosing the disease – highly trained and specialized physicians and expensive diagnostic equipment are often required to detect the disease. Pancreatic cancer accounts for about 3% of all cancers in the United States and about 7% of all cancer deaths (Rahib et al. 2014). It is estimated that 5-10% of PDAC cases have a hereditary component. The major factor associated with an increase in the incidence of pancreatic cancer compared is chronic pancreatitis – a chronic inflammation of the pancreas (Petersen 2016). In addition, smoking, diabetes and obesity have all been associated with ~2-fold increase in the risk of the disease (Bruenderman and Martin 2015). Despite recent progress in the

development of advanced imaging technologies to detect pancreatic cancer, there are currently no effective screening tools to detect asymptomatic premalignant or early malignant disease.

The pancreas is a secretory organ that serves both exocrine and endocrine functions within the digestive system. It supplies digestive enzymes and bicarbonate to the duodenum and produces peptide hormones including insulin and glucagon to regulate systemic glucose metabolism. The organ is composed of 4 main cell types – digestive enzyme-secreting acinar cells, bicarbonate-secreting ductal cells lining the pancreatic ducts, hormone-secreting islet cells and vitamin A-storing stellate cells. The acinar cells comprise the majority of the pancreas and are secretory factories with extensive endoplasmic reticula (ER), organized into functional clusters called acini. They secrete multiple digestive enzymes (proteases, amylases, lipases, ribonuclease and deoxyribonuclease) into intralobular ducts that drain into the main pancreatic duct (duct of Wirsung). The ducts are lined by simple cuboidal cells that secrete bicarbonate into the duodenum. The integrity of the duct system is of key importance in preventing entry of the exocrine enzymes into the interstitial space where they may be activated and cause tissue damage which manifests as pancreatitis. In addition to dense collagenous walls that surround the ducts, intercellular tight junctions between duct cells play a major role in preventing leakage of the duct system. The adult pancreatic islets (islets of Langerhans) constitute 1-2% of the pancreas and contain five distinct endocrine cell types – alpha, beta, delta, epsilon and PP (gamma or F) cells.

PDAC is the most common form of pancreatic cancer and accounts for >75% of all pancreatic cancer cases. PDAC is related to the ductal epithelial compartment of the pancreas. Less common neoplasms include neuroendocrine tumors (15-20%), colloid carcinomas (2%), solid pseudopapipllary carcinomas (2%), acinar cell carcinomas (2%) and pancreatoblastomas

(0.5%). Advanced PDAC has been shown to originate from three different precursor lesions: Pancreatic intraepithelial neoplasias (PanINs), mucinous cystic neoplasms (MCNs) and intraductal papillary mucinous neoplasms (IPMNs). PanINs are most common and progress into PDAC through a series of higher grade lesions (Fig. 1) (Hruban et al. 2000). PanIN-1s are the earliest precursor lesions and can be divided into PanIN-1A and 1B. PanIN-1A have characteristic flat glandular morphology composed of elongated, mucin producing epithelial cells with basally located nuclei. PanIN-1B lesions can be distinguished by their papillary or basally pseudostratified architecture. Next in the progression are PanIN-2 lesions. These can be flat or papillary and are associated with nuclear abnormalities including loss of polarity, nuclear crowding, enlarged nuclei, pseudo-stratification and hyperchromatism (the development of excess chromatin or excessive nuclear staining). PanIN-3 lesions are usually papillary with higher degree of nuclear abnormalities. They are characterized by dystrophic goblet cells (goblet cells with nuclei oriented towards the lumen and mucinous cytoplasm oriented toward the basement membrane), mitoses which may occasionally be abnormal, nuclear irregularities and prominent (macro) nucleoli. It is common to observe invasion of cells through the basement membrane into the lumen and luminal necrosis.

IPMN lesions are large cystic growths within the main pancreatic duct characterized by the production of thick mucus. They form long thin structures that project into the lumen of the duct, and histologically they are composed of tall columnar cells. These lesions can be detected in ~2.6% of healthy individuals, and their incidence correlates with age (they were detected in 8.7% of patients between 80-89 years of age) (Laffan, 2008). Early detection and surgical resection of IPMN lesions can reduce the lifetime risk associated with PDAC, and guidelines for screening of individuals at risk have been recommended (Bruenderman, 2015).

The less common MCN lesions are found predominantly in women (95%), are larger in size and are defined by the presence of ovarian stroma (Crippa, 2008).

1.2 Molecular and genetic features of PDAC

A careful molecular and pathological analysis of evolving pancreatic adenocarcinoma has revealed a characteristic pattern of genetic lesions (Fig. 1). Inspired by Bert Vogelstein's model of the step-wise genetic progression of colorectal adenocarcinoma, early efforts have ascribed similar mutational events to the progression from PanIN lesions to invasive PDAC (Staller et al. 2001a; Cubilla and Fitzgerald 1975, 1976; Hruban et al. 2000; Mutations et al. 1994). Oncogenic activating mutations in the proto-oncogene encoding the small GTPase *KRAS* are found in >95% of all patients with advanced PDAC regardless of the precursor lesion that their tumor originates from suggesting that mutant KRAS alone is not sufficient to cause histological progression of pre-neoplastic lesions, but that it might define one of the earliest genetic changes (Mutations et al. 1994). KRAS is normally tethered to the cytoplasmic face of the plasma membrane, and once activated in response to upstream receptor tyrosine kinases (RTKs), GTP-bound Kras can then facilitate the recruitment and subsequent activation of effector kinases such as Rapidly Accelerated Fibrosarcoma (Raf) kinase, Phosphoinositide 3-kinase (PI3K), and Protein Kinase B (RAF, PI3K, PKB/AKT), as well as downstream pathways that control cell proliferation such as Mitogen-activated protein kinase (Mapk) and Extracellular Signal-regulated Kinase (Erk). The most common mutations in KRAS lead to a substitution of the amino acid glycine at codon 12 to aspartic acid or valine (G12D or G12V). This causes a conformational change leading to abrogation of its GTPase activity and constitutive activation of downstream pathways. Upon nuclear import, MAPKs phosphorylate many different transcription factors, modulating their DNA binding affinity,

nuclear localization, stability, and interactions with coregulators, thereby regulating gene expression (Karin 1994).

Inactivating mutations in tumor suppressor genes cooperate with mutant *KRAS* to drive the invasive phenotype of PDAC tumors. *KRAS* mutations are the earliest to be detected in pre-neoplastic PanIN lesions (about 30% of cases) and can be found occasionally in histologically normal pancreas. Indeed, mutations in *TP53*, *CDKN2A* and *SMAD4* occur in 50–80% of pancreatic cancers, whereas other genes, including *ARID1A*, *MLL3* and *TGFBR2*, are mutated in ~10% of tumours (Raphael et al. 2017a). Those are generally the few genes that stand out among the myriad of infrequently mutated genes, which mostly occur at a prevalence of <2%, making subtyping of PDAC tumors according to mutational status difficult (Raphael et al. 2017a).

Recent efforts have focused on establishing molecular subtypes of PDAC defined by transcriptional differences. Collison et al were the first to describe three subtypes of PDAC based on gene expression - classical, quasi-mesenchymal, and exocrine-like (Collisson et al. 2011). Subsequently, using a technique called virtual microdissection, Moffitt et al. separated PDAC tumors into a classical and a basal-like subtype that resembled the basal subtypes of breast and bladder cancer (Moffitt et al. 2015a). Later studies from the Cancer Genome Atlas project have refined these subtypes to exclude tumor samples with low number of tumor cells (Raphael et al. 2017b). These studies have provided little insight into the factors that establish the distinct transcriptional subtypes. It is currently not known whether each tumor contains both 'classical' and 'basal' cells and whether the final classification is the result of simply the predominant cell type. We also do not understand whether these subtypes are 'plastic' and whether, for example, a classical cell exposed to the relevant extracellular stimuli can transition into a basal cell and vice versa. Remarkably, Moffit et al showed that all of the 2D

cancer cell lines that they analyzed were classified as 'basal-like' which either provides an answer to the question of plasticity or suggests that 2D cell culture selects for 'basal-like' tumors raising an important problem about the relevance of a homotypic *in vitro* culture systems (Moffitt et al. 2015a). The answers to these questions will be instrumental to establishing a clinically relevant use of the transcriptional classification of tumors and our understanding of the patient-to-patient heterogeneity.

1.3 Cell-of-origin in pancreatic cancer

A debated question in the field pertains to the cell of origin for PDAC. Cancer can arise from oncogenic mutations in either tissue-resident stem cells with a proliferative potential or in mature terminally differentiated cells that have transdifferentiated and now harbor the ability to proliferate. The exocrine pancreas is composed of acinar, centro-acinar and ductal cells, and they all have been suspected as the cell-of-origin. The histological appearance of PDAC tumors as dispersed ductiles in a desmoplastic stroma suggests a ductal origin, but contrasting evidence of acinar-to-ductal metaplasia observed in both human (Parsa et al. 1985) and mouse models (Sandgren et al. 1990) suggests an acinar origin. Early studies of carcinogen-induced pancreatic cancer in the Syrian golden hamster using N-nitrosobis (2-oxopropyl)amine (BOP) showed that early lesions such as focal hypertrophy, hyperplasia, goblet cell metaplasia, atypical hyperplasia and *in situ* carcinoma sequentially develop in the common duct, pancreatic duct and ductiles, but not in acinar cells (Pour et al. 1977). The histological similarity of these ductiles and associated precancerous lesions, called pancreatic intraepithelial neoplasia (PanIN), to pancreatic ductal cells suggested a lineage relationship and led to the development of tumour progression models that featured the normal ductal cell as the cellular origin of PDAC (Hruban et al. 2000). In these models, oncogenic Kras is

proposed to initiate low-grade PanIN from ductal cells. These lesions then acquire additional mutations, such as p16 or p53 loss, before becoming high-grade PanIN and invasive PDAC.

While these studies all point to the duct cell as the PDAC cell of origin, other studies suggest the acinar cell may be the originating cell. Using genetically engineered mouse models (GEMMs), multiple groups have shown that expression of oncogenic Kras in the acinar cell compartment of the pancreas can also lead to acinar-to-ductal metaplasia (ADM) and PDAC (Ji et al. 2009; Habbe et al. 2008; Kopp et al. 2012; De La O et al. 2008). To better compare the impact of cell-of-origin context on tumor development, Lee et al. relied on inducing PDAC-associated mutations (*Kras*^{G12D} and loss of *Trp53*) specifically in either ductal (*Sox9CreER; Kras*$^{LSL\text{-}G12D}$*; Trp53*$^{flox/flox}$) or acinar *(Ptf1a*^{CreER}*; Kras*$^{LSL\text{-}G12D}$*; Trp53*$^{flox/flox}$) cells.(Lee et al. 2019). The authors confirmed previous observations that both acinar and ductal cells can give rise to PDAC tumors in mice. However, they also showed that duct-derived PDAC developed earlier than acinar-derived PDAC. In addition, acinar-derived tumors had widespread metaplasia as well as both high- and low-grade PanIN lesions compared to only high-grade PanINs and advanced PDAC in duct-derived tumors. These observations are in line with the hypothesis that acinar cells undergo trans-differentiation upon transformation (ADM) and reflect the prolonged period of transition or reprogramming to initiate PDAC from those cells. In addition, acinar-derived tumors appeared more differentiated and retained features characteristic of lower-grade PanINs including Muc5ac expression and acidic mucins. These findings might provide a plausible explanation for the molecular subtypes identified in human PDAC – those patients whose tumors arose from acinar cells are more differentiated and thus belong to the classical subtype, while the duct-derived tumors have basal characteristics. Moreover, as epigenetic regulation of gene expression is

tissue-specific, the cell-of-origin that the tumor arose from might dictate transcriptional dependencies.

1.4 Non-cell autonomous transcriptional changes during PDAC

PDAC tumors are characterized by a dense desmoplastic microenvironment consisting of extracellular matrix (ECM), diffusible growth factors and cytokines, and a variety of non-epithelial cell types, including those comprising the vasculature (endothelial cells, pericytes and smooth muscle cells), those that can respond to infection and injury (lymphocytes, macrophages and mast cells), and fibroblasts. The paracrine crosstalk between epithelial cells and stromal cells is essential for both embryonic development and tumorigenesis and can influence gene expression (Gleimer and Parham 2003a).

Fibroblasts are the principal cellular component of connective tissues and are largely responsible for the synthesis of the fibrillar matrix that makes the bulk of these tissues. Fibroblasts synthesize many of the constituents of the fibrillar ECM such as fibronectin and numerous collagens (type I, type III and type V) (Tomasek et al. 2002). Fibroblasts also secrete growth factors such as TGFb, HGF, FGF and cytokines (CXCL12, CCL2, CCL5, IL6 and IL8) (Liu et al. 2016a; Orimo et al. 2005; Henriksson et al. 2011; Min et al. 2015; Jobe et al. 2016). During normal physiological conditions, fibroblasts reside within connective tissues in a resting state. However, inflammation such as tissue damage leads to the activation of resting fibroblasts which induces their proliferation and increases the secretion of ECM components (Castor et al. 1979). Fibroblasts thus play a key role in tissue fibrosis and wound healing as they help rebuild the damaged tissue. Within solid tumors, fibroblasts are in a perpetually active state and are referred to as cancer-associated fibroblasts (CAFs). In pancreatic cancer, pancreas-resident fibroblasts called stellate cells transdifferentiate into activated

myofibroblast-like cells in the context of tissue damage (Wilson et al. 2014). This activation leads to a profound change in their transcriptional program that induces a fibroinflammatory response, including secretion of extracellular matrix components, cytokines, and growth factors (Sherman et al. 2014). Therefore it is not surprising that mixing activated CAFs with PDAC cells leads to profound transcriptional effects with consistent changes in the expression of 500-800 genes in the tumor cells regardless of the underlying genetic mutations that were already harbored (Sherman et al., 2017).

Inflammatory cells within the tumor microenvironment are associated with many cancers and may facilitate tumor progression. Both adaptive and innate immune cells infiltrate tumors and whereas the latter are associated with tumor promoting effects, the former may be usually tumor suppressive. For instance, tumor-associated macrophages (TAMs), the predominant leukocyte population within PDAC tumors, support diverse phenotypes within the primary tumor, including growth, angiogenesis and invasion, by secreting a plethora of pro-tumorigenic proteases, cytokines and growth factors (Quail and Joyce 2013a). In breast cancer and glioma, TAMs facilitate tumor cell invasion through a paracrine signaling loop that involves cancer cell secreted colony-stimulating factor 1 (CSF1) and macrophage-derived epidermal growth factor (EGF) (Heeg et al. 2016a; Coniglio et al. 2012). In PDAC, pharmacological depletion of macrophages by targeting the CSFR1 receptor led to global changes in gene expression including downregulation of genes involved in cell cycle progression, DNA damage response and hypoxia/metabolism (Candido et al. 2018). These results suggest that the tumor microenvironment elicits transcriptional changes in cancer cells through paracrine secretion of growth factors and cytokines. Therefore, the crosstalk between epithelial cancer cells and stromal cells is essential in shaping the transcriptional program of tumors.

1.5 Laboratory models for studying PDAC

Good laboratory models of PDAC are essential to understanding the disease and translating findings for a clinically relevant impact on patients. Patient-derived 2D cell lines are commonly used to study cancer in laboratory settings, but multiple caveats exist that require caution when extrapolating results from cell lines to the clinical setting. First, in the case of PDAC, most published studies have relied on the same 15 cell lines thus limiting our understanding of the genetic heterogeneity of the disease (Rückert et al. 2012). Second, while epithelial cells proliferate within polarized and well-organized structures *in vivo*, PDA cell lines propagated as monolayer cultures lack this structural organization and functional differentiation. Third, the efficiency with which 2D cell lines can be derived from resected tumor is relatively low, between 11 and 14% (Grant et al. 1979; Kato et al. 1999) .

To circumvent these drawbacks our lab and others have developed 3D organoid models that allow isolated cells to self-organize into polarized 3D structures embedded in a collagenous basement membrane matrix derived from a sarcoma mouse model (Matrigel®). These organoids are supplemented with the minimal requirements for sustained growth without a mesenchyme: EGF (mitogen), R-spondin-1 (enhances Wnt signaling), Noggin (inhibits BMP signaling) and Wnt3a are indispensable maintenance factors (Boj et al. 2015). Human pancreatic organoids additionally require FGF10 (mitogen), nicotinamide (a form of vitamin B3), A83-01 (an Alk3/5 inhibitor) and prostaglandin E2 (PGE2, mitogen) for long-term expansion (Boj et al. 2015). Of note, both normal pancreatic duct-derived and preneoplastic-PanIN cells thrive in these conditions and can be expanded indefinitely. More recently, organoid cultures have been used to identify novel oncogenic mechanisms in PDAC (Quail and Joyce 2013b) as well as to predict therapeutic responses to chemotherapies in

patients (Tiriac et al. 2018). Remarkably, organoid cultures can also be used to study interactions between epithelial cancer cells and stromal fibroblasts which can aid in our understanding of the disease (Hingorani et al. 2005a; Biffi et al. 2019).

Our lab has also generated genetically engineered murine models (GEMMs) that recapitulate the progression of PDAC similar to that seen in patients by inducing pancreas-specific conditional mutations in the two most commonly altered genes in patients – *Kras* and *Trp53*. This was accomplished by replacing one of the endogenous *Kras* alleles with a $Kras^{G12D}$ allele preceded by a transcriptional STOP signal cassette and flanked by *LoxP* sites. A Cre-recombinase driven by the *Pdx1* promoter (expressed during embryonic development of the pancreas) excises the *LoxP-STOP-LoxP* cassette resulting in monoallelic expression of $Kras^{G12D}$ specifically in the pancreas. This leads to widespread PanIN lesions through the pancreata of these KC ($Kras^{G12D}$*; Pdx-Cre*) mice once they reach 8-10 weeks of age. These PanIN lesions eventually progress to advanced PDAC (Hingorani et al. 2003). Addition of a $Trp53^{R172H}$ allele accelerates onset of advanced PDAC in KPC ($Kras^{G12D}$*;* $Trp53^{R172H}$*; Pdx-Cre*) mice (Hingorani et al. 2005b). The deletion or mutation of other tumor suppressors in the KC model, such as Smad4 (*Dpc4*) (Oslowski and Urano 2011; Kojima et al. 2007; Izeradjene et al. 2007), *Tgfbr2* (Ijichi et al. 2006), and Ink4a/Arf (*Cdkn2a*) (Aguirre 2003), has led to phenotypes ranging from IPMN-like cystic tumors to aggressive PDAC.

1.6 Transcriptional changes during PDAC progression

PDAC tumors exhibit significant changes in gene expression compared to normal pancreatic exocrine cells, but only few of those changes could be explained by genetic alterations (Gutiérrez et al. 2015; He et al. 2012). Therefore, researchers have spent a lot of effort on the epigenetic regulation of gene expression during pancreatic cancer progression.

The term 'epigenetic' refers to changes that are 'beyond' the DNA sequence. A more formal definition proposed by Berger et al. is that "an epigenetic trait is a stably heritable phenotype resulting from changes in a chromosome without alterations in the DNA sequence" (Berger et al. 2009a). Multiple epigenetic mechanisms control gene expression during tumorigenesis including DNA methylation, post-translational histone modification nucleosome remodeling, and regulation by non-coding RNAs (ncRNAs).

DNA methylation of cytosine bases (converting cytosine to 5-methylcytosine) within regions of the DNA called CpG islands (CG dinucleotides) in promoters or gene bodies is one of the better understood mechanisms of epigenetic inheritance. Hypermethylation is linked to the repression of transcription, whereas DNA demethylation of normally methylated promoters is frequently associated with increased gene expression. While DNA methylation plays essential roles in development, genomic imprinting, X-chromosome inactivation for monoallelic expression, changes in DNA methylation patterns are observed in many cancers including PDAC. One of the commonly inactivated tumor suppressor genes in PDAC, *CDKN2A* (p16), is epigenetically silenced by promoter methylation in 14 to 21% of PDAC cases. (Schutte et al. 1997). In addition, several proto-oncogenes were found to be hypomethylated and overexpressed in PDAC relative to normal cells including genes for chromatin enzymes (e.g., histone methyltransferase SETD8, histone deacetylase KDM6A and the histone acetylase EP400) and oncogenes (JUNB, MYB, and FOS). Although the targeted methylation/demethylation of specific genes is poorly understood, large scale alterations of the cellular 'methylome' are often observed in cancer including PDAC (Nones et al. 2014). DNA methylation is carried out by three DNA methyltransferases (DNMT1, DNMT3a, and DNMT3b), and alterations of their function or expression in PDAC has been previously reported (Connor et al. 2017).

The majority of RNA molecules from the human genome are non-coding, and their function has only recently begun to be elucidated. ncRNAs can be broadly divided by size into small non-coding RNAs (sncRNAs) of less than 200bp and long non-coding RNAs of more than 200 bp (Mercer et al. 2009). These RNAs can fold to form secondary and tertiary structures that allow them to interact with DNA, RNA or proteins and affect multiple steps of gene expression including transcription, splicing and translation. lncRNAs, for example, can also interact with chromatin remodeling complexes and affect gene expression. The lncRNA *MALAT-1* has been shown to bind to and downregulate the expression of E-cadherin by recruiting the EZH2 complex to its promoter, ultimately promoting migration and metastasis in PDAC (Han et al. 2016). sncRNAs include miRNAs that can recognize and bind to sequences within untranslated regions (usually the 3′ end) of mRNAs and regulate their expression either by inducing RISC-mediated mRNA degradation or post-transcriptional translation inhibition (Murchison and Hannon 2004). Multiple oncogenic miRNAs (oncomirs) are overexpressed in PDAC tumors and control important tumorigenic processes. For example, miR-221/222 silences the expression of the MMP2/MMP9 inhibitor TIMP2 in pancreatic cancer cell lines leading to an increase in migration and invasiveness (Xu et al. 2015).

Another mechanism of epigenetic gene expression regulation is nucleosomal remodeling. Nucleosomes are the basic unit of chromatin and comprise DNA wrapped around proteins. Each nucleosome consists of an octamer of histones (two molecules each of histones H2A, H2B, H3 and H4) and 146 bp of DNA, which is wrapped around the octamer. Heterochromatic regions of the genome with little transcriptional activity are characterized by tightly packed nucleosomes whose remodeling is necessary to activate gene expression. ATP-dependent chromatin modifying enzyme complexes such as Swi/Snf (switch

defective/sucrose non-fermentable) alter nucleosome position on the DNA strand, resulting in more open or closed chromatin structure (Wilson and Roberts 2011). Mutations of the SWI/SNF complex members *ARID1A*, *PBRM1* or *SMARCA4* (Raphael et al. 2017a). Post-translational modifications of histones by methylation, acetylation or SUMO-ylation are thought to influence gene expression by recruiting chromatin modifying complexes or transcriptional activators and repressors (Berger 2002). However, there is extensive debate over whether these modifications directly induce gene expression changes or whether they merely reflect the present state of gene expression at that loci. Importantly, many transcription factors (TFs) can recruit chromatin modifying complexes and thus change chromatin accessibility regardless of the current chromatin state (Zaret and Carroll 2011).

1.7 Pioneer transcription factors can initiate chromatin remodeling at transcriptionally inactive genomic loci

An important question in transcriptional regulation is how do DNA-binding factors find and bind to their targets amidst the tightly wound nuclear chromatin. Early studies of the FoxA TF's ability to bind its target sequence within tightly packed nucleosomal DNA established the concept of pioneering TFs (Cirillo and Zaret 1999a). These factors are characterized by a set of features that distinguish them from opportunistic TFs: the abilities to bind DNA within closed or unmarked chromatin; 2) initiate chromatin remodeling at target sites; 3) allow binding of other TFs to the newly opened sites; and 4) the ability to establish a stable change in chromatin structure associated with epigenetic memory (Mayran and Drouin 2018). Binding of a pioneer factor to its target sequence often allows for the activation of otherwise silent genes, and many such factors play essential roles during development and cell fate specification.

Notably, chromatin opening activity is intrinsic to a pioneer factor binding to its target in chromatin and does not require ATP or an ATP-dependent nucleosome remodeler (Mayran and Drouin 2018). However, this does not mean that pioneering TFs can bind all of their target sequences in the genome unrestrictedly. Their occupancy seems to be cell type-dependent: for example, Sox2 binds different targets in the mouse cortex and spinal cord suggesting the presence of additional determinants of their binding (Wei et al. 2010). Importantly, pioneer factors are unable to bind to target sequences within constitutive heterochromatin and first recognize 'permissive' heterochromatin sequences. Initial binding to this facultative heterochromatin leads to subsequent recruitment of chromatin modifying complexes and nucleosomal depletion. Therefore, it is not surprising that alterations in pioneer TFs are often observed in cancer. Many of these factors are expressed during embryonic development but their expression is silenced in adult cells only to be re-activated again during tumorigenesis (Katoh et al. 2013). For example, in ER^+ breast cancer, Foxa1 is overexpressed and it is important for ER binding to many target sites thus regulating hormone response in these tumors (Carroll et al. 2006). In pancreatic cancer, our lab has previously shown that enhancer reprogramming driven by Foxa1 overexpression in metastatic organoids is essential for invasive tumor growth and metastasis formation (Roe et al. 2017).

1.8 Cooperation between transcription factors to control gene expression

Genome-wide occupancy studies have shown that many TFs only occupy a small fraction of their consensus binding sites in the genome (Harbison et al. 2004). Chromatin state and cooperation between TFs are both important aspects that can determine where and when a TF binds. Cooperative binding can occur by several means but the most common way is through protein-protein interactions (Morgunova and Taipale 2017). Results from single-

molecule imaging studies confirm that binding sites are occupied longer when multiple TFs bind together (Chen et al. 2014; Gebhardt et al. 2013). Molecular modeling and structural analyses provide further explanation of the cooperative nature of TFs. The cooperativity could also be DNA-dependent: for example, DNA could facilitate the contact between the two proteins, or the binding of one TF could alter the shape of the DNA and promote the binding of the other (as is the case with the IFN-beta enhanceosome) (Panne 2008). Taken together, these studies highlight the complexities involved transcriptional regulation of gene expression and the essential role that cooperation plays in how TFs function.

1.9 Deregulation of transcription factors in cancer

Somatic mutations in tumors provide only marginal insight into the actionable dependencies of each cancer. Another approach to identify key pathways essential for tumorigenesis is to understand the drivers of the deregulated transcriptional programs in cancer. Transcriptional programs are often disrupted in cancer by genetic alterations and abnormal paracrine stimuli. These altered programs invariably carried out by deregulated transcription factors. It is clear that cancer arises from the collaborative interplay between oncogenic events acquired during multi-step tumor formation with and tissue-specifying gene expression. Deregulated TFs in cancer can be classified into 4 main groups: (1) TFs involved in organizing cell identity, (2) TFs involved in proliferation control, (3) TFs that amplify transcriptional output, and (4) signaling TFs involved in dynamic changes in response to extracellular signals (Bradner et al. 2017). It is not uncommon for cancer cells to activate TFs that are either expressed in early development or early in a specific cell lineage. For example, TAL1 plays an important role in hemopoietic differentiation but is aberrantly expressed in >40% of cases of T cell acute lymphoblastic leukemia. In those cancers, TAL1's

regulatory program is hijacked by cancer cells to induce the expression of genes characteristic of more embryonic states (Sanda et al. 2012). On the other hand, transcription factors like MYC are frequently deregulated to amplify proliferative transcriptional programs and induce other oncogenic pathways to promote tumorigenesis (Lin et al. 2012). Transcriptional signaling proteins that alter gene expression but do not necessarily bind directly to DNA are exemplified by the Mediator complex (Allen and Taatjes 2015). Genetic alterations of Mediator-complex-encoding genes are observed frequently in prostate cancer and in many uterine myomas (Barbieri et al. 2012; Makinen et al. 2011).

1.10 Structure and function of Myc and Max as opportunistic transcription factor dimers

The C-MYC oncogene features prominently in human cancers, being overexpressed or activated in more than 70% of malignancies (Dang 2012). It is a member of the MYC family of transcription factors including also N-MYC and L-MYC. C-MYC's protein product (referred to as Myc hereafter) controls a number of essential cellular processes including proliferation, DNA replication, protein biogenesis, metabolism, angiogenesis as well as paracrine regulatory programs – all essential pathways for neoplastic growth and maintenance (Li et al. 2016).

Myc is a basic helix-loop-helix (bHLH) transcription factor that lies at the crossroads of many growth promoting signal transduction and bioenergetic pathways. It forms a heterodimer with another small bHLH protein, MAX, which allows the complex to bind promoters and enhancers containing the canonical E-box sequence (CACGTC) and activate gene expression by recruiting multiple co-activator complexes. Similar to other regulatory transcription factors, Myc contains two separable domains: a bHLH/leucine zipper DNA

binding and dimerization domain at its C-terminus and a transactivation domain at its N-terminus. Myc has low affinity for DNA and does not form homodimers (Darzynkiewicz et al. 1980a; Littlewood et al. 1992; Amati et al. 1992a). Therefore, its interaction with Max is essential for carrying out its oncogenic function whereby Myc supplies a strong transactivating domain and Max provides a high affinity E-box DNA binding domain (Amati et al. 1992a, 1993). Max, on the other hand, can form both homodimers as well as heterodimers with members of the Mxd protein family capable of binding E-box sequences (Ayer et al. 1993). Despite the lack of a transactivating domain, Max can indirectly inhibit the transcriptional activity of Myc by competing for E-box binding (Amati et al. 1992a). Additionally, Max-Mxd heterodimers antagonize Myc-Max by direct transcriptional repression of E-box-containing target genes (Ayer et al. 1993). Myc-Max complexes can also forms oligomers with the Miz-1 transcription factor leading to transcriptional repression of Miz-1 target genes (Gebhardt et al. 2006; Staller et al. 2001b; Herold et al. 2002). The repressive role of the cooperation between Myc-Max and Miz-1 has also been shown to promote tumorigenesis (Walz et al. 2014; Heeg et al. 2016b).

Understanding the transcriptional effects of Myc activation would, in principle, allow us to explain its oncogenic properties. The advent of next generation sequencing and whole genome occupancy analyses, such as ChIP-seq, revealed that Myc directly regulates the expression of thousands of genes (Guccione et al. 2006; Lawlor et al. 2006; Li et al. 2005; Schlosser et al. 2005; O'Connell et al. 2003). The binding of Myc is also dose-dependent: at low physiological levels Myc selectively engages with promoters containing the canonical E-box motif but when overexpressed, Myc binding is less selective and binds to E-box variant motifs as well as distant sites (Lin et al. 2012; Nie et al. 2012; Walz et al. 2014; Sabò et al. 2014). A debate in the field pertains to the question of whether oncogenic Myc acts as a transcriptional

amplifier of all expressed genes in a cell or whether it regulates a distinct subset of target genes in a tumor-specific manner. Recent studies have argued that high levels of Myc lead to engagement with all active regulatory elements leading to global increase in transcription and total RNA levels per cell (Nie et al. 2012; Lin et al. 2012). These results support a hypothesis that Myc serves to merely sustain or promote the transcriptional program already active in each cell. On the other hand, it is also important to consider that Myc endows cells with specific physiological changes that could indirectly account for the increased transcriptional activation (e.g. in cell size, energy metabolism, translation and nucleotide biosynthesis) (Cunningham et al. 2014; Padovan-Merhar et al. 2015; de Gramont et al. 2017). In addition, total RNA content is a well-established correlate of cell proliferation, and since induction of Myc in all of these models leads to increased proliferation, change in total RNA content might not be necessarily dependent on Myc (Darzynkiewicz et al. 1980b).

1.11 The Myc transcriptome - controlling all aspects of the 'hallmarks of cancer'

The tight regulation of Myc protein levels and function is essential for normal cell homeostasis. Early genetic studies of the role of Myc in murine embryonic development showed that Myc is an essential gene, and its homozygous loss leads to lethality at 9.5-10.5 days of gestation (Davis et al. 1993). Surprisingly, Myc was dispensable for proliferation of embryonic stem cells or embryos before that time suggesting that certain organs/systems are more dependent on Myc than others. On the other hand, constitutive overexpression of Myc *in vitro* and *in vivo* leads to neoplastic transformation (Coppola and Cole 1986) but also apoptosis (Evan et al. 1992).

In contrast to other oncogenes, MYC is usually deregulated not by mutations in its protein coding sequence but by alterations of the levels or timing of its expression by other signaling pathways or mutational processes such as insertional mutagenesis, chromosomal translocations or amplifications (Dang 2012). In addition, control of MYC's mRNA turnover as protein stability by post-transcriptional modifications can enhance its activity in cancer cells (Sears 2000). Multiple oncogenic pathways can alter the activity of Myc by regulating its gene expression or protein stability. The half-life of the Myc protein is only ~20 mins in cell culture due to its rapid degradation by the ubiquitin/26S ribosome pathway (Hann and Eisenman 1984; Ciechanover et al. 1991). Mitogenic stimulation leads to stabilization of Myc by inhibition of its proteasome-dependent degradation by direct phosphorylation of Myc at serine 62 by the Ras/Raf/MAPK pathway (Sears et al. 1999). In addition, beta-catenin directly upregulates Myc expression downstream of the APC pathway which is commonly inactivated in cancer (Moffitt et al. 2015b). Overall, Myc's steady-state activity is altered in at least 70% of human cancers and is believed to be deregulated in most cancers (Li et al. 2016).

Early studies suggested that deregulation of Myc alone is not sufficient for transformation, and co-operating oncogenes such as Ras are required for tumorigenesis in part because elevated Myc levels cause apoptosis in normal cells (Yancopoulos et al. 1985a; Podsypanina et al. 2008; Evan et al. 1992; Amati et al. 1993; Land et al. 1983). However, using an elegant *in vivo* system to modulate the levels of Myc, Murphy et al. showed that although high levels of Myc led to ARF/p53-induced apoptosis, sustained expression of low levels of Myc from the *Rosa* locus was sufficient to drive cell proliferation and oncogenesis bypassing those cell death pathways (Quail and Joyce 2013c). More recently, using a similar model of sustained but reversible deregulated Myc expression, Kortlever et al. showed that co-activation of Myc and $Kras^{G12D}$ in the lung leads to the formation of highly proliferative and

inflammatory lung adenocarcinomas (Kortlever et al. 2017). The authors clearly showed a non-cell autonomous role of Myc in promoting tumorigenesis and immune suppression through regulating the expression of the CCL9 and IL-23 (Kortlever et al. 2017). Surprisingly, when a similar module was utilized but this time driven by a pancreas-specific promoter, Myc's highly tissue-specific mechanism of action was revealed. In Myc/Kras^{G12D}-induced PanIN lesions, Myc activation leads to rapid expression of PD-L1 in epithelial cells which promotes an immunosuppressive phenotype (Sodir et al. 2019). In both models, the Myc-induced transcription programs and tumorigenesis were immediately and completely reversible. Earlier studies have also shown tumors are dependent on the powerful oncogenic role of Myc even if Myc is not the initiating oncogene. For example, systemic inhibition of Myc in both the well-established LSL–Kras^{G12D} murine model of non-small cell lung cancer (Soucek et al. 2008, 2013)and the RIP1-Tag2 model of pancreatic insulinomas driven by SV40 T/t antigens (Sodir et al. 2011) triggered rapid and wholesale regression of incipient and established tumors. Altogether these results are a clear testament to the pleiotropic functions of Myc and suggest that tissue- and tumor-specific dependencies exist which could be exploited therapeutically.

1.12 ETS family of transcription factors - effectors of mutant Kras signaling

The E26 transformation-specific (ETS) family of transcription factors includes 28 different proteins that play various roles in development (Maroulakou and Bowe 2000). While some are ubiquitously expressed, others are expressed in a tissue- and cell type-specific manner (Hollenhorst et al. 2011b). All members of the family share the highly conserved ETS DNA binding domain that recognizes an invariable GGAA/T core flanked by 3-4 other less conserved nucleotides (Wei et al. 2010). In addition, some members contain a pointed domain

(PNT) that has been shown to be involved in protein-protein and protein-RNA interactions and could serve as a docking site for ERK2 (Seidel 2002). The transcriptional transactivation domains, similar to other transcription factors, display minimal stable secondary or tertiary structure. The regulation of the activity of ETS factors is mostly carried out by transcriptional and post-translational modifications affecting the total protein levels inside the cell as well as interaction with other transcription factors (Hollenhorst et al. 2011b).

The ETS factors are present throughout the metazoan family and seem to have evolved by large-scale duplications of vertebrate genomic regions (Degnan et al. 1993). Based on their homology, the 28 human ETS factors can be grouped into four classes (Hollenhorst et al. 2011b). This classification is important because closely related members of a subfamily may display redundant functions, whereas those in different subfamilies may have unique biochemical properties that could be utilized in distinct biological pathways. The diverse phenotypes that these factors play a role in, despite the similarities of the DNA motif they recognize, is exemplified by the mouse genetics experiments and summarized in Figure 1.2. This diversity suggests that ETS factors carry out distinct biological functions which are often achieved by specific signaling cascades and cooperation with other transcription factors. The Ras pathway has been shown to be a crucial upstream regulator of multiple members of the ETS family (Wasylyk et al. 1998). Molecular details of these interactions have been well illustrated by the Ets1/Ets2 transcription factors. Downstream of Ras, MAPK phosphorylation of threonine and serine residues immediately preceding the PNT domains of Ets-1 and Ets-2 leads to stimulation of their transcriptional activities by promoting interactions with transcriptional activator complexes (Wasylyk et al. 1997; Yang et al. 1996). In addition, through cooperation with other transcription factors a Ras-responsive element (RRE) could be identified in promoters of genes whose expression is regulated by Ras-

induced ETS activation (Imler et al. 1988). For examples, serum-response elements are present in many immediate early genes (C-fos, Egr1, Egr2, Vinculin) and function as RREs that mediate responses to many extracellular stimuli. In this case, SRF cooperates with Ras-induced TCF proteins.

1.13 Spdef is a unique ETS transcription factor

The SAM Pointed Domain Containing ETS Transcription Factor (Spdef) is a unique ETS family member that defines a secretory lineage of epithelial cells. It is the sole member of ETS protein Class IV because of differences in the sequence of its DNA-binding domain which lead to its unique preference for a GGAT core sequence instead of GGAA (Oettgen et al. 2000). It was originally discovered as a key interactor of the androgen receptor in controlling prostate-specific antigen (PSA) gene expression (Oettgen et al. 2000). Subsequently, Spdef's expression was shown to be increased in multiple cancers, including breast and prostate compared to the normal tissue (Sood et al. 2007). While the ETS1/2 transcription factors are expressed ubiquitously in all cell types, Spdef's expression is restricted to epithelial cells and has been shown to be essential for the maturation of the mucus-secreting Goblet cells in the intestinal epithelia and the differentiation of Clara cells to Goblet cells in lung epithelial tissues (Gregorieff et al. 2009). In Goblet cells, Spdef was shown to directly regulate the expression of multiple genes involved with mucin secretion including mucins (*Muc5ac*), genes involved in protein folding (*Agr2*) and glycosylation enzymes (*Gcnt3*) (Park et al. 2007). These studies establish an essential role of Spdef in a well-defined secretory cell lineage during development.

Multiple studies have implicated a functional role for Spdef in tumorigenesis. Surprisingly, in cancer, Spdef's mechanistic role appears to be distinct from its developmental

program. For example, Spdef is highly upregulated in luminal breast cancer compared to normal breast epithelial cells and may promote tumorigenesis by negatively regulating the expression of the death ligand Fas (Buchwalter et al. 2013). In addition, Spdef was also found to regulate invasion and cell motility by cooperating with the receptor tyrosine kinase Erbb4 in breast cancer cell lines (Gunawardane et al. 2005). In prostate cancer, besides the Spdef's role in cooperating with the androgen receptor, Spdef expression was reported to inhibit advanced disease and metastasis although the mechanism was not determined (Steffan et al. 2012). More recently, conditional ectopic expression of Spdef with $Kras^{G12D}$ in the lungs of transgenic mice was shown to induce malignant mucinous lung tumors while $Kras^{G12D}$ alone led to the formation of benign lung tumors (Guo et al. 2017). Interestingly, Spdef is not essential for development in mice (Marko et al. 2013).

1.14 The Unfolded Protein Response

The majority of secreted and membrane-bound proteins are folded into their native confirmation and modified post-translationally in the endoplasmic reticulum (ER). The ER is essential in monitoring the folded state of proteins and repairing any misfolding mistakes. This process requires protein oxidation to generate disulfide bonds. The major redox buffer in the cell is glutathione. In the cytoplasm, the ratio of reduced glutathione to oxidized glutathione is >50:1. In contrast, in the ER, this ratio is 1:1 to 3:1. Disulfide bond formation in the ER is catalyzed by protein disulfide isomerases like Agr2 and PDI which are also part of protein homeostasis (Ma and Hendershot 2004). If the influx of nascent, unfolded polypeptides exceeds the folding and/or processing capacity of the ER, the normal physiological state of the ER is perturbed. Aberrant protein conformations are a major cause of disease, and as such, the ER has mechanisms in place to respond to misfolded proteins. If

misfolded proteins are detected, signal transduction pathways originating in the ER are activated to increase its folding capacity or induce cell death if the stress to the ER persists. This response, which is called the unfolded protein response (UPR), is a conserved physiological mechanism that ensures proper protein folding.

ER stress can be caused by overexerting the protein folding capacity of the ER. ER stress can be created by the synthesis of large and heavily modified proteins, the global overexpression of proteins, or by the damage to nascent polypeptides caused by reactive oxygen species (ROS). Notably, ROS are generated by activation of oncogenic signaling, hypoxia or nutrient deprivation, conditions that all occur in the context of tumors. Two options exist to restore the folding capacity of the ER following ER stress: the cell can either decrease the folding demand or increase the folding capacity. To decrease the folding demand, either selective downregulation of the expression of secretory proteins or global decrease in protein translation could be employed. Alternatively, and usually concurrently, ER folding capacity can be increased by the upregulation of ER resident molecular chaperones and enzymes required for protein folding and disulfide bond formation, or by increasing ER size. Unresolved ER stress ultimately triggers cell death pathways.

The UPR is a network of multifaceted signaling pathways that is activated to limit the accumulation of unfolded proteins in response to ER stress. In mammals, three main pathways respond to increased protein folding demand in the ER – the Ire1α/ Ire1β (encoded by Ern1/2), Atf6 and Perk pathways (Ma and Hendershot 2004) (Figure 1.3). Ern1 and Ern2 are paralogues, and while Ern1 is expressed ubiquitously in the body and is required for murine development (Iwawaki et al. 2009), Ern2 expression is restricted to tissues of the gastrointestinal tract is a non-essential gene (Bertolotti et al. 2001; Ghosh et al. 2010; Martino et al. 2013). As a type I transmembrane proteins, Ire1α/β contain an amino-terminal ER

luminal domain and carboxy-terminal cytoplasmic kinase and RNase domains. Their activation in the presence of ER stress requires the formation of Ire1α/b homo- or hetero-oligomer by self-association of their ER luminal domain (Li et al. 2010).

The ER resident chaperone BiP (also known as Grp78) is the major sensor of unfolded proteins in the ER. In addition to its function in facilitating protein folding as a chaperone, BiP is also involved in restricting UPR activation in the absence of unfolded proteins. When unfolded proteins are not present, BiP associates with the luminal domains of Ire1α/β and Perk to prevent their oligomerization (Pincus et al. 2010; Shen et al. 2002). However, when the concentration of unfolded proteins in the ER increases, BiP dissociates and binds to exposed hydrophobic regions (the thermodynamic hallmark of an unfolded protein), and this allows Ire1α and β to dimerize which leads to their activation (Bertolotti et al. 2000; Okamura et al. 2000; Shen et al. 2002). Additionally, the luminal domains of both Ire1α and Ire1β contain an MHC-like structure that can bind to hydrophobic domains of unfolded proteins, but this mechanism of sensing ER stress is likely employed only by Ire1β (Pochampalli et al. 2007b; Karagöz et al. 2017).

Dimerization of Ire1α and β induces trans-autophosphorylation of the proteins which causes a conformational change in their RNAse domains. This conformational change activates their effector function of cleaving the Xbp1 mRNA (Korennykh et al. 2009). In mammals, Ire1α excises a 26 bp intron within the *Xbp1* mRNA which shifts the open reading frame of the mRNA, and the resulting short protein isoform of Xbp1 (Xbp1s) contains a strong transcriptional activating domain (Shen et al. 2002). In cellular models of ER stress, Xbp1s controls the expression of genes encoding factors that modulate protein folding, secretion, Endoplasmic Reticulum Protein Degradation (ERAD), protein translocation into the ER, and lipid synthesis (Acosta-Alvear et al. 2007). In addition, non-specific cleavage of multiple

RNAs by Ire1α, a process called **r**egulated **I**re1-**d**ependent **d**ecay (RIDD) can occur that may serve to alleviate the ER from further protein synthesis (Hollien and Weissman 2006).

The transcription factor Atf6 interacts with BiP with its luminal domain, and upon ER stress it translocates to the Golgi apparatus where it is proteolytically cleaved releasing its cytoplasmic domain which is a potent transcription factor (Yancopoulos et al. 1985b). Atf6 regulates the expression of UPR genes, including those that reinforce the ERAD pathway (Yamamoto et al. 2007).

Perk, another ER resident kinase, is activated in the presence of ER stress. It phosphorylates the translation initiation factor eIF2a which leads to shutting down global translation and a paradoxical concomitant increase in the translation of the Atf4 transcription factor (Harding et al. 2000; Berger et al. 2009b). The latter induces the transcription of select genes whose functions are to restore proteostasis (Fusakio et al. 2016). A notable target of Atf4 is Chop – a transcription factor responsible for activating the expression of multiple ER chaperones as well as apoptotic genes (Nishitoh 2012).

The role of the unfolded protein response in tumorigenesis still remains poorly understood. As the tumor becomes larger, it experiences increasing hypoxia, nutrient starvation and acidosis until the microenvironment becomes limiting, suggesting that conditions within tumors may promote ER stress. Indeed, several studies have reported evidence of involvement of the UPR in various tumors. Activation or overexpression of IRE1, XBP1, ATF6, CHOP, BiP (GRP94) and GRP170 have been shown to be important in tumorigenesis (Li et al. 2017; Ojha and Amaravadi 2017a; Shuda et al. 2003; Fernandez et al. 2000; Gazit et al. 1999; Chen 2002; Song et al. 2001). One hypothesis posits that the UPR protects tumor cells from ER stress-induced apoptosis. Additionally, multiple studies have established a link between activation of the UPR and angiogenesis. Vegf is a pro-angiogenic

protein that is synthesized and processed in the ER. Its expression is induced by an ATF4-dependent pathway and there is evidence to suggest that increased levels of BiP could mediate Vegf folding (Roybal et al. 2004; Ikeda et al. 1997). It has also been suggested that, in metastatic pancreatic cancer, UPR induction promotes a dormant state instead of apoptosis which could serve to protect tumor cells from clearance by the adaptive immune system (Pommier et al. 2018).

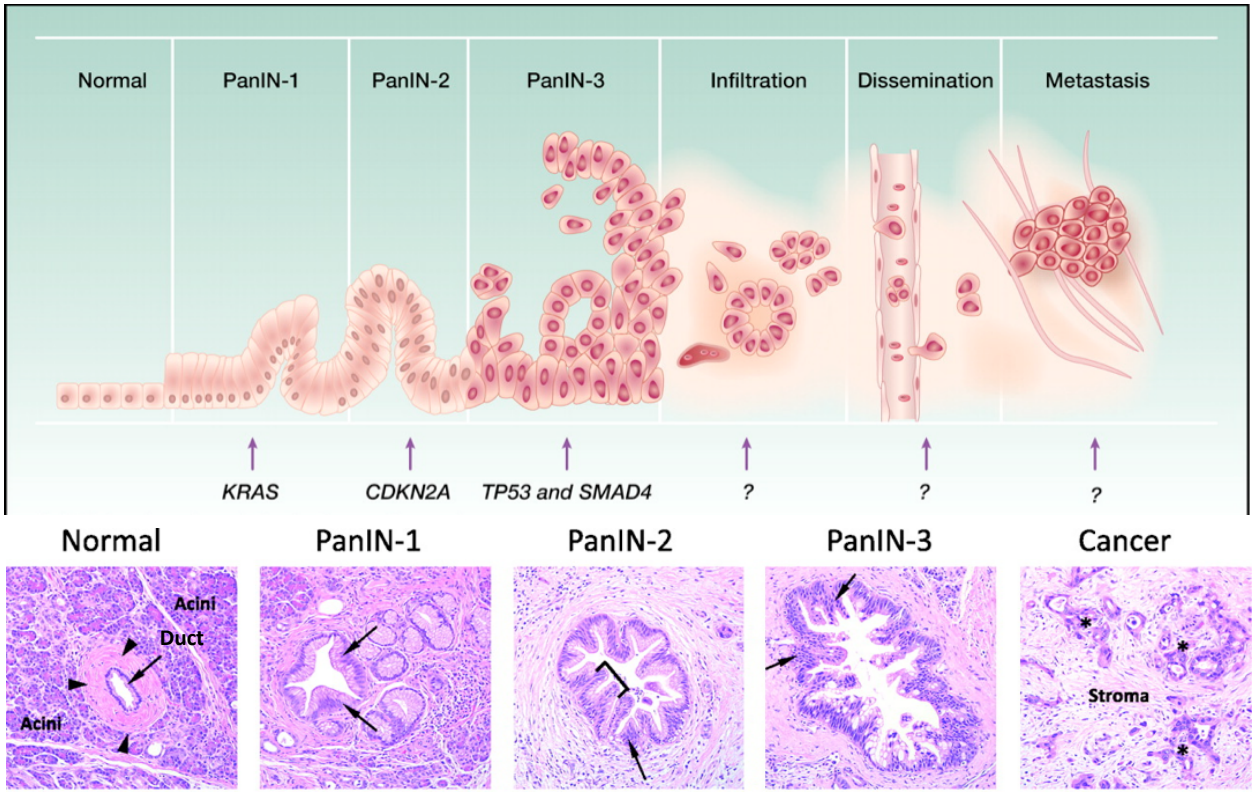

Figure 1.1 Histological and molecular progression of pancreatic ductal adenocarcinoma. Top panel shows a schematic of the histological progression in PDAC from normal epithelial ducts to PanIN, advanced PDAC and metastasis and the common mutations associated with each stage. Bottom panel shows representative H&E images of normal pancreatic ducts, PanIN1-3 and PDAC histology (adapted from Iacobuzio-Donahue et al 2012).

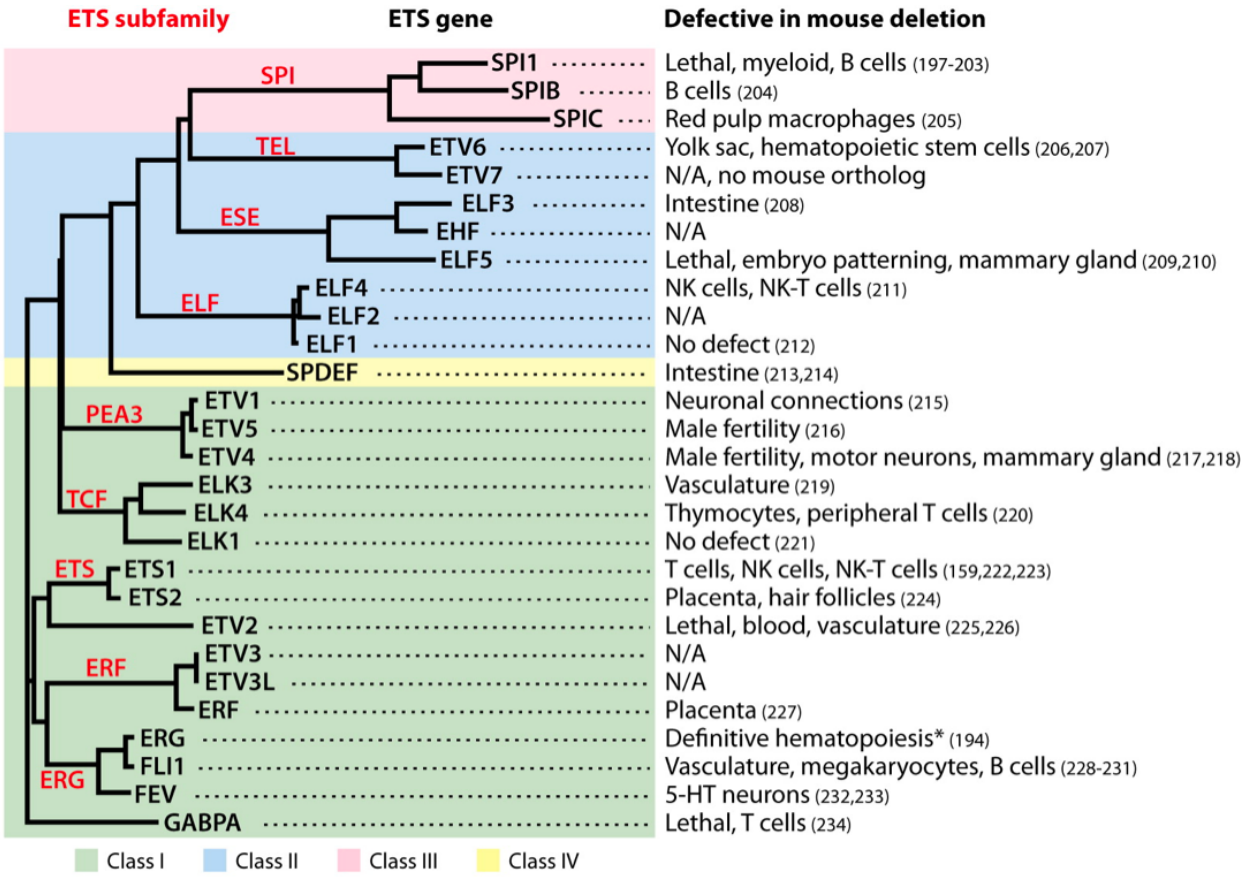

Figure 1.2 The ETS family of transcription factors and their relatedness based on sequence homology (adapted from Hollenshorst et al 2011)

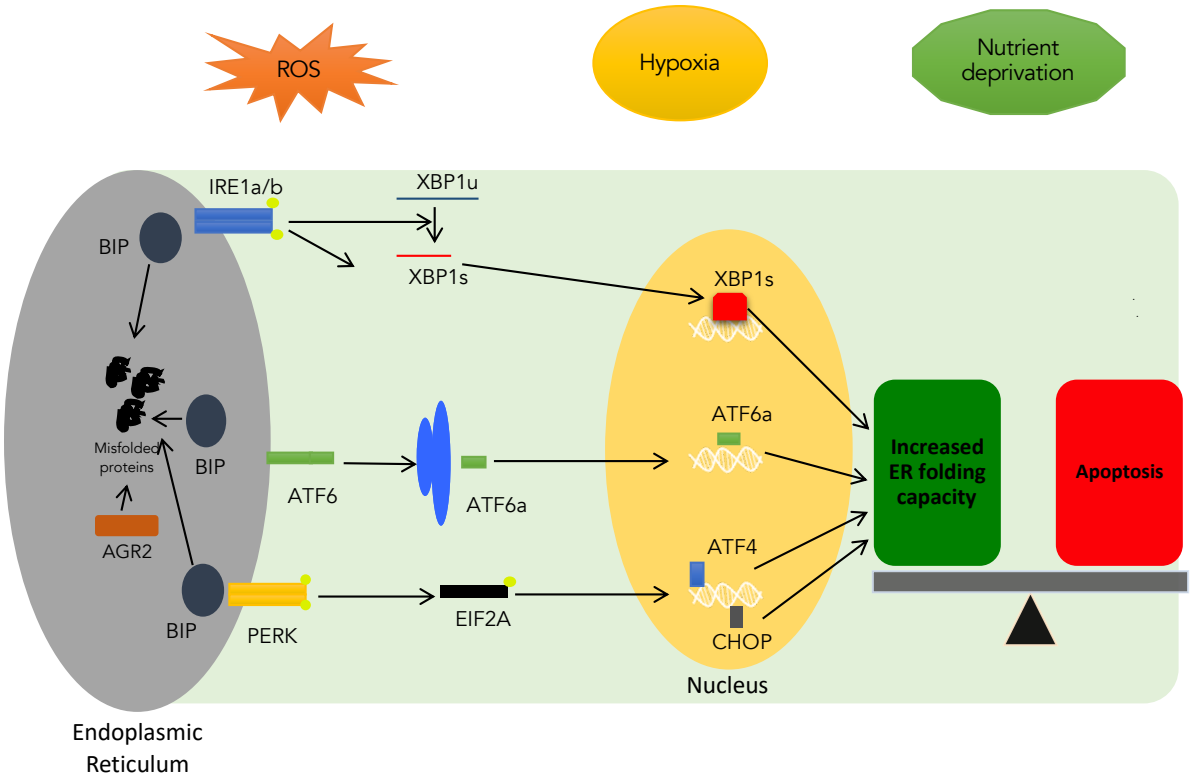

Figure 1.3 The three arms of the mammalian unfolded protein response pathway: IRE1, ATF6 and PERK. Endogenous stressors including ROS, hypoxia and nutrient deprivation lead to accumulation of unfolded proteins in the ER which activate the unfolded protein response. The BIP protein binds to the 3 major effectors of the UPR IRE1a/b, ATF6 and ATF4. High concentration of misfolded proteins in the ER leads to dissociation of BIP from the UPR proteins and causes their activation. IRE1a/b's endonuclease function initiates non-canonical splicing of Xbp1; ATF6 is proteolytically cleaved in the Golgi and translocates into the nucleus and PERK causes phosphorylation of the translation initiation factor EIF2A.

CHAPTER 2. REGULATION OF C-MYC ACTIVITY IN PANCREATIC CANCER ORGANOIDS

Introduction

A central theme in molecular oncology is that tumors remain dependent on the activity of the oncogenic pathways that drive tumorigenesis (Weinstein 2002). This phenomenon, coined "oncogene addiction", has been demonstrated to be a feature of tumors even when MYC is not the initiating oncogenic event, thus rendering MYC a plausible therapeutic target (von Eyss and Eilers 2011). Genetic studies performed in animal models have revealed that suppression of Myc activity leads to rapid tumor regression due to inhibition of cell proliferation, induction of senescence, apoptosis, as well as remodeling of the tumor microenvironment (Soucek et al. 2008; Sodir et al. 2011; Soucek et al. 2013). By overexpressing a mutated version of the Myc bHLH domain (Omomyc), which acts in a dominant negative fashion to endogenous Myc, Soucek *et al* showed that systemic Myc inhibition can eradicate tumors in a mutant Kras-driven GEMM of lung cancer with only mild and fully reversible side-effects on proliferating tissues (Soucek et al. 2008). These proof-of-concept genetic studies, although not feasible in the human setting, establish the dependency of tumors on Myc activity even in cases where Myc is not the initiating oncogene. Based on these findings, additional studies have been performed to explore the inhibition of MYC's expression or activity as a therapeutic approach. For example, the BET bromodomain small molecule inhibitor JQ1 was identified to have a powerful therapeutic effect in murine models of a number of blood cancers by shutting down the expression of *MYC* (Delmore et al. 2011). Small molecule inhibitors of MYC-MAX dimerization have also been described but have shown no efficacy *in vivo* due to their short terminal half-life and rapid metabolism (Whitfield

et al. 2017). More recently cell-penetrating Omomyc peptides showed promising activity against solid tumors in mouse models but, due to the limited clinical success of other peptide-based therapies, will require further validation before advancing to the clinic (Wang et al. 2019; Beaulieu et al. 2019). Given these unsuccessful attempts to target MYC in solid tumors, new approaches to inhibit its function are warranted.

The role and regulation of MYC in PDAC progression have not been fully elucidated (Eser et al. 2014). Amplifications of *MYC* have been documented in a subset of PDAC tumors (<10%) and activation of the MEK-Erk pathway by mitogens or oncogenic KRAS has been shown to stabilize MYC (Sears 2000). Post-translational modifications (PTMs) of the N-terminus of MYC can regulate its stability as well as activity (Hann 2006). Phosphorylation, ubiquitination, O-linked glycosylation and acetylation have all been found on MYC with phosphorylation (at residues S62, S71, S82 and S164) being the only functionally relevant modification *in vivo* (Hann 2006). Most of these modifications affect the stability of the MYC protein, however, phosphorylation of MYC at S62 by ERK has been reported to also regulate its interaction with specific target genes (Li et al. 2005a). Studies have also shown that Myc is essential for the deregulation of a number of other metabolism pathways important for PDAC and that its knockdown affects early stages of PDAC development (Saborowski et al. 2014). In a Kras-driven mouse mode of PDAC, Kras promotes metabolic reprogramming in these tumors by regulating anabolic glucose metabolism downstream of MYC (Ying et al. 2012). Additionally, deletion of a single allele of Myc significantly increased the survival of KPC mice exemplifying the dependency of PDAC tumors on Myc (Walz et al. 2014). To investigate the progression of PDAC and explore therapeutic applications, our lab previously generated a physiologically-relevant murine model of early and late stage PDAC by conditionally expressing endogenous $Kras^{LSL\text{-}G12D}$ (KC) or both the $Kras^{LSL\text{-}G12D}$ and $Trp53^{LSL\text{-}R172H}$ (KPC)

alleles in developing pancreatic tissues through the use of pancreas-specific Cre recombinase alleles (Hingorani et al. 2005b, 2003). Early stage pancreatic intraepithelial neoplasms (PanINs) can be studied using the KC model, while the KPC model allows for characterization of advanced, invasive and metastatic PDAC. To complement these mouse models, in collaboration with Hans Clevers's laboratory, we recently developed an *ex vivo* three-dimensional organoid system to study normal ductal (mN), PanIN (mP) and tumor (mT) cells as well as cells from distant metastases (mM) (Boj et al. 2015). This system provides us with the ability to compare primary normal to primary neoplastic cells and follow the progression of the disease from initiation to metastasis.

2.1. C-myc's activity is induced in pancreatic cancer organoids despite no difference in protein levels between normal and tumor cells

To determine the status of Myc activation in our organoid cultures, we analyzed the RNA-seq expression data from Boj et al. 2015. GSEA revealed that canonical and previously described Myc target gene sets were significantly upregulated in tumor organoids when compared to normal (Fig.2.1A and B). Surprisingly, this upregulation of Myc targets was not observed in PanIN organoids, suggesting that mutant Kras alone could not explain the activation of Myc and points to Kras-independent hyperactivation of c-Myc in advanced PDAC.

We hypothesized that upregulation of Myc itself in tumor organoids might explain the increased expression of its target genes. However, we did not observe induction of c-Myc at the mRNA (Fig.2.2A) or protein level (Fig. 2.2B) when we compared a panel of normal, PanIN and tumor organoids. Interestingly, in our organoid cultures, acute activation of

mutant Kras using the LSL-KrasG12D organoids did not lead to stabilization or increase of c-Myc at the protein level (Fig. 2.2C).

2.2. Tumor-specific promoter occupancy by Myc defines transcriptional changes of its target genes

Gene expression can be altered by dynamic changes in enhancer states and functional changes establishing novel regulatory regions typically occur in a cell type-specific manner (Rada-Iglesias et al. 2012). For example, in normal non-proliferative B cells most Myc peaks are located within promoter regions whereas, during progression of the Eu-Myc-driven B-cell lymphoma, a larger percentage of Myc peaks are found in distal elements (Sabò et al. 2014). Since we did not observe any differential expression of Myc in Kras-mutant and wildtype organoids, we hypothesized that in tumor organoids, although Myc levels remained unchanged, Myc could be binding to novel enhancer sites regulating the expression of its target genes. To address this hypothesis, we optimized a chromatin immunoprecipitation (ChIP) protocol for immunoprecipitation of DNA-bound Myc from organoid cultures and performed ChIP-seq experiments comparing Myc occupancy between normal and tumor organoids (Fig.2.3). Ultimately, 1 ng of ChIP DNA was used to prepare Illumina compatible libraries sequenced to ~10-15 million reads. The reads were mapped to the mm10 version of the Mus musculus genome and peaks, i.e. Myc-occupied regions, were called using the MACS software by comparing input samples to IP samples. When all peaks from all four samples were combined, 25% were located within promoter regions, defined as within 2kb of transcription start sites (TSS) (Fig.2.4A). Remarkably, this ratio differed between normal and tumor organoids. Both normal organoid lines had a larger number of peaks at distal elements (<2kb upstream or downstream of transcription start sites (TSS)) compared to promoter

elements (Fig. 2.4A). In both tumor samples, however, peaks were evenly distributed between promoter and distal regions (Fig. 2.4A). One explanation of these results might be that many of the normal distal peaks are peaks with low enrichment, also known as "weak" peaks, that have passed the threshold of detection but are not biologically significant. After comparing the enrichment scores of the promoter and distal peaks, however, we found that the normal and tumor peaks had very similar distributions (Fig. 2.5A). Surprisingly, the distal peaks of the tumor samples were significantly less enriched compared to the promoter ones suggesting that Myc has lower affinity for distal binding sites in tumor organoids. Comparison of the number of reads mapping within 2kb of each peak also revealed that, largely, there are few novel Myc binding sites in any sample but rather sites where Myc binds with higher affinity in tumor organoids compared to normal (Fig.2.4B and C)

We analyzed all samples to identify overlapping peaks present in all samples, which should represent the core, common Myc target sites and thus provide valuable information about the quality of the dataset generated. As expected, the Myc E-box binding motif was identified with high significance in those peaks (Fig.2.6A). Interestingly, 2/3 of the common peaks were located at promoter regions and 1/3 at distal (Fig. 2.6B). As expected, due to the similar levels of total Myc among samples, the overall enrichment of normalized reads did not differ between samples; however, we did identify an enrichment of Myc at the peaks that fall within promoter regions (Fig. 2.6D, E and F). Myc's affinity for distal sites remained similar between the samples at these overlapping peaks (Fig. 2.6D). Gene ontology analysis of the genes in the vicinity (i.e. within 2kb of TSS) of these common Myc binding sites identified canonical Myc-regulated pathways involved in transcription, translation and proliferation (Fig. 2.6G).

To determine the tumor-specific Myc binding sites, we analyzed all peaks that were present in both tumor samples but absent from both normal samples. 841 peaks were unique to the tumor organoids and 75% of these peaks localized to promoter regions (Fig. 2.7A). Surprisingly, despite not being identified as significant peaks by our algorithm, there were still reads mapping to these sites in normal organoids, enriched around the center of the tumor specific peaks (Fig. 2.7B and C). Therefore, most tumor-specific peaks are not novel Myc binding sites but rather sites that Myc occupies with higher affinity in the tumor organoids. To confirm that these novel peaks were not low-affinity Myc binding sites, we compared the fold enrichment of reads mapping to all peaks to those mapping to the novel peaks and did not observe any significant differences (Fig.2.7D). The putative set of genes bound by Myc in a tumor-specific manner were significantly upregulated in tumor cells as revealed by GSEA of RNA-seq performed concomitantly (Fig. 2.8A). The tumor-specific binding sites occurred near genes involved in both previously documented Myc-regulated cellular processes (e.g. promoter opening by PolII) as well as less studied functions of Myc (e.g. telomere maintenance) (Fig. 2.8B).

With similar levels of Myc observed in normal and tumor organoids, one hypothesis to explain the higher affinity binding of Myc in tumor organoids is the existence of a co-factor of Myc that is present or active only in the tumor organoids. Previous studies have reported cooperation between Myc and other transcription factors such as HIF1A and TWIST (Valsesia-Wittmann et al. 2004; Dang et al. 2008). To determine if this putative co-factor is a transcription factor, we analyzed the DNA sequence underlying the tumor-specific peaks for the presence of transcription factor binding motifs. As expected the most commonly identified and centrally located motif was the E-box. However, we also identified the Stat1 and Spdef binding motifs to be significantly enriched proximal to the E-box motif suggesting that these

two TFs might be cooperating with Myc in pancreatic cancer cells to alter Myc's function (Fig. 2.9A).

Phosphorylation of Stat1 leads to its nuclear translocation where it regulates the expression of multiple genes involved in antimicrobial activities, cell proliferation and cell death (Meissl et al. 2017). Interferon signaling leads to phosphorylation of residue Y701 of Stat1 by Jak1 while PDGFR/MAPK activation through Erk1 causes phosphorylation of S727. WB analysis for both of these phospho residues as well as for total levels of Stat1 revealed that Stat1 is downregulated in tumor organoids suggesting that Stat1 is either a negative regulator of, or not important for, the expression of Myc-regulated genes (Fig. 2.9B). On the other hand, the ETS transcription factor Spdef, is significantly upregulated in tumor organoids. Spdef has previously been implicated as an oncogenic driver in breast cancer so we decided to investigate its role in cooperating with c-Myc further (Fig. 2.9C).

2.3. A model of cooperation between Myc and Spdef to control target gene expression

We hypothesized that if a direct interaction between Myc and Spdef existed, it could be supported by analyzing the RNA-seq data. We would expect to find the Spdef binding motif proximal to the center of each Myc peak, either in an upstream or downstream fashion, with an adjacent gap accounting for the physical occlusion of the Ebox by Myc. By plotting a histogram of the frequency of occurrence of the Spdef motif relative to the center of each Myc peak, we observed a symmetrical enrichment of the Spdef motif approximately 18bp in either direction (Fig. 2.10A). We also analyzed the absolute distance of each Ebox motif from the nearest Spdef motif and found a peculiar periodicity of ~16-18bp. These results increase confidence that Spdef and Myc might interact directly in tumor cells (Fig. 2.10B).

To confirm the direct interaction between Myc and Spdef, we cloned and stably co-expressed a cDNA for each gene in a an organoid-derived KPC line (mT10-2D) using a retroviral vector. Due to an unavailability of an Spdef antibody at that time, we fused peptide tags to each protein for ease of detection (a Flag tag for Myc and an HA-tag for Spdef). Co-immunoprecipitation of each tag revealed that the exogenously expressed Spdef-HA and Myc-Flag could, indeed, interact under these conditions and we were able to reproduce this experiment using bead-conjugated antibodies (Fig. 2.11A and B). However, when we performed this experiment using antibodies against the endogenous Myc and Spdef proteins we were unable to replicate these results. The enrichment for Spdef compared to input was minimal suggesting that the antibody for the endogenous Spdef protein might bind with low affinity. Alternatively, the ectopic overexpression of these two proteins created an artificial environment that allowed them to co-precipitate.

2.4. dMax is a naturally occurring isoform of Max and can be exploited to inhibit Myc activity

The DNA binding activity of Myc as a monomer is relatively weak[30]. Its activity is dependent upon its transactivation via the formation of a heterodimeric complex with Max. An alternatively spliced version of Max exists, termed dMax, in which exon 3 is excluded from the final mature Max mRNA (Arsura et al. 1995) (Fig 2.12A). dMax can still bind to MYC and form the heterodimer but lacks the DNA binding domain thus abrogating the transactivation activity of Myc *in vitro (*Fig. 2.12B). Importantly, the expression of this isoform has been detected in a number of tissues but its physiological role has not been fully elucidated.

We hypothesized that dMax is involved in normal tissue homeostasis and acts as a tumor suppressor to repress oncogenic Myc activity. We first wanted to evaluate the potential role of a splice variant of Max (dMax) as a dominant negative regulator of Myc. We hypothesized that Myc's function could be inhibited in normal cells by high expression of dMax while in neoplastic cells, dMax levels are reduced which leads to activation of Myc. To confirm that this splice isoform is indeed expressed in the pancreatic organoids we designed SybrGreen RT-qPCR primers for both the splice variant and the full-length mRNA of Max. qPCR results showed that the dMax transcript is expressed in both normal and tumor organoids but did not detect any difference in the expression levels (Fig. 2.13A). Unfortunately, the antibodies used in the original paper characterized dMax are no longer available and we were unable to confirm these results at the protein levels using two commercially available antibodies.

Induction of splice-switching oligonucleotide (SSO) technology to promote dMax expression could be exploited as therapeutic approach to target Myc. The SSO technology relies on masking a splice site or an exon-internal exonic splicing enhancer (ESE) in the pre-mRNA (Kole et al. 2012). This prevents the proper assembly of the spliceosome on the exon and redirects splicing to another pathway, inducing skipping of the targeted exon. These oligos, upon chemical modifications, can be delivered to the patient and have already shown promising results for the systemic treatment of Duchenne muscular dystrophy and SMA (Finkel et al. 2017). Accordingly, we wanted to investigate the dominant negative effects of dMax on Myc function and its potential as a therapeutic tool. We expressed either dMax or WT Max fused to a flag tag using a TetON doxycycline-inducible retroviral system in a 2D KPC cell line. We confirmed that the cDNAs were expressed (Fig. 2.13B) and translated into stable proteins (Fig. 2.13C). At the protein level, both dMax-Flag and WT Max-Flag were

expressed at levels similar to those of endogenous Max. To investigate the effect of ectopic dMax overexpression on the proliferation of KPC 2D lines, we monitored their proliferation by CellTiterGlo in the presence of doxycycline and, thus, continuous induction of either WT Max, dMax, or an empty control vector. We did not observe a significant difference in the proliferation of any of the aforementioned cell lines (Fig. 2.13D). This experimental approach does not model use of an SSO because endogenous full-length Max mRNA is still expressed in the cells expressing dMax ectopically. To circumvent this issue, we designed five shRNAs targeting Max at the 5′ UTR region, which was absent from the cloned cDNAs, to ensure that only the endogenous Max was being silenced. We achieved ~50% knockdown of both endogenous WT and dMax mRNA (Fig. 2.13E). To assess the effects of ectopic dMax on Myc's transcriptional activity, we analyzed the expression of canonical Myc target genes (Bcat1, Hmga1, Ccnb1, Ccnd2) in KPC cells upon either dMax expression, endogenous Max knockdown, or simultaneous dMax expression and endogenous Max knockdown. Surprisingly, dMax overexpression alone or Max knockdown alone led to an induction in Myc and the majority of its target genes (Fig. 2.13F). However, when the two conditions were combined, modeling the splice switching approach, we observed a significant reduction in the expression of the majority of Myc target genes suggesting that dMax could act as a Myc antagonist in our system (Fig. 2.13G).

2.5 Discussion and future experiments

Previous efforts to understand Myc's oncogenic function have suffered from the lack of appropriate models for the comparison of cancer and normal cells. Most of those studies relied on comparing either different tissues (e.g. normal fibroblasts to cancer cells), cells with different proliferation rates (before and after serum stimulation), or used models of oncogenic

Myc activation that led to an extreme overexpression (e.g. >1000-fold increased levels) of Myc. To our knowledge, our data reveals the first comparison of Myc's activity between normal proliferating pancreatic ductal and cancer cells. Our results showed that, in tumor cells, Myc is significantly enriched at >800 sites, which correlates with increased expression of nearby genes. In addition, we propose a model of cooperation between Myc and the pioneer ETS factor Spdef that occurs early in tumorigenesis.

The cooperation between oncogenic Ras and Myc has been explored previously. The current model posits that Ras signaling affects Myc by two basic mechanisms: Pi3k inhibits phosphorylation of Myc at T58, which blocks its proteolysis by the ubiquitin proteasome system, while activated Erk phosphorylates Myc at S62, which increases its stability. It was surprising that steady-state Myc protein levels did not change significantly in PanIN or tumor organoids despite the presence of an endogenous $Kras^{G12D}$ mutation. A plausible explanation is that our organoid cultures provide more physiologically relevant growth conditions that do not rely on serum supplementation and therefore limit the hyperactivation of Myc. Alternatively, presence of EGF in the media may stimulate high levels of PI3K/MAPK signaling that leads to high levels of Myc even in the proliferating normal cells. It is also important to note that in previous studies co-expression of Myc and Ras led to significant increase in cell proliferation and that our normal and PanIN/Tumor organoid cultures do not exhibit differences in proliferation. Importantly, our results suggest that despite similar steady-state levels, Myc is indeed more active in the tumor organoids suggesting that deregulation of its expression might be even more important than mere accumulation of Myc protein.

It has been previously shown that, in normal quiescent B cells, Myc is expressed at very low levels and occupies mostly promoter regions whereas in the mouse model of B cell

lymphoma, the high levels of Myc driven by the Eu promoter lead to saturation of Myc at those promoters and invasion of distal elements (Sabò et al. 2014). Our results, however, suggest that in normal pancreatic organoids, the majority of Myc peaks are located at distal sites while in Tumor organoids Myc peaks are evenly split between promoter and distal sequences. Remarkably, while there is no difference in the enrichment of reads between distal and promoter peaks in normal organoids, Myc is recruited at higher levels at promoter peaks than for distal peaks in Tumor organoids. In addition, the majority of tumor-specific peaks identified by the algorithm are located at promoters. These results suggest that in tumor organoids, Myc is recruited better to promoters which explains the increased expression of genes proximal to these promoter peaks which has been shown previously (Sabò et al. 2014). The role of Myc at these distal sites in both normal and tumor organoids remains poorly understood and future elucidation of the functional consequences of the depletion of Myc from distal sites in Normal versus Tumor organoids will be important.

Our results also suggest that despite being called as tumor-specific peaks by our algorithm, most of the novel Myc binding sites are also occupied by Myc in Normal organoids, albeit at much lower levels. It is important to keep into consideration the averaged, population-based nature of ChIP-seq experiments: the differences that we observe, most likely, reflect the heterogeneity of Myc occupancy within the sampled cell population. Therefore, our results suggest that Myc is recruited to those tumor-specific sites in a higher proportion of tumor organoid cells.

As an opportunistic transcription factor, Myc has previously been shown to cooperate with pioneer transcription factors such as Foxr2 (Lo et al. 2017). The ETS family of transcription factors are known to be important effectors of mutant Kras signaling (Wasylyk et al. 1998) and members of this family (e.g. TCF) can interact with other bHLH-containin

transcription factors (Stinson 2003). Our results show that the binding motif of the ETS transcription factor Spdef is enriched around the Ebox motif in tumor-specific peaks and that Myc and Spdef can interact in cells when expressed ectopically. Spdef is very lowly expressed in normal organoids and its expression increases throughout the progression of PDAC with it peaking in tumor organoids. Two different models could explain how Spdef recruits Myc to tumor-specific sites. As a pioneer transcription factor, Spdef could function to convert facultative heterochromatin into an accessible state that would allow subsequent binding by the Myc/Max dimer. Alternatively, direct recruitment by Spdef might explain the occupancy of Myc at those sites in a tumor-specific manner, only when Spdef is highly expressed. Remarkably, shRNA-mediated depletion of Spdef in tumor organoids did not lead to a significant change in the expression of genes associated with the tumor-specific peaks (genes shown in Chapter 2.3). These results support the former model of Spdef affecting chromatin accessibility and thus being dispensable after any changes in chromatin state have been made. Further experiments to analyze the chromatin dynamics of these loci in normal, PanIN and tumor organoids could help elucidate the mechanism of Spdef-mediated Myc activity. In addition, analysis of Myc occupancy following ectopic expression of Spdef in PanIN or normal organoids would allow us to determine whether Spdef is sufficient for the recruitment of Myc to those tumor-enriched peaks.

As a central node on which multiple oncogenic pathways converge, Myc is a coveted therapeutic target. Encouraged by examples in the literature of rapid and sustained tumor regression following Myc inhibition (Soucek et al. 2008; Sodir et al. 2011; Soucek et al. 2013) and the success of oligonucleotide therapies in clinical trials (Finkel et al. 2017), we proposed the use of SSOs inducing dMax as a therapeutic strategy against Myc. Our preliminary results show that modeling splice-switching by depleting endogenous Max mRNA and expressing

dMax cDNA leads to a reduction in the expression of canonical Myc target genes. Unfortunately, due to time constraints, we did not investigate this further but our preliminary results warrant a more thorough investigation of the potential for using SSOs that induce dMax and thus Myc inhibition.

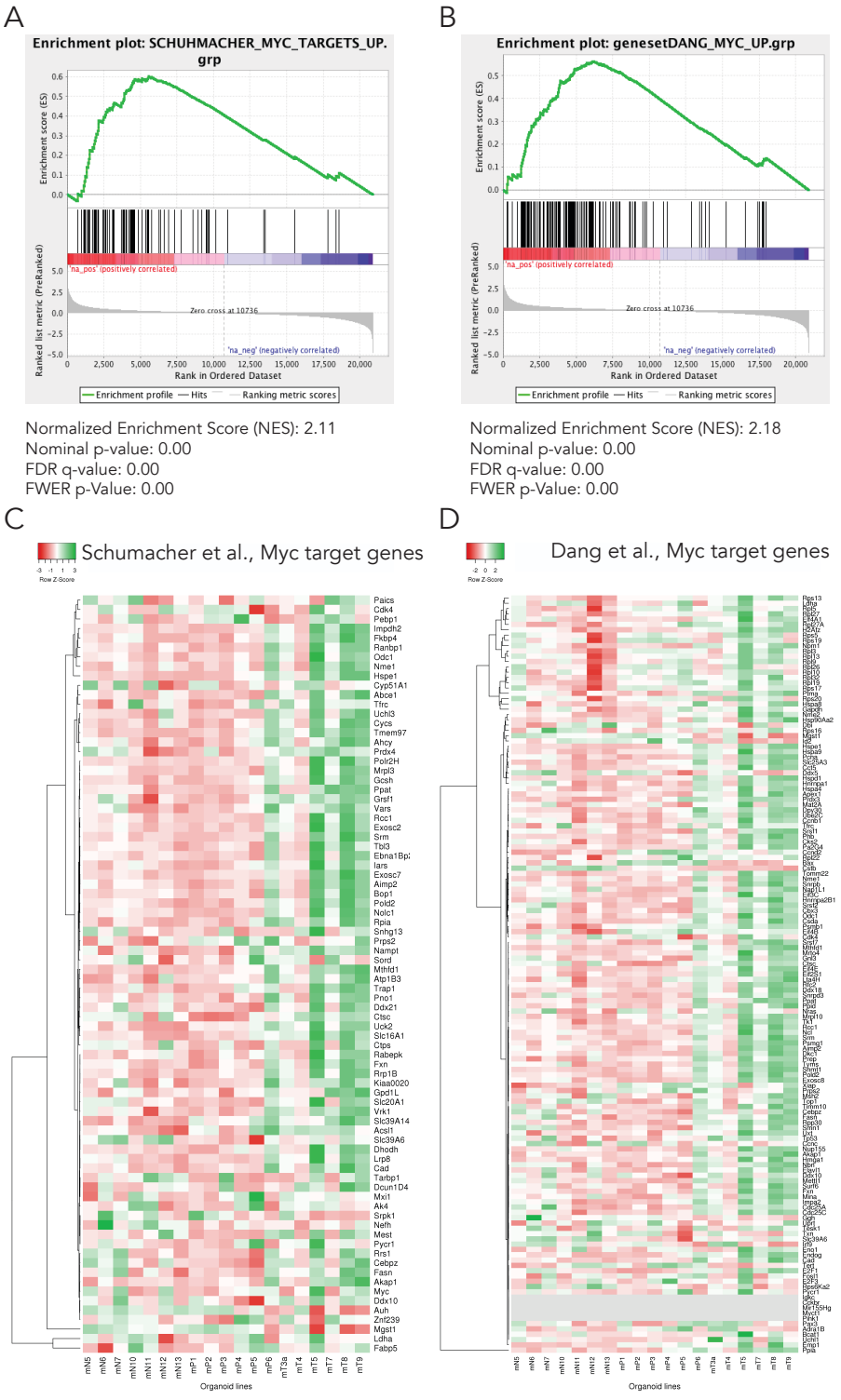

Figure 2.1 Myc's transcriptional program is activated in tumor organoids
A) and B) Gene Set Enrichment Analysis (GSEA) of Tumor versus Normal RNA-seq from Boj et al., 2015 for 2 published Myc target gene sets (Schuhmacher et al 2001; Zeller et al 2003).
C) and D) Heatmap plot of the normalized expression for genes from the pathways in A and B of 7 Normal, 6 PanIN and 6 Tumor organoid lines as calculated by DESeq2.

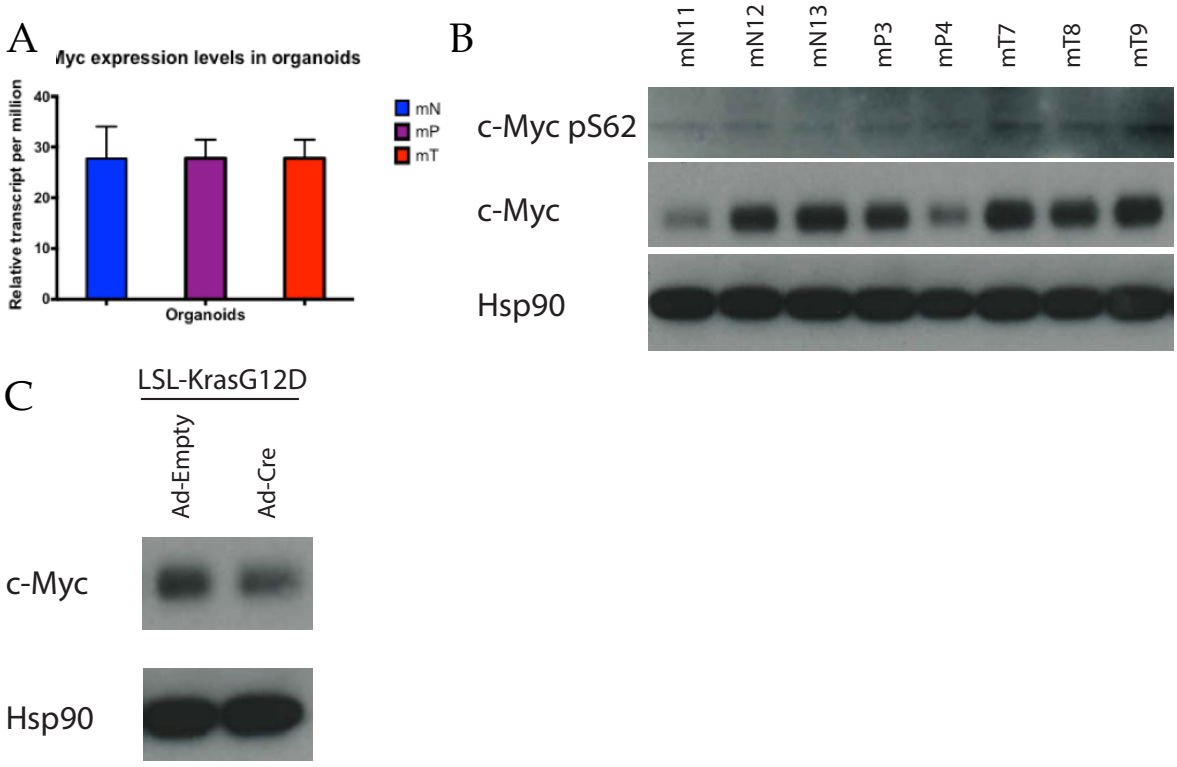

Figure 2.2 Myc expression does not change significantly in organoid model of murine PDAC progression

A) Normalized RNA-seq expression of Myc averaged across 7 Normal, 6 PanIN and 6 Tumor organoid lines as calculated by DESeq2
B) WB analysis of pS62, total c-Myc and Hsp90 (loading control) in 3 normal, 2 PanIN and 3 tumor organoid lines.
C) WB analysis for c-Myc following acute activation of $Kras^{G12D}$ in LSL-KrasG12D organoids

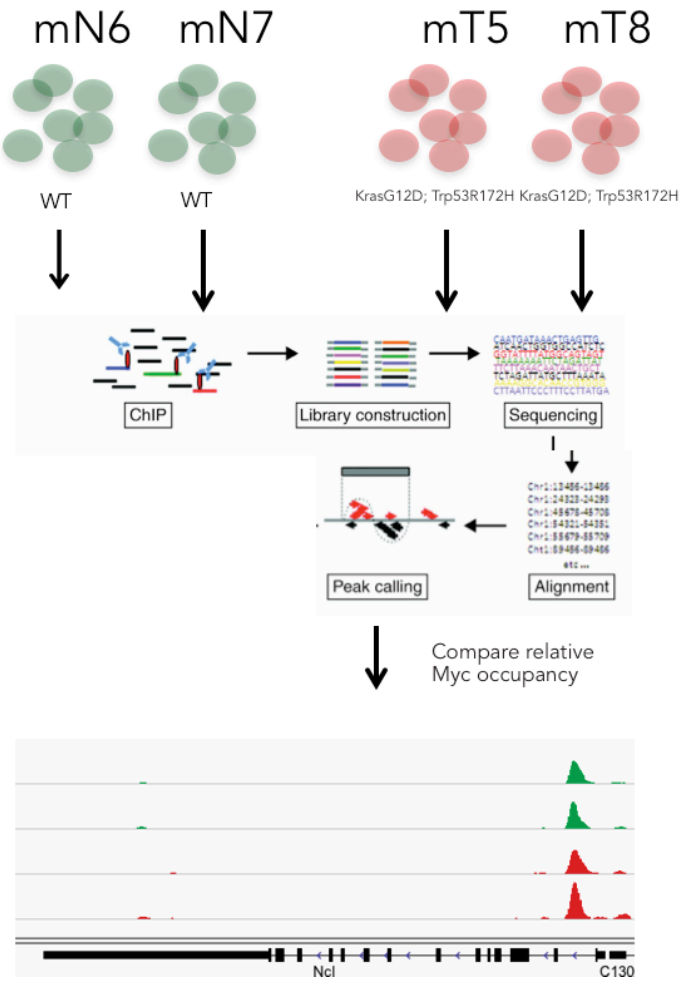

Figure 2.3 Worklfow of ChIP-seq experiment. Two normal and tumor organoids were cross-linked and ChIP was performed using a polyclonal anti-Myc antibody. Immunoprecipitated DNA was used for library construction followed by next-generation Illumina sequencing. Reads were aligned to the genome and peaks were called using the MACS2 algorithm..

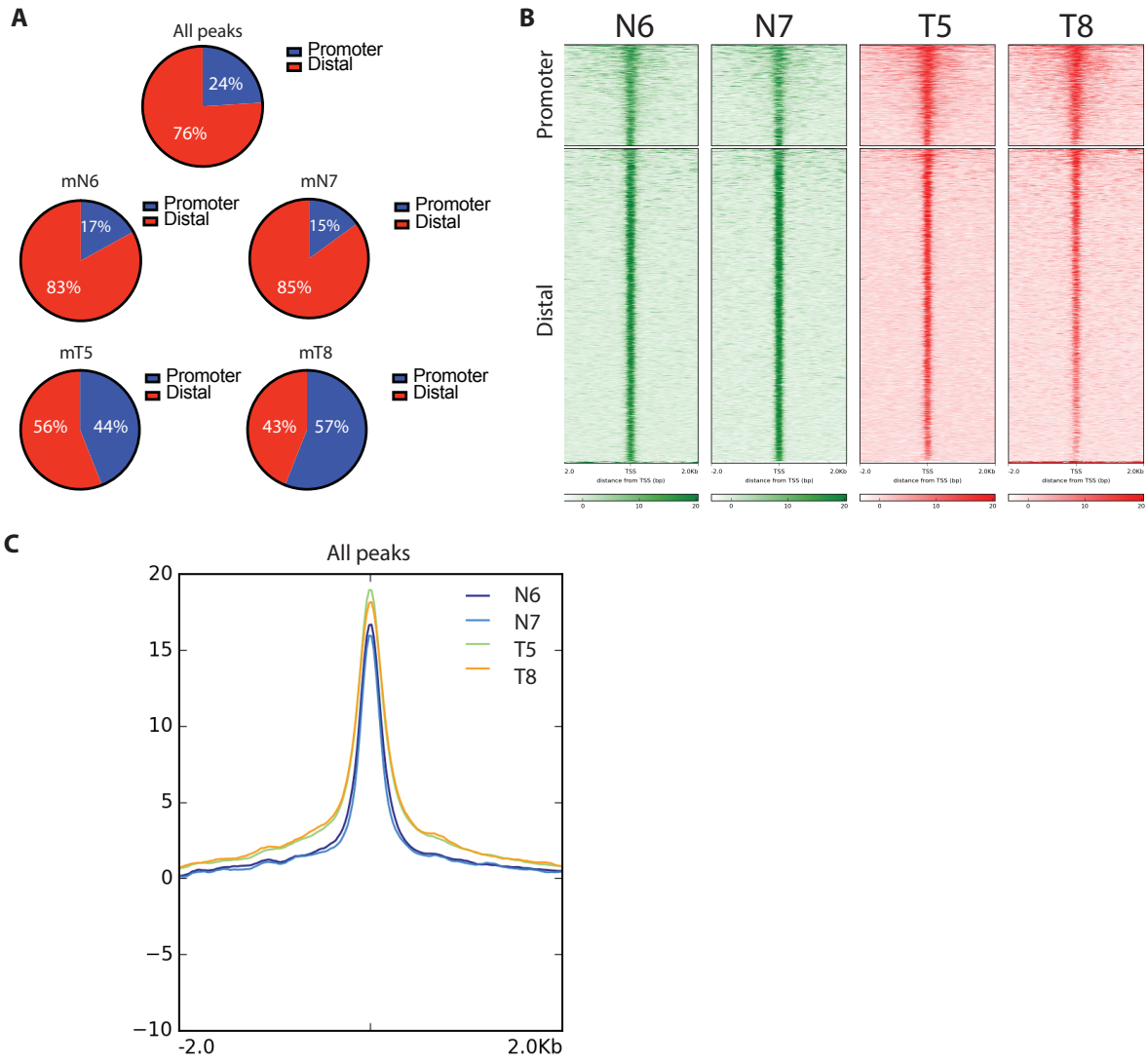

Figure 2.4. Promoter and distal distribution of all peaks from Myc ChIP-seq experiments
A) Distribution of Myc peaks in promoter (+/-2kb of TSS) and distal sites of murine normal (N6 and N7) and tumor (T5 and T8) organoids.
B) Density plot of Myc ChIP-seq datasets in murine normal (N6 and N7) and tumor (T5 and T8) organoids. Data is centered on 5,135 high-confidence Myc-occupied elements. Each row represents a 4-kilobase interval surrounding a single peak.
C) ChIP-seq meta-profiles comparing Myc occupancy at all peaks identified in murine normal (N6 and N7) and tumor (T5 and T8) organoids.

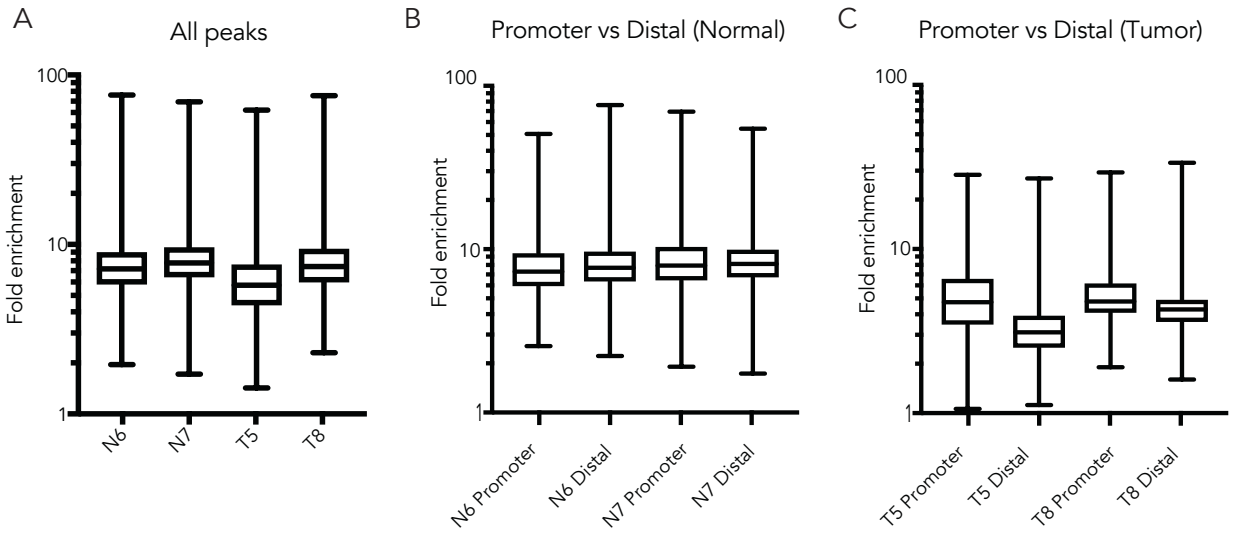

Figure 2.5 Comparison of enrichment between Myc peaks.

A) Box-plot of the normalized Myc enrichment of all peaks in murine normal (N6 and N7) and tumor (T5 and T8) organoids.

B) Box-plot of the normalized Myc enrichment of promoter and distal peaks within normal (N6 and N7) organoids

C) Box-plot of the normalized Myc enrichment of promoter and distal peaks within tumor (T5 and T8) organoids

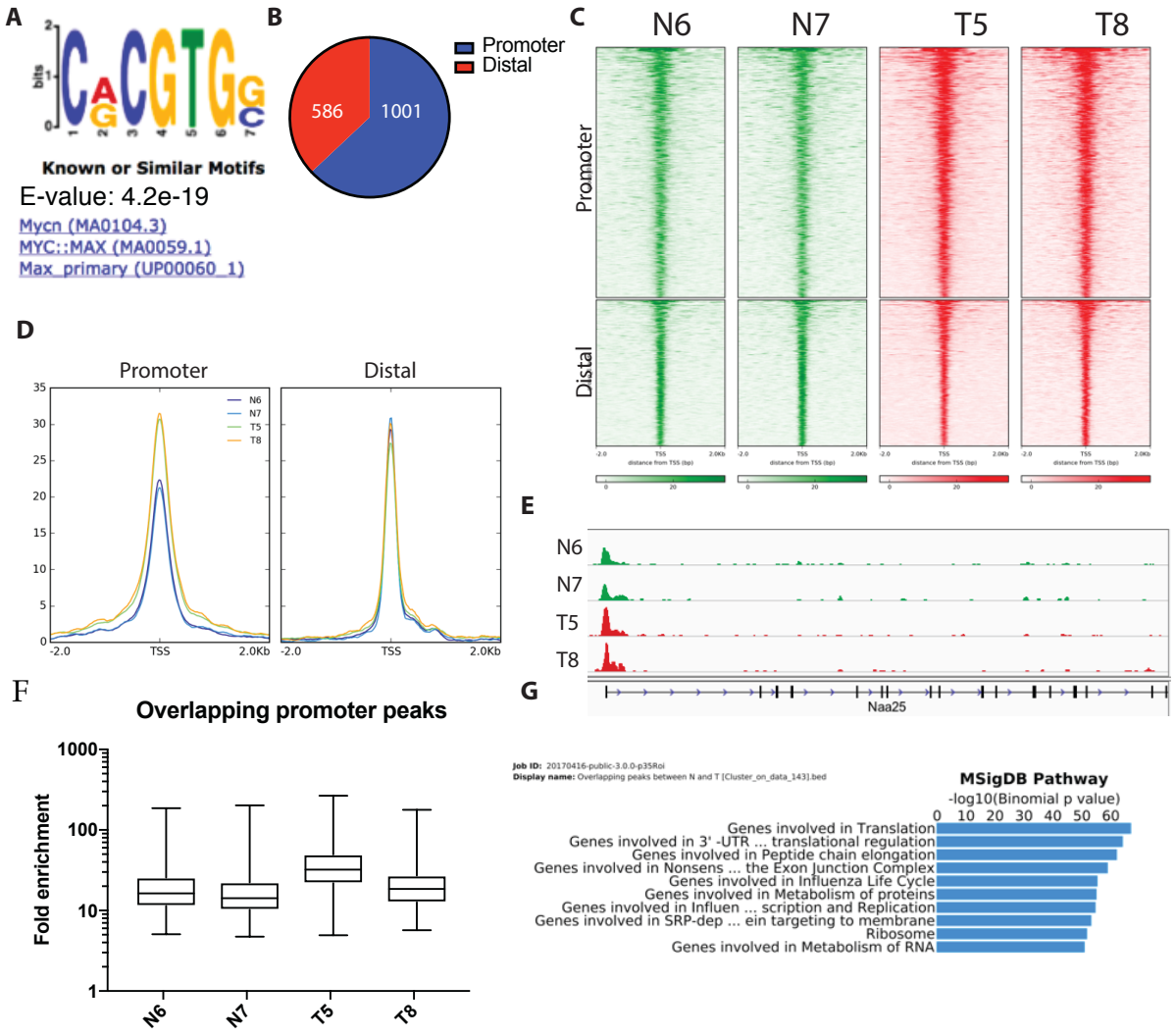

Figure 2.6 Evaluation of overlapping Myc peaks (peaks that were identified in all 4 samples) between normal and tumor organoids

A) MEME ChIP-seq motif analysis of overlapping peaks.
B) Distribution of overlapping peaks Myc peaks in promoter (+/-2kb of TSS) and distal sites
C) Density plot of Myc ChIP-seq datasets in murine normal (N6 and N7) and tumor (T5 and T8) organoids. Data is centered on all overlapping Myc peaks. Each row represents a 4-kilobase interval surrounding a single peak.
D) ChIP-seq meta-profiles comparing Myc occupancy at overlapping peaks between normal (N6 and N7) and tumor (T5 and T8) organoids at promoter or distal elements
E) Example of a ChIP-seq occupancy profile for Myc at the promoter of Naa25
F) Box-plot of the normalized Myc enrichment at overlapping peaks in murine normal (N6 and N7) and tumor (T5 and T8) organoids
G) Gene ontology terms from GREAT analysis of genes proximal to overlapping peaks

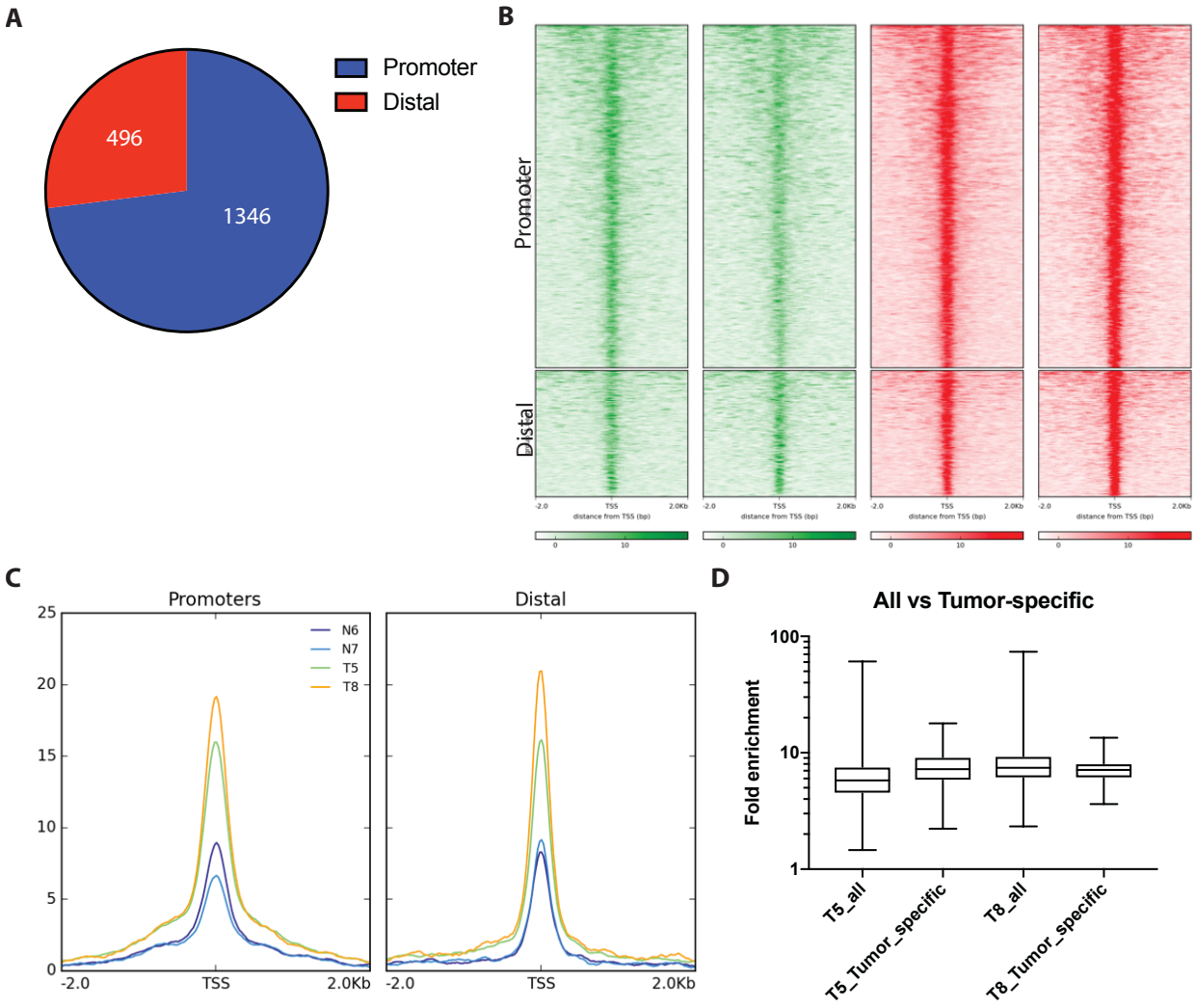

Figure 2.7 Analysis of tumor-specific Myc peaks

A) Distribution of tumor-specific Myc peaks in promoter (+/-2kb of TSS) and distal sites
B) Density plot of Myc ChIP-seq datasets in murine normal (N6 and N7) and tumor (T5 and T8) organoids. Data is centered on all tumor-specific Myc peaks. Each row represents a 4-kilobase interval surrounding a single peak.
C) ChIP-seq meta-profiles comparing Myc occupancy at tumor-speicifc peaks between normal (N6 and N7) and tumor (T5 and T8) organoids at promoter or distal elements
D) Example of a ChIP-seq occupancy profile for Myc at the promoter of Naa25
E) Box-plot comparing the normalized Myc enrichment at tumor-specific peaks versus all peaks in tumor (T5 and T8) organoids

A

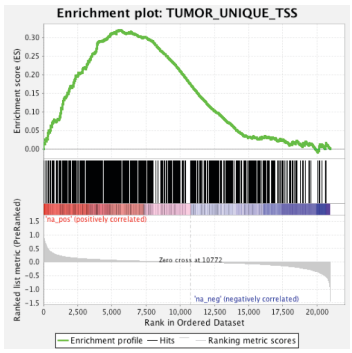

Normalized Enrichment Score (NES): 1.43
Nominal p-value: 0.00
FDR q-value: 0.00
FWER p-Value: 0.00

B

Gene Set Name	# Genes in Gene Set (K)	# Genes in Overlap (k)	k/K	p-value	FDR q-value
MARSON_BOUND_BY_E2F4_UNSTIMULATED	728	12	0.0165	8.42E-11	3.70E-07
REACTOME_RNA_POL_I_PROMOTER_OPENING	62	6	0.0968	1.62E-10	3.70E-07
MARSON_BOUND_BY_FOXP3_UNSTIMULATED	1229	14	0.0114	2.34E-10	3.70E-07
KEGG_SYSTEMIC_LUPUS_ERYTHEMATOSUS	140	7	0.05	4.87E-10	5.76E-07
WANG_RESPONSE_TO_GSK3_INHIBITOR_SB216763_DN	374	9	0.0241	9.07E-10	6.58E-07
KOBAYASHI_EGFR_SIGNALING_24HR_DN	251	8	0.0319	9.29E-10	6.58E-07
REACTOME_AMYLOIDS	83	6	0.0723	9.73E-10	6.58E-07
REACTOME_MEIOTIC_RECOMBINATION	86	6	0.0698	1.21E-09	7.15E-07
REACTOME_RNA_POL_I_TRANSCRIPTION	89	6	0.0674	1.49E-09	7.83E-07
FUJII_YBX1_TARGETS_DN	202	7	0.0347	6.27E-09	2.97E-06
REACTOME_MEIOSIS	116	6	0.0517	7.41E-09	3.19E-06
REACTOME_RNA_POL_I_RNA_POL_III_AND_MITOCHONDRIAL_TRANSCRIPTION	122	6	0.0492	1.00E-08	3.68E-06
LEE_BMP2_TARGETS_DN	882	11	0.0125	1.01E-08	3.68E-06
REACTOME_TELOMERE_MAINTENANCE	75	5	0.0667	3.96E-08	1.34E-05
REACTOME_CELL_CYCLE	421	8	0.019	5.18E-08	1.62E-05
ZHANG_TLX_TARGETS_60HR_DN	277	7	0.0253	5.48E-08	1.62E-05
MUELLER_PLURINET	299	7	0.0234	9.21E-08	2.54E-05
DANG_BOUND_BY_MYC	1103	11	0.01	9.74E-08	2.54E-05
SARRIO_EPITHELIAL_MESENCHYMAL_TRANSITION_UP	180	6	0.0333	1.02E-07	2.54E-05
HORIUCHI_WTAP_TARGETS_DN	310	7	0.0226	1.18E-07	2.78E-05

Figure 2.8 Analysis of pathways that genes in the vicinity of tumor-specific Myc peaks belong to
A) GSEA of RNA-seq data of normal and tumor organoids for a geneset composed of genes proximal to tumor-specific Myc peaks
B) Gene ontology terms from GREAT analysis of genes proximal to tumor-specific peaks

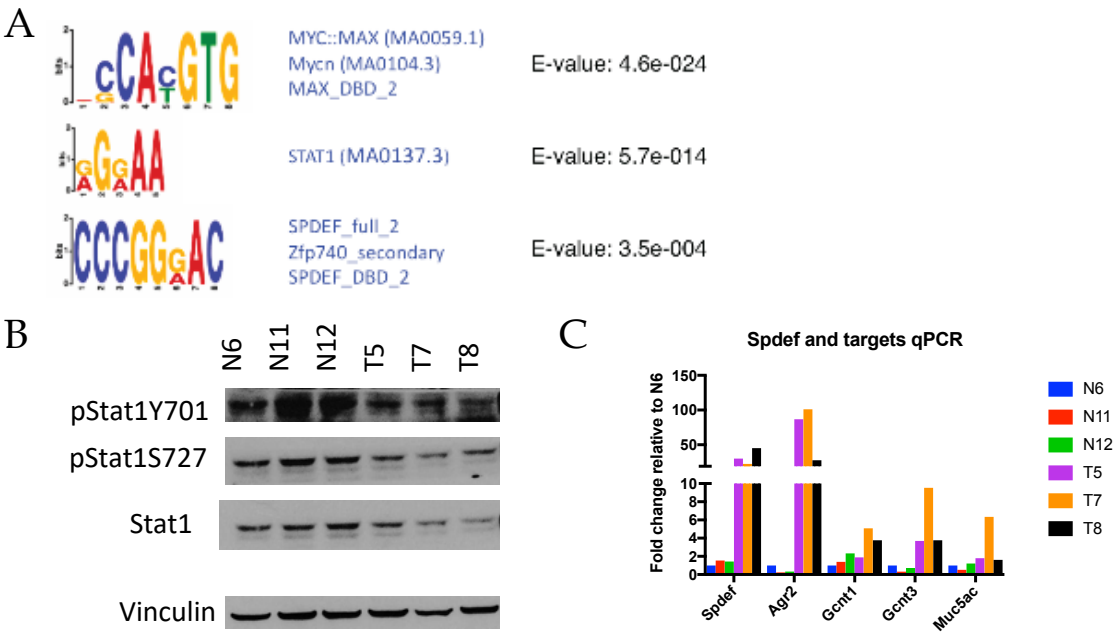

Figure 2.9. Putative co-operators of Myc in tumor organoids

A) MEME ChIP-seq analysis of transcription factor motifs enriched within a 200bp interval surrounding the summit of each tumor-specific Myc peak.

B) WB analysis of normal and tumor organoids for total Stat1 and pY701 and pS727.

C) RT-qPCR of normal and tumor organoid for Spdef, Agr2, Gcnt1, Gcnt3 and Muc5ac

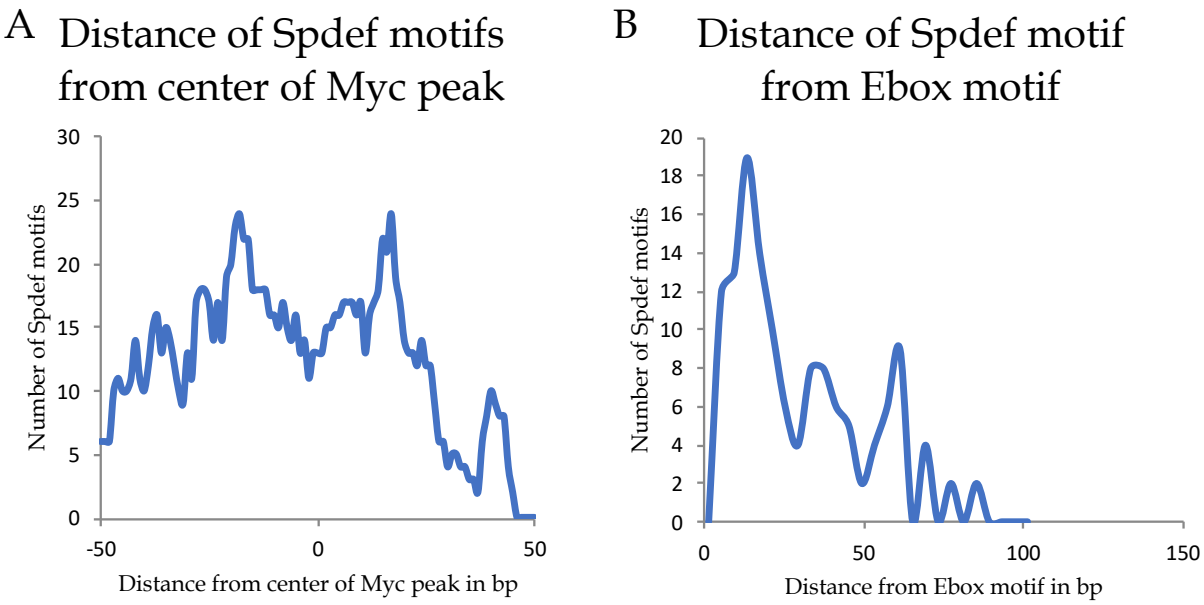

Figure 2.10 Distance of Spdef motif from Myc peaks and Ebox motif in tumor-specific peaks

A) Histogram of the abundance of Spdef motifs plotted against the distance from the center of each Myc tumor-specific peak

B) Histogram of the abundance of Spdef motifs plotted against the distance from E-box motifs in each tumor-specific peak

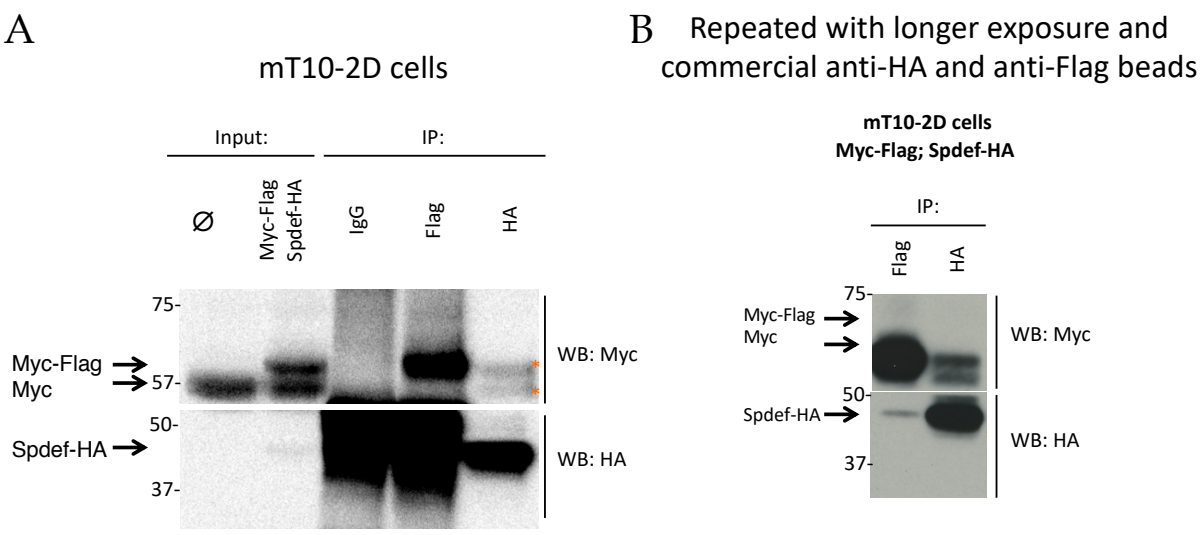

Figure 2.11 Ectopically expressed Myc and Spdef co-immunoprecipitate

A) Co-IP of ectopically expressed Myc-Flag and Spdef-HA in a murine PDAC 2D cell line

B) Co-IP of ectopically expressed Myc-Flag and Spdef-HA in a murine PDAC 2D cell line using commercially conjugated anti-Flag and anti-HA magnetic beads

A

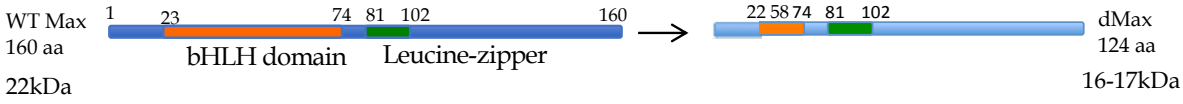

B

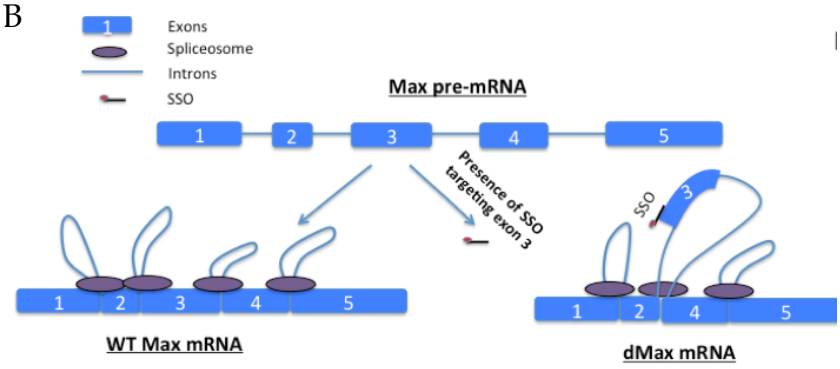

Figure 2.12 Schematic of dMax and SSOs.
A) Schematic of full length Max and dMax proteins
B) Alternative splicing diagram of Max pre-mRNA to full length Max and dMax.

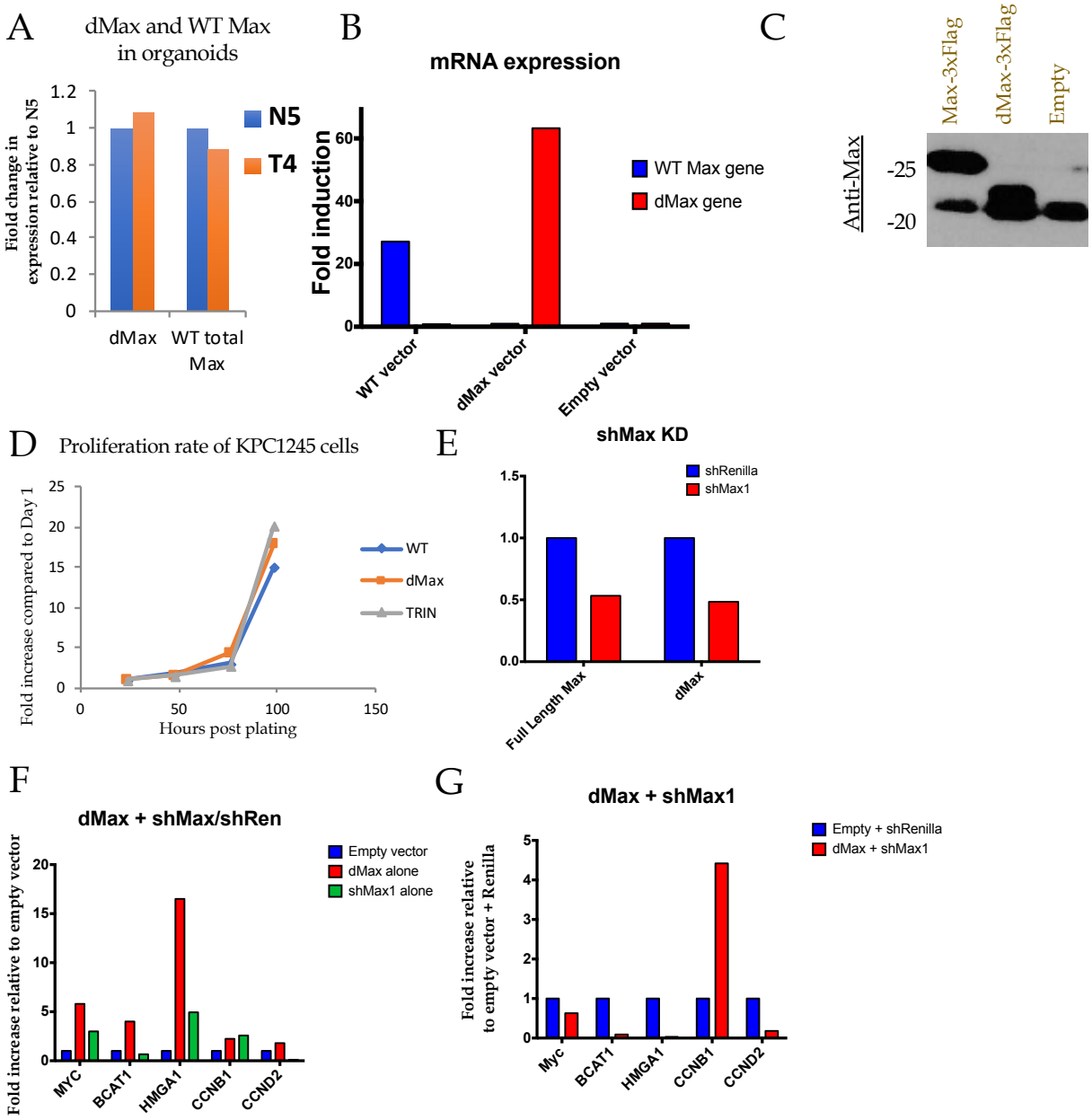

Figure 2.13 Evaluation of antagonistic effects dMax on Myc in pancreatic cancer cells

A) RT-qPCR for full-length Max (WT) and dMax in normal and tumor organoids
B) RT-qPCR for full-length Max and dMax in cells expressing ectopically either full-length Max cDNA or dMax
C) WB analysis for Max in cells expressing ectopically either full-length Max cDNA or dMax
D) CellTiterGlo proliferation assay for KPC1242 2D cells lines expressing either full-length Max, dMax or empty vector control (TRIN). Relative luminescence was normalized to Day 1 and measured every 24 hours for 4 days.
E) RT-qPCR for full-length Max and dMax in cells expressing shRNA hairpins against Max or a Renilla control
F) RT-qPCR for Myc target genes in cells expressing dMax, shMax1 or empty vector.
G) RT-qPCR for Myc target genes in cells expressing dMax and shMax1 compared to cells expressing an empty vector control and shRenilla (control)

Chapter 3. Spdef expression correlates with progression of pancreatic cancer

3.1 Introduction

The ETS family of transcription factors (TFs) includes 28 different proteins that play various roles in development (Maroulakou and Bowe 2000). Some are ubiquitously expressed, while others are expressed in a tissue- and cell type-specific manner (Hollenhorst et al. 2011b). All members of the family share the highly conserved ETS DNA binding domain that recognizes an invariable CCGA/T core flanked by 3-4 less conserved nucleotides (Hollenhorst et al. 2011b). In addition, some members contain a pointed domain (PNT) that has been shown to be involved in protein-protein and protein-RNA interactions and could serve as a docking site for ERK2 to elicit specific responses downstream of the RAS/MAPK pathway (Seidel 2002). The activity of ETS factors is most commonly regulated transcriptionally or by post-translational modifications affecting the total protein levels inside the cell. Based on their homology ETS factors can be grouped into four classes with class IV comprising a single gene, Spdef, due to differences in its DNA binding and PNT domain sequences (Hollenhorst et al. 2011b).

While, for example, the Ets1 and Ets2 TFs are expressed ubiquitously in all cell types, Spdef's expression is restricted to epithelial cells and has been shown to be essential for the maturation of the mucus-secreting Goblet cells in the lung and other epithelial tissues (Gregorieff et al. 2009; Hollenhorst et al. 2011b). GenePaint is an online database that provides spatial *in situ* RNA hybridization information on multiple mammalian genes (Visel 2004). E14.5 represents the single time point covered by GenePaint for whole embryo analysis, which is highly useful as a first-level screen because, at this the timepoint, the developing pancreas contains a large number of pancreatic progenitor cells, some differentiated exocrine

and endocrine cells, and a significant portion of pancreatic mesenchymal tissue. We analyzed *in situ* hybridization data available from GenePaint and found co-expression of Spdef with the pancreas-specific Pdx1 transcription factor suggesting that Spdef is expressed the embryonic development of the exocrine pancreas in mice, which was also reported by Kobberup et al. (Fig. 3.2B) (Kobberup et al. 2007). Remarkably, in the organoid model of pancreatic cancer development, Spdef is one of the top overexpressed genes in tumor cells when compared to normal (Fig. 3.2C). Out of all ETS transcription factors, Spdef is the only one that is overexpressed in tumor organoids (Fig. 3.2D and E). In this study, we sought to further investigate the induction and regulation of Spdef expression in PDAC.

3.2 Development and validation of polyclonal antibodies against Spdef

Since we had previously identified Spdef as a highly upregulated gene in tumor organoids, we first sought to determine the level of Spdef protein in pancreatic epithelial cells during the progression of PDAC. Due to the unavailability of specific antibodies against Spdef, we generated polyclonal rabbit antibodies against murine Spdef with Thermo Fisher. Based on hydrophobicity, hydrophilicity, and specificity scores obtained from a proprietary Thermo Fisher algorithm and the NIH AbDesigner tool (https://hpcwebapps.cit.nih.gov/AbDesigner/), we selected two peptides (spanning amino acids 33-50 and 75-91) of the mouse Spdef protein to use as antigens (Figure 3.2A). Each peptide was used to immunize two rabbits. This was followed by three subsequent boosts (day 14, 42 and 56) and bleeds were collected 72 days following initial immunization. The isolated antibodies were affinity purified using the immunizing peptide. Pre-immune sera were tested on lysates from cells with varying levels of expression of Spdef: normal organoids (with no detectable Spdef transcripts by RNA-seq), tumor organoids, and Rosa and Spdef

knockout tumor organoids generated by CRISPR/Cas9 showing no background activity (Fig. 3.2B). Despite a background band of unknown identity at ~50kDa, the 1161 antibody was the most sensitive antibody with a putative Spdef band at ~37kDa, that was absent from normal organoids and Spdef KO organoids (Fig. 3.2C). The sera from rabbits immunized with the 33-50 region of Spdef reacted with multiple non-specific bands and we are currently awaiting their affinity purification (Fig. 3.2C)

Antigens present on fully linearized and denatured proteins (i.e. those used for WB) will not necessarily be present or accessible on cross-linked partially folded proteins (i.e. those used for IHC/ChIP). To assess whether the 1163 antibody can also be used for chromatin immunoprecipitation, we performed ChIP-qPCR for the previously annotated promoter region of Agr2 containing the Spdef motif. *In silico* motif analysis suggests that an Spdef binding motif is present ~200bp downstream of the Agr2 transcription start site. The 1161 antibody successfully immunoprecipitated Spdef-bound Agr2 promoter DNA with a significant enrichment compared to pre-immune sera (Fig. 3.2D). To validate the 1161 antibody for the detection of endogenous Spdef protein in formalin-fixed and paraffin embedded (FFPE) tissues by immunohistochemistry (IHC), we used sections from a FFPE KPC tumor. Whereas staining was not observed in non-epithelial cells, tumor epithelial cells had strong nuclear staining for Spdef (Fig. 3.2E). These results make the 1161 antibody an indispensable tool to study Spdef, especially after the discontinuation of the only published Spdef antibody used for ChIP (previously distributed by Santa Cruz) .

3.3 Spdef expression is elevated in pancreatic tumors *in vivo* in both the KPC mouse model and PDAC patient samples

Previous analysis by our lab on the expression of Spdef by RNA-seq of a panel of normal, PanIN, tumor and metastatic organoids showed that its expression was marginally induced in PanIN organoids and further increased with tumor progression (Fig. 3.3A). The expression of previously described Spdef target genes including Agr2, Gcnt1, Gcnt3 and Muc5ac, as revealed by RT-qPCR correlated well with Spdef levels suggesting that Spdef's activity increased during PDAC progression (Fig. 3.3B). The upregulation of Spdef and its target genes at the mRNA level in tumor organoids led us to further investigate the regulation of its expression during PDAC progression.

To confirm the observed changes at the protein level, we analyzed four normal, three PanIN, three tumor and three metastatic organoid lines derived from our KPC mouse model for Spdef expression by western blotting using the newly developed antibody. Spdef protein levels correlated well with its mRNA levels. Normal organoids had either undetectable (N6) or barely detectable levels of Spdef (Fig. 3.4A). While Spdef was significantly induced in PanIN organoids, its levels were highest in organoids derived from advanced PDAC tumors (T5, T8, T69a). Metastatic organoids had higher levels of Spdef than normal and PanIN ones, but lower levels when compared to tumor organoids. To confirm that the observed changes in Spdef expression in the organoid model were also present *in vivo*, we evaluated the levels of Spdef by immunohistochemistry in murine PanIN lesions (KC), PDAC (KPC), and diaphragm metastases (KPC). Higher levels of Spdef were observed in early acinar-to-ductal metaplasia lesions as well as throughout the PanIN1-3 stages when compared to morphologically normal ducts in KC mice (Fig. 3.4B). In PDAC lesions of KPC mice, strong nuclear staining for Spdef was observed in most neoplastic epithelial cells while stromal cells were negative for staining. Similarly, in diaphragm metastatic lesions, tumor cells stained positively for Spdef while normal cells were negative. These results confirm that Spdef

expression is induced during the early stages of PDAC development and its levels are maintained even in metastatic lesions.

To confirm that Spdef is also induced in human PDAC, we analyzed its expression by RNA in a large dataset of normal and tumor patient-derived PDAC organoids. Spdef was significantly upregulated in the majority of tumor organoids (Fig. 3.5A; ~3-fold, $p<0.01$). To compare the expression of Spdef between normal and PDAC human specimens, we used an RNA-seq dataset published by the TCGA consortium. Spdef expression was significantly induced in the PDAC samples compared to the normal pancreas (Fig. 3.5B). We confirmed the induction of Spdef at the protein level *in vivo* using a human PDAC tissue microarray comprising FFPE sections from 38 cases of adenocarcinoma, five adjacent normal pancreata and five non-pancreatic normal tissues. IHC staining for Spdef showed strong nuclear staining in tumor epithelial cells when compared to adjacent normal areas consistent with the gene expression data (Fig. 3.5C).

Analysis of Spdef expression across all cancer types included in the TCGA research network database (https://www.cancer.gov/tcga) revealed that PDAC ranked fifth according to Spdef levels (Fig. 3.6A). Recently, Rau et al developed a computational algorithm that analyzes the heterogeneity of expression for a target gene within a subset of cancers to predict the molecular source of variation driving those differences in expression (Rau et al. 2018). Using this software we found that methylation and transcription factor-driven variations of Spdef expression in PDA are more prominent than other cancer types (Fig. 3.6B). To compare the methylation status of the Spdef promoter between normal pancreas and PDAC samples we analyzed bisulphite sequencing data from the TCGA consortium. We observed a small but significant decrease in methylation of a marker within the Spdef

promoter in tumor over normal samples that could partially contribute to the increase in Spdef expression seen in PDAC tumors (Fig. 3.6C).

3.4 Tgfβ inhibition and Wnt signaling are necessary for Spdef expression in organoid cultures

To better understand the relevance and regulation of Spdef's expression *in vivo*, we first sought to understand the signaling pathways that regulate Spdef expression in organoids. Surprisingly, when 2D cell lines derived from tumor organoids were grown in DMEM media supplemented with 10% fetal bovine serum (DMEM/FBS), Spdef expression was downregulated ~100-fold (Fig. 3.7A). To understand whether this change in expression was driven by the media composition or the 3D culture conditions, we grew the same organoid line in 2D or embedded in Matrigel (3D) and cultured them in DMEM/FBS or complete organoid media. We observed that the organoid media induced Spdef expression regardless of the cell culture condition (2D vs 3D) (Fig. 3.7B). The complete media used for maintenance of the organoid cultures contains growth factors (EGF and FGF), Tgfβ pathway inhibitors (A83, mNoggin), Wnt pathway activators (R-spondin), vitamins and supplements (B27, nicotinamide). Spdef's expression is 100-fold upregulated in complete media compared to the basal media media (Advanced DMEM/F12 with glutamine, HEPES and Pen/Strep), which has none of those factors added (Fig. 3.7C). To understand which components of the media are necessary and sufficient for Spdef expression, we either removed individual components from the complete media composition or added them one by one to the basal media. Removal of the Activin receptor-Like Kinase3/5 (Alk3/5) inhibitor A83 reduced Spdef expression to the basal media levels supporting previously published reports that the Tgfβ pathway has been previously reported to inhibit Spdef expression (Fig. 3.7C) (McCauley et

al. 2014). However, the addition of A83 to the basal media had no effect on Spdef expression, suggesting that while A83 relieves the inhibition of Spdef by the TGFβ pathway, additional exogenous activators in our complete media are required to express Spdef. (Fig. 3.7D). In addition, removal of R-spondin, a Wnt agonist, caused a 50% reduction in expression (Fig. 3.7C). The addition of R-spondin alone also had no effect on Spdef's expression (Fig. 3.7D). To test synergies between Tgfβ pathway inhibition and other factors in the complete media, we added each factor individually in the presence of A83. These experiments showed that both R-spondin and nicotinamide synergize with A83 to induce Spdef levels but neither was sufficient to induce expression levels to that observed in complete media (Fig. 3.7D). Importantly, adding these three factors (A83, Nicotiamide and R-spondin) together led to increased Spdef expression similar to that in complete media suggesting that a convergence of these three pathways is responsible for the regulation of Spdef in organoids.

The TGFβ pathway is commonly inactivated in PDAC tumors by deletion or frameshift mutations in either TGFBR1 or SMAD4. Our lab has previously developed a mouse model to study the cooperation between $Kras^{G12D}$ and Smad4 deletion ($Kras^{LSL\text{-}G12D/+}$; $Smad4^{fl/fl}$; Pdx-Cre). To evaluate the effect of Smad4 deletion on Spdef expression, we compared the levels of Spdef between organoids derived from the KPC model to those derived from the $Smad4^{fl/fl}$ model. Surprisingly, we did not detect a constitutive increase in Spdef expression in the Smad4 deleted organoids when compared to the KPC organoids, which suggests that the Alk inhibitor A83 is sufficient for Tgfβ pathway inhibition in these conditions (Fig. 3.7E).

To confirm the role of the Tgfβ pathway in regulating Spdef expression in PDAC tumors *in vivo*, we analyzed single cell RNA-seq data of KPC tumors. Single cells from three KPC tumors were captured following enzymatic digestion and sequenced using a droplet-

based approach (Senapati et al. 2011a). Density based clustering of the expression data for each cell was used to identify distinct clusters. Signature genes within each cluster were cross-referenced with known markers of cell populations from the literature to identify the different cell types that are represented by the clusters. We focused on the epithelial cell cluster, where we expected to see the highest Spdef expression based on our IHC results. Overall, we found that Spdef expression was relatively low in this population, a feature typical of transcription factors, which could be a caveat with the low coverage of single cell RNA-seq approaches. Based on our IHC results that show Spdef expression in the majority of epithelial cells, we took a binary approach to classify all epithelial cells where Spdef transcript was detected as $Spdef^{high}$ and compare those to epithelial cells where Spdef was not detected, $Spdef^{low}$ (Fig. 3.8B). Differential gene expression analysis revealed that the known Spdef target genes including Agr2, Gkn3, Muc6, Tff2, and Tff3 are higly expressed in the $Spdef^{high}$ cells (Fig. 3.8C), whereas multiple genes (Nefl, Crabp2, Ank, Inhba, Acta2, Serpine1, Gpx8) downstream of the Tgfβ signaling pathway are downregulated in the $Spdef^{high}$ population (Fig. 3.8C). We identified multiple genes downstream of the Tgfβ signaling pathway to be downregulated in the $Spdef^{high}$ population (Nefl, Crabp2, Ank, Inhba, Acta2, Serpine1, Gpx8) (Fig. 3.8C). Gene ontology pathway analysis confirmed this observation and multiple pathways related to Tgfβ signaling and epithelial-to-mesenchymal transition were significantly downregulated in the $Spdef^{high}$ cells. Taken together, our study showed that Tgfβ pathway inhibition is necessary for high Spdef expression (Fig. 3.8D).

3.5 Mutant Kras is necessary but not sufficient for Spdef expression.

Mutant Kras has previously been shown to activate Wnt signaling and canonical Wnt signaling is required for Kras-induced pancreatic cancer. Moreover, it has been shown that

mutant Kras signaling can suppress TGFβ signaling *in vitro*. In addition, PDAC-associated fibroblasts express high levels of Rspo1 and are absent from the normal pancreas. Additionally, Spdef expression was induced in Kras-mutant PanIN organoids compared to Kras-wildtype normal organoids, albeit to a lesser degree than was seen in tumor organoids. We hypothesized that oncogenic Kras may regulate Spdef expression directly or indirectly. To test whether mutant Kras is sufficient for the upregulation of Spdef in organoid cultures, we used organoids derived from pancreatic ducts of mice harboring a $Kras^{G12D}$ allele, preceded by an intact Lox-STOP-Lox (LSL) cassette. The LSL cassette encodes a premature stop codon upstream of the mutant Kras allele preventing its expression. Cre-recombinase expression allows for the excision of the LSL cassette and subsequent expression of the mutant Kras allele. Infection of the LSL-$Kras^{G12D}$ organoids with adenovirus encoding the Cre gene therefore leads to acute activation of mutant Kras. RT-qPCR for Spdef in LSL-$Kras^{G12D}$ organoids infected with either an empty vector or Cre did not show a difference in the expression of Spdef following acute $Kras^{G12D}$ activation (Fig. 3.9A).

To assess the necessity of mutant Kras for Spdef expression, we used another model developed in our lab – the FPC model. In this mouse model, *Frt-LSL-KrasG12V* allele was crossed to *LSL-p53R172H, PDX1-Cre and* $Rosa26^{FlpOERT2}$ alleles to generate **F**rt-LSL-$Kras^{G12V}$;LSL-**p**53^{R172H}, PDX1-**C**re;$Rosa26^{FlpOERT2}$ (FPC) mice. We isolated tumor organoids from the FPC model. The FlpO recombinase is fused to the estrogen receptor (ER) ligand binding domain, restricting Flp to an inactive state in the cytoplasm sequestered by heat-shock proteins bound to the ER domain. Upon addition of tamoxifen (Tam) (*in vivo*) or 4-hydroxytamoxifen (4-HT) (*in vitro*), FlpO recombinase translocates into the nucleus and nicks the Frt sites excising exon 1-$Kras^{G12V}$, which results in a knock-out for the mutant Kras allele. Treating FPC-derived tumor organoids with 4-OHT for 72 hours was sufficient to excise the

majority of the mutant Kras alleles leading to downregulation of canonical genes activated by mutant Kras signaling (Etv4, Dusp6 – data not shown). Inactivation of mutant Kras led to a consistent ~50% reduction in the mRNA expression of Spdef in 3 biological replicates (Fig. 3.9B). Therefore, although mutant Kras is not sufficient to induce Spdef expression in normal duct-derived organoids, it is necessary for its sustained expression in organoids derived from advanced PDAC.

3.6 Discussion and Future Directions:

In this study, we describe the successful development of polyclonal antibodies against Spdef and examination of the expression and regulation of Spdef in pancreatic cancer. We found that Spdef is expressed during the early pre-neoplastic stages of pancreatic cancer and its expression is sustained in advanced PDAC and distant metastases in the autochthonous KPC mouse model as well as in murine organoids. Spdef is also upregulated in human PDAC tumor cells compared to the normal ductal cells both *in vivo* and *ex vivo* in organoid cultures. We also observed that Spdef expression in organoids is ~50-fold higher than that in organoid-derived 2D lines, highlighting the unprecedented potential of organoid cultures to uncover physiologically- and disease-relevant biology. In addition, we also showed that Tgfβ pathway inhibition, Wnt signaling, and nicotinamide are necessary to induce Spdef expression in pancreatic tumor organoids, which might provide additional insights into its regulation *in vivo* and potential opportunities for therapeutic targeting.

It is well established in the literature that developmental programs are often hijacked by cancer cells. Spdef is expressed in the early stages (E13.5) of the development of the exocrine pancreas but is silenced shortly after and is undetectable in the adult pancreas (Kobberup et al. 2007). Our work showed that Spdef is re-expressed in late stage PanIN lesions

and its expression is maintained throughout the progression of the disease to advanced and metastatic PDAC. In patient samples, we noticed a trend of higher Spdef expression in lower grade, more differentiated lesions compared to higher grade, more undifferentiated tumors. This is consistent with Spdef's function in goblet cells differentiation and mucus secretion, two prominent features of early PanIN lesions in patients (Kaur et al. 2013). Mucins, the highly glycosylated gel-forming proteins abundant in mucus, have been shown to mediate receptor growth factor signaling (Pochampalli et al. 2007c, 2007a; Li et al. 2005c), interactions with the tumor microenvironment (Komatsu et al. 1999; Senapati et al. 2011b) and oncogenic signaling (Singh and Hollingsworth 2006) and the potential role that Spdef plays in those processes is an exciting future direction for these studies.

It was interesting to note the inter-patient and inter-organoid heterogeneity of Spdef expression. Here we showed that mutant Kras can regulate Spdef expression *in vitro.* Copy number variation data of both patient tumors and KPC tumors has shown common amplifications of the mutant Kras locus (Mueller et al. 2018). Therefore, the amplification status of mutant Kras could explain the difference in Spdef expression between different lines.

Goblet cells, the cell type where Spdef is most highly expressed is physiologically restricted to, are only observed in differentiated glands within advanced PDAC tumors. Interestingly, our work showed a more ubiquitous expression of Spdef in both primary tumors and distant metastases. Previous studies of Spdef in breast and prostate cancer also suggest a tissue- and disease-specific target gene repertoire. For example, Spdef promotes luminal breast cancer by negatively regulating the expression of the death ligand Fas (which we did not observe by IHC staining – data not shown), while in prostate cancer it cooperates with the androgen receptor to regulate the expression of the prostate-specific antigen, PSA. Thus, Spdef's role in advanced PDAC might extend beyond regulating the expression of

mucin genes and we performed additional studies, described in Chapter 4, to address this question.

Another important question pertains to the transcriptional regulation of Spdef expression in pancreatic cancer. Our results from the FPC model of endogenous mutant Kras deletion suggest that, to an extent, mutant Kras regulates Spdef expression in tumor organoids. However, the observed change in Spdef expression (~50%) does not explain the difference in expression between normal and tumor organoids. Multiple Kras-dependent and independent pathways may be inducing Spdef expression in PanIN and tumor cells. We showed that Spdef expression at the protein level is significantly induced in PanIN organoids which was not reflected by the change of its mRNA levels. Previous reports have shown that the phopshorylation of ETS transcription factors containing a PNT domain by RAS/MAPK signaling leads to their stabilization and accumulation (Hollenhorst et al. 2011a). Thus, post-transcriptional regulation of Spdef by mutant Kras might add another level of regulation of this transcription factor in pancreatic cancer.

The striking differences in the expression of Spdef between 2D cell lines and 3D organoid cultures led us to also suspect the role of endogenous factors in the transcriptional regulation of Spdef expression. Indeed, we showed that A83 (a Tgfβ pathway inhibitor), R-spondin (a Wnt agonist) and Nicotinamide are necessary and sufficient for Spdef expression in 2D tumor organoid-derived cell lines. Tgfβ has previously been shown to be required for the restriction of goblet cell differentiation in adult mice by Smad3-mediated transcriptional silencing of Spdef expression in mice (McCauley et al. 2014). In addition, Spdef has been reported as a direct transcriptional target of the basix helix-loop-helix transcription factor, Atoh1. In neural progenitor cells, Atoh1 expression is upregulated by β-catenin suggesting a direct link between Wnt pathway activation and Spdef expression (Li et al. 2005b). Both TGFβ

and WNT signaling have been implicated in pancreatic cancer. Somatic mutations leading to TGFβ pathway inactivation are found in >37% of patients with PDAC (Raphael et al. 2017a) and mutant Kras has been shown to repress TGFβ signaling through Smad4 degradation *in vitro* (Saha et al. 2001). Additionally, canonical WNT signaling is also critical for the progression of pancreatic cancer (Cirillo and Zaret 1999b). These studies suggest that TGFβ inhibition and WNT signaling are prominent features of PDAC in humans and could explain the induction of Spdef expression that we described in this chapter. However, since both normal and tumor organoids are grown using the same media, cell intrinsic factors like mutant Kras might also be involved in regulating Spdef in tumor cells by providing a necessary context to facilitate signal transduction or transcription. Additionally, since most Tgfβ and Wnt ligands are secreted by stromal cells, the availability of ligands in close proximity to the tumor cells might also influence the expression of Spdef.

Because of their tertiary structure and lack of enzymatic sites, transcription factors, with the exception of those that are ligand-inducible, are notoriously hard to inhibit with small molecule inhibitors. Therefore, understanding the regulation of Spdef expression in PDAC could elucidate new therapeutic approaches of indirectly targeting Spdef. Our results implicate Tgfβ, Wnt, and mutant Kras signaling in the regulation of Spdef expression in tumor organoids.

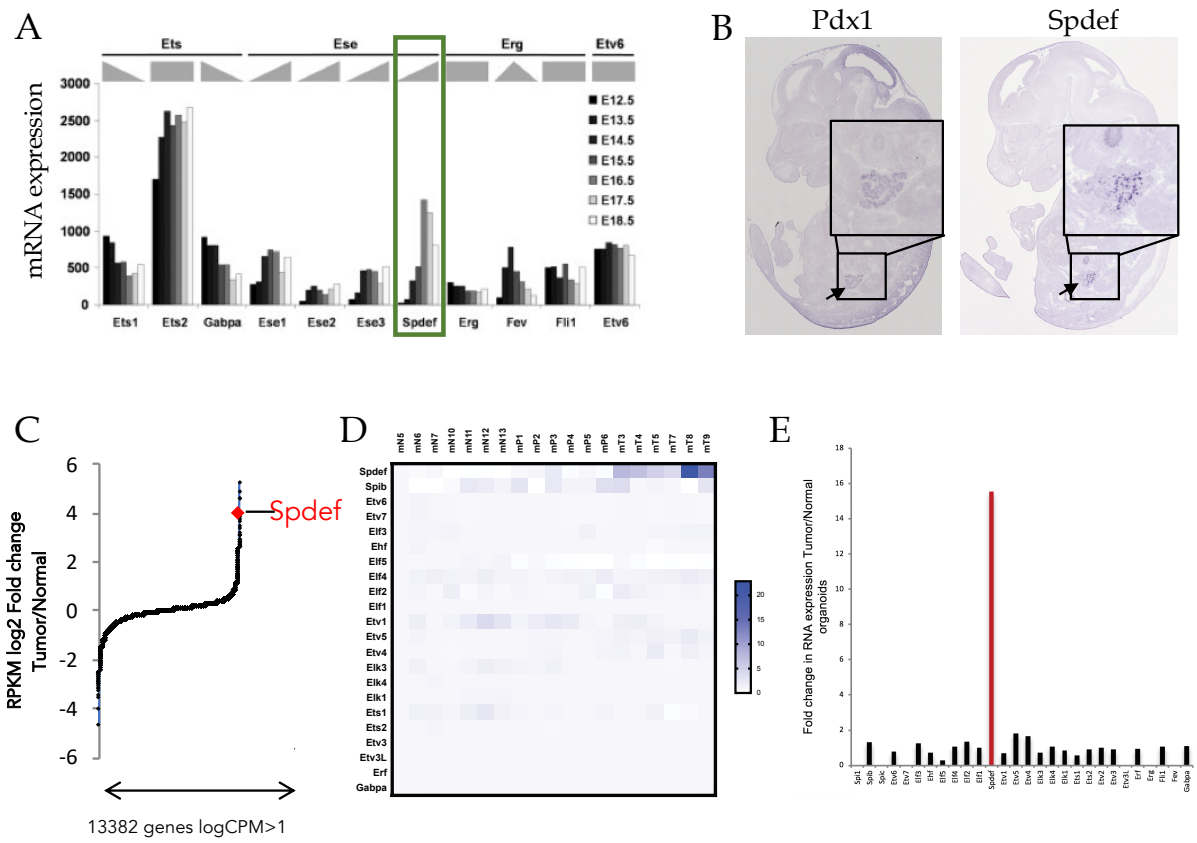

Figure 3.1 Spdef is the most overexpressed transcription factor during PDAC progression.

A) qPCR analysis of ETS factors expressed during embryonic development of the pancreas (Kobberup et al 2007)

B) In situ RNA hybridization for Pdx1 and Spdef in E14.5 embryos from GenePaint. Arrow indicate pancreas

C) RNA-seq analysis of gene expression changes between normal and tumor organoids. Averaged RPKM values for 5 tumor organoid lines were normalize to mRNA levels in normal organoid lines. Genes with RPKM<1 in the normal sample were excluded. Genes are plotted from the most down-regulated genes on the left to the most upregulated genes on the right. (Normal: n=5; Tumor: n=6).

D) Heatmap of RNA-seq mRNA expression of ETS family genes between normal, PanIN and tumor organoids normalized to N6.

E) mRNA Expression of ETS family genes in tumor organoids plotted as fold change over normal organoids

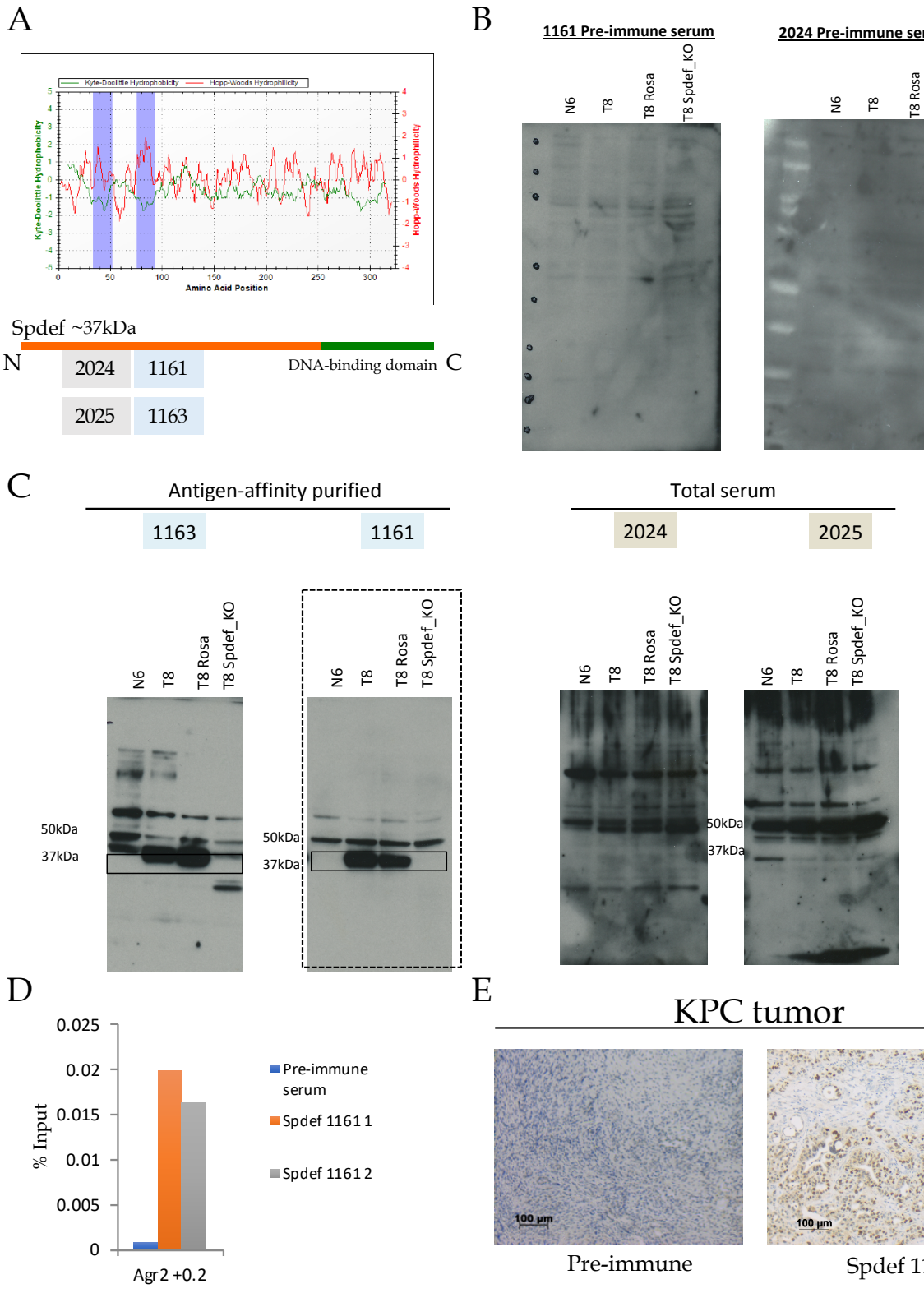
A
Kyte-Doolittle Hydrophobicity
Hopp-Woods Hydrophilicity
Amino Acid Position
Spdef ~37kDa
N
2024
1161
2025
1163
DNA-binding domain
C
B
1161 Pre-immune serum
2024 Pre-immune serum
N6
T8
T8 Rosa
T8 Spdef_KO
C
Antigen-affinity purified
1163
1161
Total serum
2024
2025
50kDa
37kDa
D
% Input
Pre-immune serum
Spdef 1161 1
Spdef 1161 2
Agr2 +0.2
E
KPC tumor
100 µm
Pre-immune
Spdef 1161

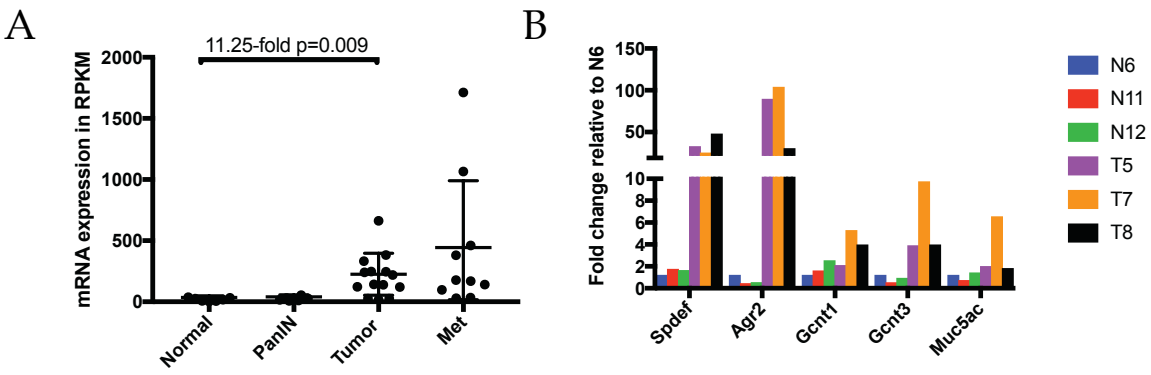

Figure 3.3 Spdef and its target genes are overexpressed in tumor and metastatic murine organoids.
A) mRNA expression of Spdef measured in RPKM by RNA-seq in normal, PanIN, tumor and metastatic organoids
B) RT-qPCR for Spdef and Agr2, Gcnt1, Gcnt3, Muc5ac in normal (N6, N11, N12) and tumor (T5, T7, T8) organoids

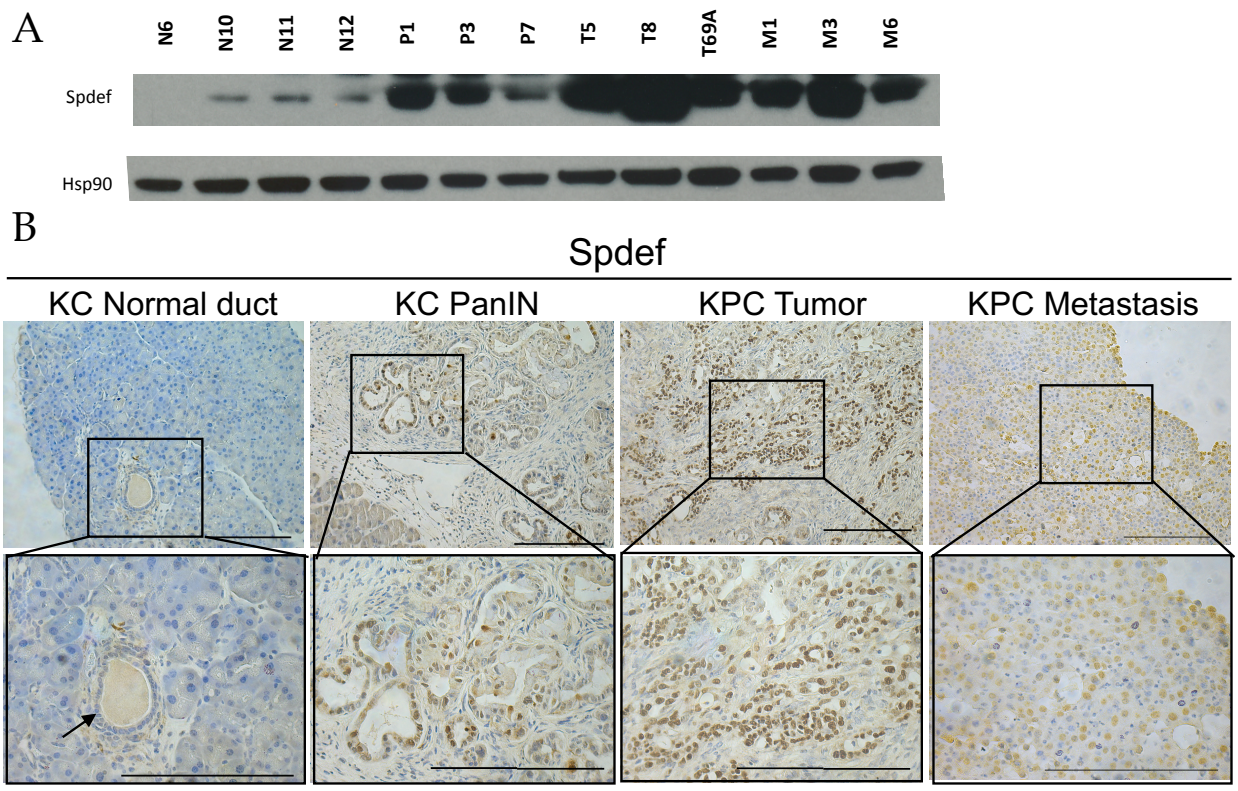

Figure 3.4 Spdef protein levels increase with PDAC disease progression in a murine mouse model

A) WB for Spdef in normal, PanIN, tumor and metastatic organoids. Hsp90 was used as a loading control

B) Immunohistochemistry for Spdef in normal ducts, KC (PanIN), KPC (Tumor) and KPC (diaphragm metastasis) sections. Top panel: 20x magnification; Bottom panels: 40x magnification. Scale bars = 200um

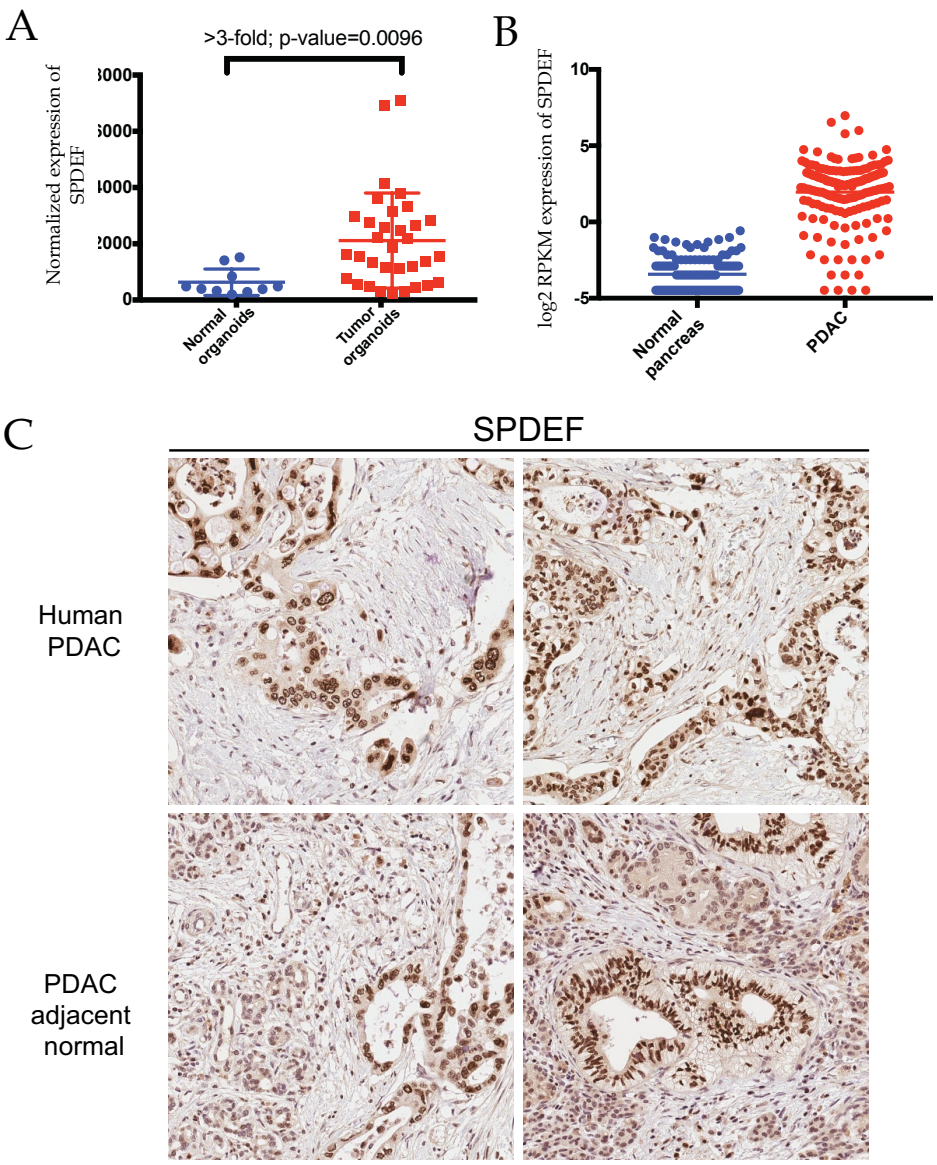

Figure 3.5 Spdef is induced in human PDAC tumors
A) RPKM expression of Spdef in normal pancreas and PDAC tumors.
B) Normalized Spdef expression in human normal and tumor organoids
C) Immunohistochemistry for Spdef in human PDAC with adjacent normal sections.

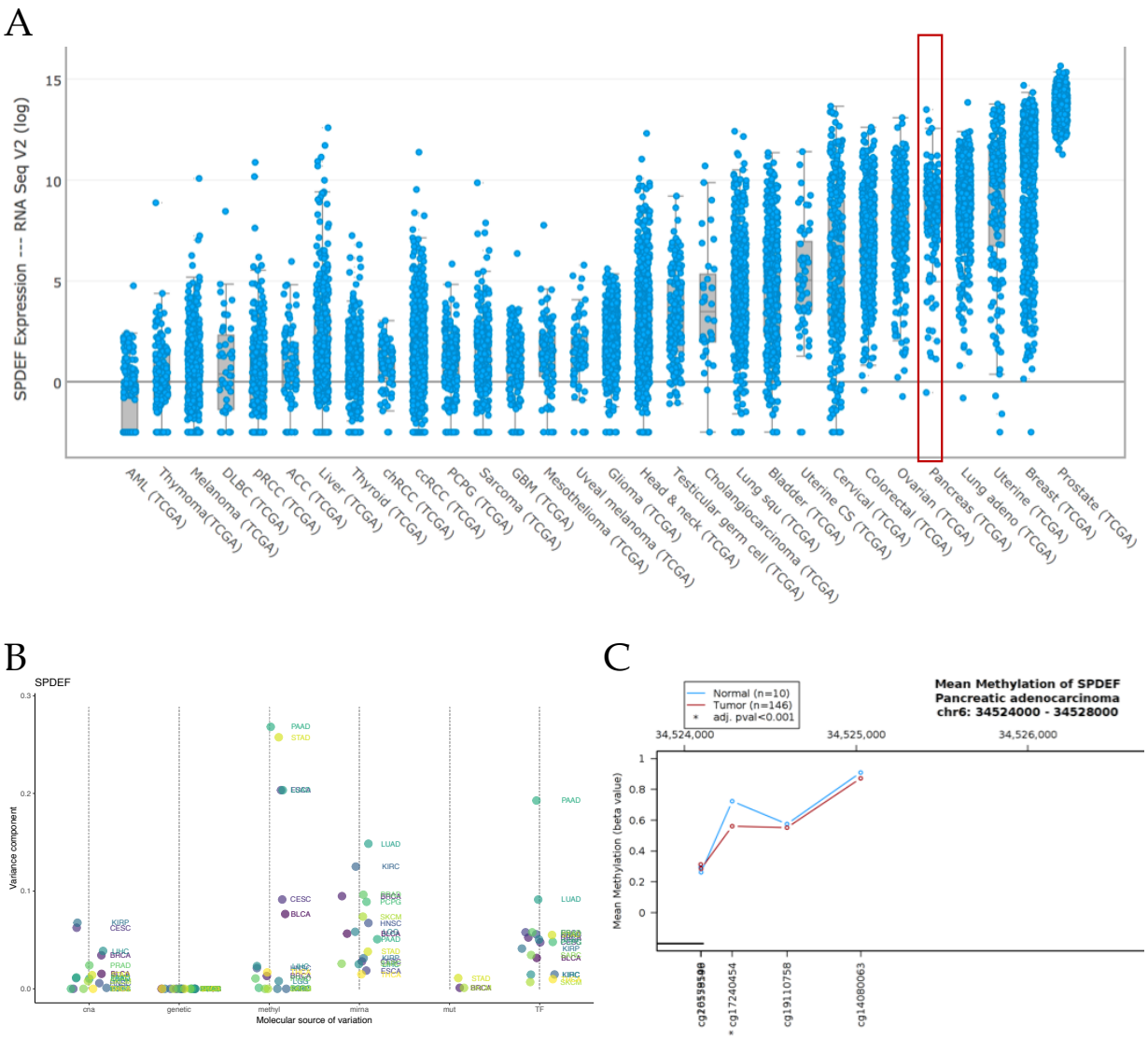

Figure 3.6 Pancreas cancer has the 5th highest expression of Spdef.

A) Comparison RPKM expression of Spdef in TCGA tumor types
B) Molecular source of variation analysis for Spdef in TCGA datasets
C) Bisulfide sequencing of Spdef promoter methylation levels in normal pancreas and PDAC tumor samples.

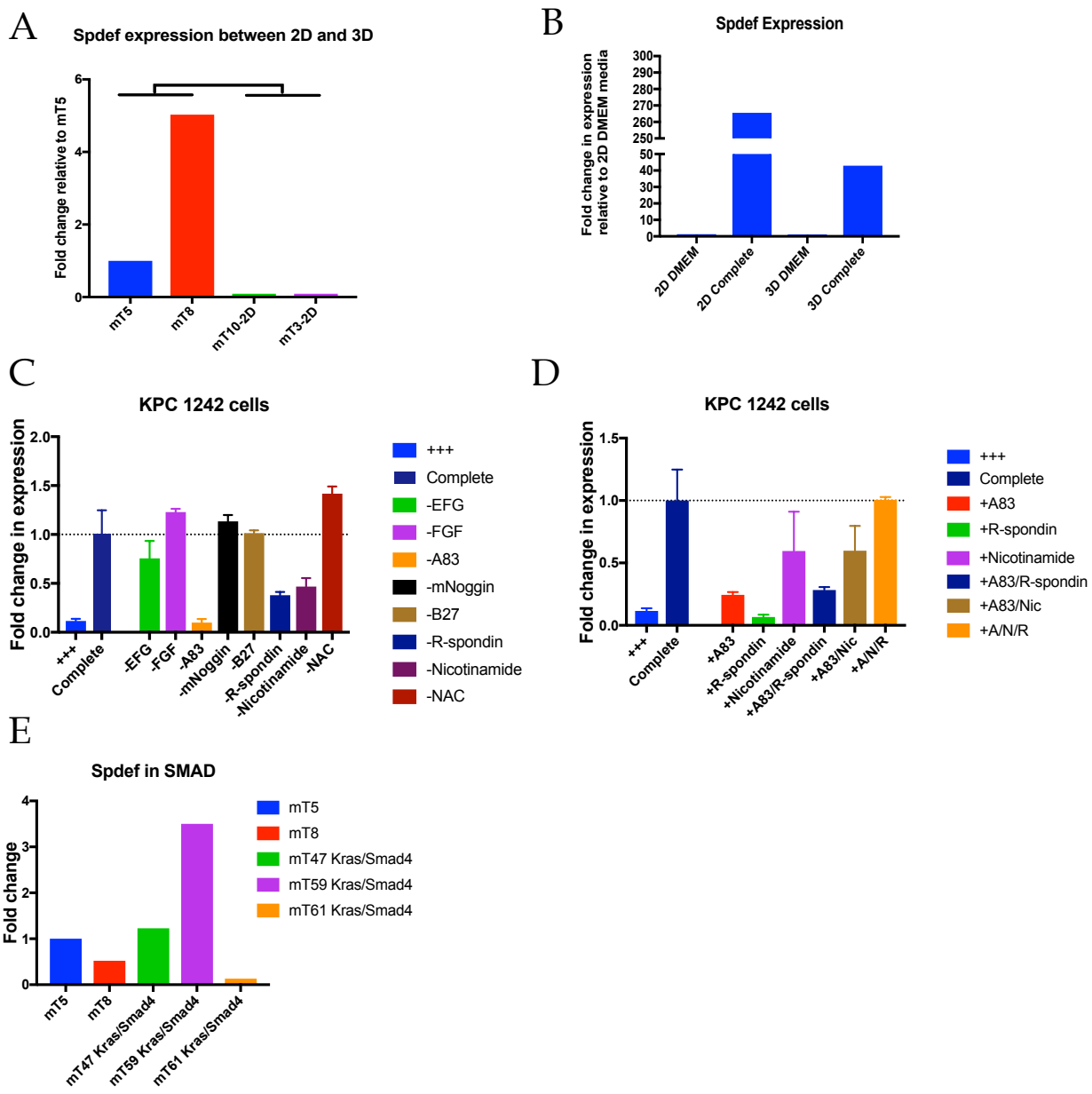

Figure 3.7 Spdef is expressed in organoid cultures and not in 2D lines and its expression is controlled by exogenous factors

A) RT-qPCR for Spdef in organoids (mT5 and mT8) and organoid-derived 2D lines (mT10-2D and mT3-2D)

B) RT-qPCR for Spdef in 2D cell lines grown either in 2D or 3D conditions and supplemented by either DMEM/10%FBS or Complete organoid media

C) RT-qPCR for Spdef in KPC1242 2D cell lines grown in complete organoid media following removal of indicated growth factors

D) RT-qPCR for Spdef in KPC1242 2D cell lines grown in basal organoid media conditions supplemented with the indicated factors

E) RT-qPCR for Spdef in KPC-derived tumor organoids (mT5, mT8) or $Kras^{G12D}/Smad4^{fl/fl}$ –derived organoids

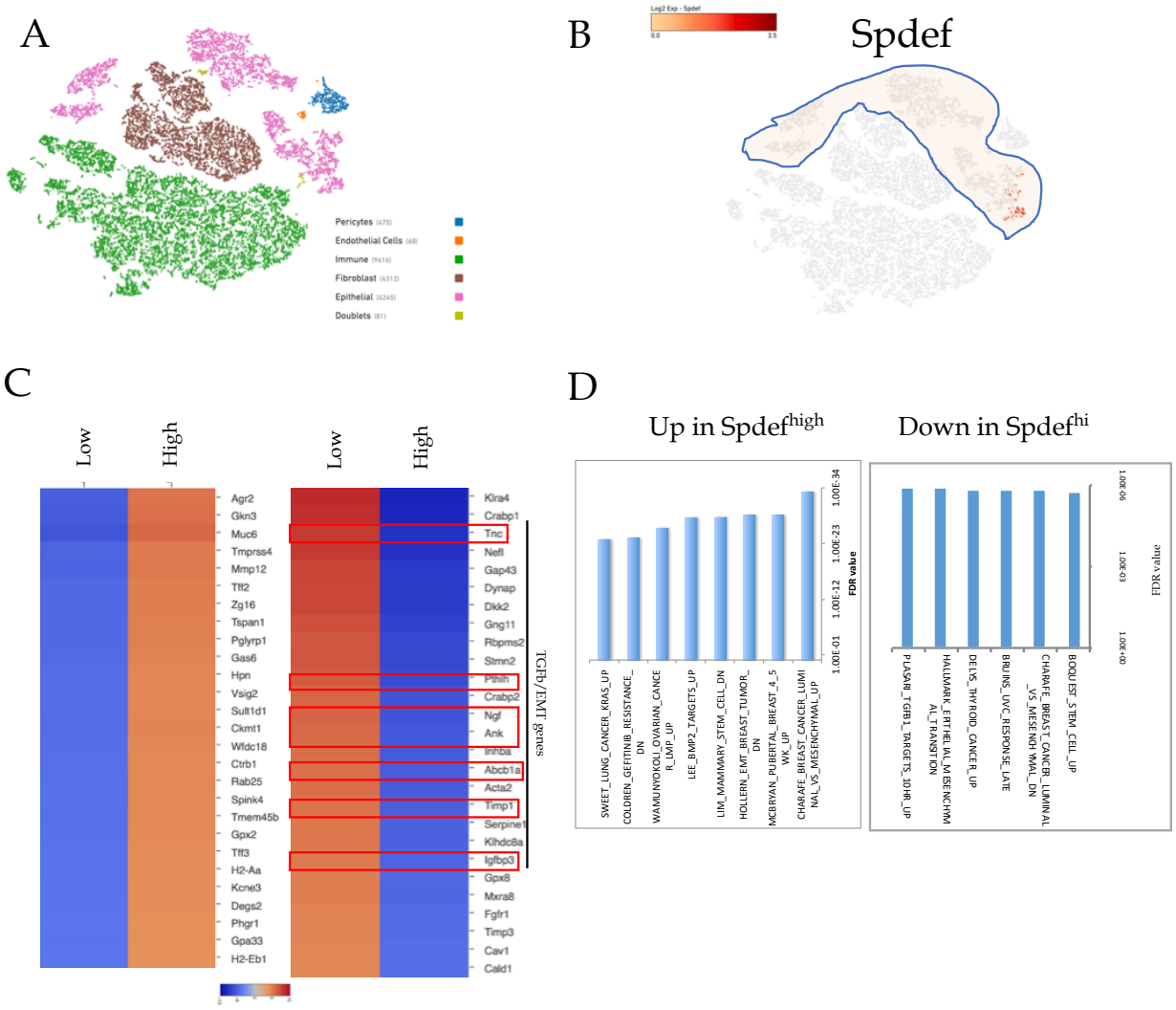

Figure 3.8 Single Cell RNA-seq analysis of Spdef expression in tumor epithelial cells from KPC PDAC mouse model.

A) Graph-based clustering of cells isolated from 3 KPC tumors by cell type. Cells belonging to each cell type are colored accordingly (see legend).
B) Expression of Spdef within tumor cells
C) Differentially expressed genes between Spdef^{hi} and Spdef^{low} cells.
D) Gene ontology pathway analysis of upregulated and downregulated genes in Spdef^{hi} population plotted by FDR q-value

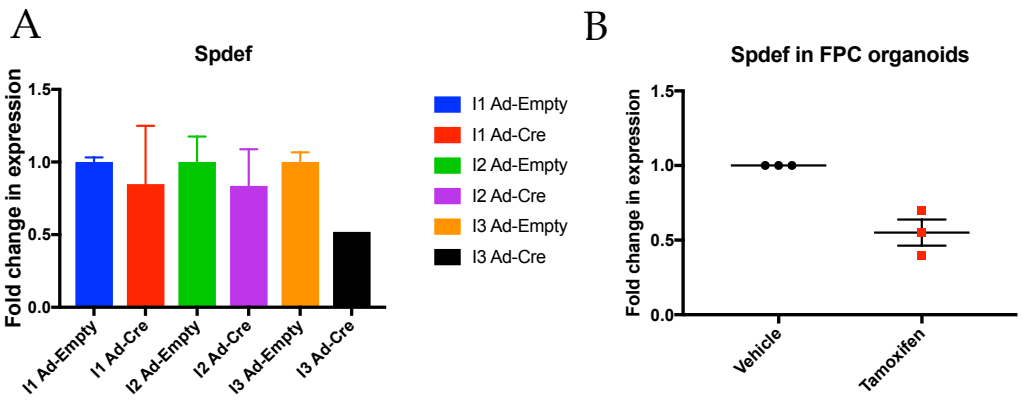

Figure 3.9 Mutant Kras is necessary but not sufficient for Spdef expression

A) RT-qPCR for Spdef expression in LSL-Kras^{G12D} organoids infected either with Ad-Empty or Ad-Cre. Error bars represent standard deviation (n=2).

B) Spdef expression following Kras^{G12V} excision in 3 FPC-derived organoid lines normalized to vehicle-treated control. Error bars represent standard error of the mean (N=3).

CHAPTER 4. SPDEF PROMOTES PANCREATIC CANCER BY REGULATING ENDOPLASMIC RETICULUM HOMEOSTASIS

4.1 Spdef is dispensable for organoid proliferation *in vitro* but impairs the growth of tumor organoids *in vivo*

In the RNA-seq analysis of mouse pancreatic organoids, Spdef is the fourth-most transcriptionally upregulated gene and the most upregulated transcription factor overall in tumor compared to normal organoids (Boj et al. 2015). To address the functional consequences of high Spdef expression in tumor organoids and the dependency of tumor organoids on sustained Spdef expression, we generated Spdef-knockout (KO) tumor organoids. To do so, we modified and adapted an inducible CRISPR-Cas9 system previously described by the Sordella group at CSHL (Senturk et al. 2017). In this system, an engineered mutant peptide from the human FKBP12 protein, or "degron domain" (DD), is fused to Cas9 to generate DD-Cas9. The DD peptide leads to rapid degradation of Cas9 by the proteasome complex, which can be prevented in the presence of a small molecule compound named Shield-1. Therefore, in the absence of Shield-1, Cas9 is degraded, whereas the addition of Shield-1 to the growth media leads to stabilization of Cas9 and genome editing. In addition, separated by an P2A self-cleaving peptide, the fluorescent protein Venus was cloned immediately downstream of Cas9. To ensure that DD-Cas9 is expressed in all cells infected with this lentiviral vector, we engineered the system and replaced the Venus cDNA with a puromycin resistance cassette. We tested five gRNAs spanning regions within the 2nd and 3rd exons of Spdef to select two with the highest efficiency of protein knock-out. Cas9-mediated gene editing can lead to either in-frame (~25%) or out-of-frame insertions or deletions (Sander and Joung 2014). To ensure

that we were working with a clonal Spdef KO population, we generated and selected an organoid clone that was KO for Spdef for both gRNAs (Fig. 4.1A).

To assess the effect of deleting Spdef on the proliferation of tumor organoids, we compared the growth of two independent organoid lines KO for Spdef to a Rosa gRNA control. Surprisingly, we did not observe a significant difference in the growth of Spdef WT and KO organoids *in vitro* when we followed proliferation by Incucyte imaging (Fig. 4.1B – one organoid line shown). However, when transplanted orthotopically into the pancreata of immunodeficient host mice (athymic, nu/nu mice), Spdef KO lines displayed significantly delayed tumor formation in two independent organoid lines using clones derived from two gRNAs (Fig. 4.2A and B). H&E staining of Rosa control tumors revealed a highly cellular PDAC morphology, similar to that seen in the KPC model (Fig. 4.3A). However, examination of the pancreata from Spdef KO transplants in which we did not observe any macroscopic tumor lesions, revealed cystic, PanIN-like lesions at the site of injection that had not progressed to invasive PDAC (Fig. 4.3B). It has previously been reported that loss of the WT copy of Trp53 (loss of heterozygosity, LOH) leads to accumulation of the mutant p53 protein in the nucleus, which can be detected by immunostaining (Olive et al. 2004). The organoids used in this experiment, mT69a, have been demonstrated to be LOH for Trp53 based on genotyping of for the LSL-Trp53^{R172H} and WT alleles (Roe et al. 2017). We performed IHC staining for p53 to confirm that the observed cystic lesions are composed of the tumor organoids that we transplanted and observed nuclear accumulation of p53 in the nucleus of the cells lining the cysts, confirming their tumor origin (Fig. 4.3C). These results suggest that Spdef is required for progression to PDAC but not for engraftment of transplanted cells.

To investigate the mechanism for the impaired tumor progression, we compared the proliferative capacity of the Rosa tumors and the Spdef KO lesions at endpoint. Ki67 is a well-

established marker of proliferation that accumulates in the nucleus of dividing cells (Scholzen and Gerdes 2000). IHC staining for Ki-67 did not show a substantial difference in the proliferation rates between the Rosa and the Spdef KO lesions (Fig. 4.4A). The difference in the growth and progression of these tumors could also be caused by increased cell death in the Spdef KO lesions. Caspase 3 cleavage is an initial step of the caspase-dependent apoptotic pathway. However, staining for cleaved Caspase 3 by IHC did not reveal any differences between the two genotypes (Fig. 4.4B).

Since we observed that Spdef KO organoids could give rise to tumors, albeit smaller in size than those tumors formed from Rosa control organoids, we wanted to examine any differences in the survival of animals that were transplanted with WT vs KO Spdef organoids. Although this experiment is currently ongoing, at 173 days post transplantation, all mice transplanted with Rosa control organoids have succumbed to malignant disease, while 9/10 mice transplanted with Spdef KO organoids are still alive and tumor-free (Fig.4.5).

To confirm that the phenotype observed *in vivo* is due to Spdef KO and is not an off-target effect of the gRNA or a feature of selected organoid clones, we cloned the mouse Spdef cDNA into a retroviral expression vector (MSCV) with a hemagglutinin (HA) tag either at its N- (HA-Spdef) or C-terminus (Spdef-HA) and stably infected Spdef KO organoids to rescue its expression. Because of the inducible nature of DD-Cas9, the ectopic Spdef cDNA should not be cleaved in the absence of Shield-1. Surprisingly, Spdef-HA did not express well so we used the HA-Spdef organoids for all further experiments. Re-expression of HA-Spdef in the Spdef KO organoids was able to successfully rescue the *in vivo* phenotype with HA-Spdef organoids, forming similar tumors to Rosa controls in the same time period (Fig.4.6A and B).

One of the benefits of the DD-Cas9 system is that the Shield-1 compound can be administered *in vivo* to study the effects of Spdef KO on tumor maintenance. To perform this

experiment, we transplanted five mice with tumor organoids expressing a gRNA targeting the Rosa locus and five mice with organoids expressing a gRNA targeting Spdef. Once tumors reached an enrollable size (5x6 mm), as measured by ultrasound imaging, we began dosing the mice with Shield-1, administered by intraperitoneal injection every other day. Ultrasound scans were taken 7 days and 14 days after enrollment and mice were sacrificed on the 15th day after enrollment. We did not observe any significant differences in the growth kinetics or final tumor volumes between the Rosa and the Spdef KO cohorts. To confirm that Shield-1 was effective in stabilizing DD-Cas9 and inducing cleavage, we digested tumors harvested at endpoint and enriched for cancer cells by negative selection for stromal cells using an antibody cocktail binding stromal-specific protein conjugated to magnetic beads. A surveyor assay showed that the genomic region targeted by the gRNA was indeed intact in cancer cells showing that Cas9-mediated DNA cleavage did not occur, possibly due to inefficient stabilization of the DD-Cas9 following administration of Shield-1.

4.2 Spdef regulates the expression of mucins and genes involved in the UPR

The striking phenotype that we observed *in vivo* prompted us to determine the mechanism by which Spdef controls tumor growth. During development, Spdef is known to directly regulate the expression of genes important for goblet cell maturation and mucus production, and additional studies in breast and prostate cancer have revealed a tissue- and disease-specific repertoire of SPDEF target genes (Oettgen et al. 2000; Buchwalter et al. 2013; Park et al. 2007). To define the genes that Spdef regulates in pancreatic cancer, we analyzed the transcriptome of three independent tumor organoid lines following shRNA-mediated Spdef knockdown by RNA-seq. Spdef was downregulated at least 0.5-fold in all three pairs of organoids infected with shRNAs against Spdef (Fig. 4.7A, B and C). The analysis revealed

69 genes that were differentially expressed upon Spdef knockdown (Fig. 4.7D). When genes with low baseline expression were excluded, the only pathway that stood out was related to the regulation of the secretory phenotype of goblet cells. Spdef has been previously described as a transcriptional activator of both mucins and genes involved in protein folding (Park et al. 2007). In addition to the previously reported Spdef target genes (Agr2, Muc2, Muc6, Muc5ac), we found that a putative novel Spdef target gene, also involved in protein folding, (Ern2) was significantly downregulated in all three lines (Fig. 4.7B and D).

4.3 Egfr signaling is not perturbed in Spdef KO tumor organoids

It has been previously reported that Spdef cooperates with Erbb2 signaling to promote breast cancer metastasis (Gunawardane et al. 2005). In addition, a central characteristic of mucins are their EGF-like domains, which can interact with members of the EGF receptor family to regulate their activity (Hollingsworth and Swanson 2004). Therefore, attenuation of Erbb signaling might explain the severe phenotype of Spdef KO organoid transplants *in vivo*. To assess whether Spdef KO leads to attenuation of Erbb signaling we performed a time-course EGF stimulation experiment of growth factor deprived Rosa and Spdef KO organoids and assessed the activation status (by phosphorylation) of Egfr and two downstream kinases: Akt and Erk. These experiments showed no significant attenuation of Egfr signaling in the setting of Spdef KO (Fig. 4.8A). In addition, Spdef KO did not affect the sensitivity of tumor organoids to the Egfr/Erbb2 inhibitor Neratinib (Fig.4.8B). Therefore, the decreased expression of mucin genes in Spdef KO organoids did not affect Erbb signalling.

4.4 Spdef is a direct transcriptional activator of Ern2

Both Agr2 and Ern2 are significantly upregulated in tumor and metastatic organoids compared to normal organoids (Fig. 4.9 A and B). To confirm that Ern2 is a direct target of Spdef, we performed ChIP of endogenous Spdef, followed by qPCR for a region within the promoter of Ern2. We observed a significant enrichment of Spdef at Ern2's promoter when compared to an isotype control antibody suggesting that Spdef directly binds to the promoter of the gastric-specific Ern2 gene to regulate its expression, which has never been reported in the literature before (Fig. 4.10). To confirm that Ern2 is induced in human PDAC samples, we analyzed IHC staining for Ire1β in normal and PDAC specimens performed in the Human Protein Atlas project (Uhlen et al. 2015). While normal acinar cells did not stain positively for Ire1β we did observe staining in stellate cells within the normal pancreas. However, in PDAC sections, we observed a significant increase in the staining for Ire1β specifically in tumor epithelial cells confirming our observation of increased Ern2/ Ire1β in murine tumor organoids (Fig. 4.11A). To determine if SPDEF expression correlates with ERN2 expression in patients, we analyzed TCGA gene expression data from PDAC, breast and prostate adenocarcinoma tumors (Fig. 4.11B). Surprisingly, while ERN2 was the most positively correlated gene with SPDEF in PDAC, we found little correlation between these two genes in breast and prostate cancer (Fig. 4.11C,D and E). These results show that ERN2 is significantly upregulated in PDAC and suggest a tissue-specific regulation of its expression by SPDEF specifically in pancreatic cancer.

4.5 Spdef KO attenuates Xbp1 splicing in tumor organoids

Cancer cells are particularly dependent on the induction of a robust UPR due to their exposure to exogenous and endogenous stresses that cause the accumulation of misfolded

proteins – e.g. ROS, hypoxia, nutrient deprivation etc. The protein encoded by Ern2 (Ire1β), but not Ern1 (Ire1α), promotes efficient protein folding and secretion in the ER of goblet cells and Ern2 expression is typically restricted to the GI tract (Tsuru et al. 2013). Activation by phosphorylation of the Ire1α/β kinases/RNAses induces non-canonical splicing of the Xbp1 transcription factor converting it into its active form, Xbp1s (Li et al. 2010). Our observation that Ern2 expression is significantly downregulated upon Spdef knockdown encouraged us to explore the UPR pathway in the context of Spdef loss.

To determine whether Spdef is essential for robust activation of the unfolded protein response *in vitro*, we treated Spdef knockout tumor organoids with the ER-stress inducing compound thapsigargin (TG) and measured the induction of Xbp1 splicing by RT-qPCR. TG is a non-competitive inhibitor of the endoplasmic reticulum Ca^{2+} ATPase, SERCA, and treatment with TG leads to a drop in the ER Ca^{2+} levels reducing the folding capacity of Ca^{2+}-dependent chaperones which causes accumulation of unfolded proteins in the ER. As expected, in Rosa control organoids, treatment with TG led to a rapid induction of Xbp1s two hours after treatment which peaked and plateaued at six hours. Knockout of Spdef resulted in attenuated splicing of Xbp1 while the levels of the unspliced Xbp1 mRNA remained the same regardless of the treatment in both Spdef KO and Rosa control organoids (Fig. 4.12A and B). Concurrently, Spdef KO led to reduced induction of Xbp1s-specific target genes (Hspa5, Ddit3) upon TG treatment, supporting the finding of impaired Xbp1s activation (Fig. 4.12C). Unresolved ER stress leads to cell death through apoptosis, so we analyzed the expression of the pro-apoptotic gene Puma, a known mediator of ER-stress-induced cell death (Fig. 4.12D). Spdef KO organoids displayed higher induction of Puma following TG treatment supporting the hypothesis that those organoids are unable to resolve ER stress which leads to cell death.

4.6 Spdef KO sensitizes tumor organoids to ER-stress-induced cell death

To test whether unresolved ER stress sensitized Spdef KO tumor organoids to ER-stress induced cell death, we first used previously described conditions known to induce ER stress: nutrient deprivation, hypoxia and anchorage-independent growth. Surprisingly, the Spdef KO organoids showed no differential sensitivity to those stresses (Fig. 4.14 A, B and C). To assess whether Spdef KO organoids were sensitized to TG-induced ER stress, we monitored the growth of Spdef KO and control (Rosa) organoids over four days in the presence of varying concentrations of TG (0.1-500 nM). The Rosa control tumor organoids exhibited high sensitivity to TG (GI: 41.7-68.2 nM) but both lines of Spdef KO organoids had ~5-fold reduction in the GI50 concentration for TG (7.6-17.3 nM) (Fig. 4.15 A, B and C).

4.7 Ectopic expression of Xbp1s rescues the sensitivity of Spdef KO to thapsigargin

To confirm that the increased sensitivity of Spdef KO organoids is due to attenuated activation of the Xbp1s transcription factor, we cloned the sequence for the mouse Xbp1s cDNA by Gibson cloning into the MSCV retroviral vector to generate Spdef KO organoids that stably overexpress Xbp1s to levels similar to those of TG-treated WT organoids. At baseline (untreated) conditions, ectopic expression of Xbp1s led to an induction in the expression of its ER-stress associated target genes (Hspa5, Dnajb9, Tspan9) confirming that the protein product was correctly expressed (Fig. 4.16B and C). Surprisingly, we also noted that Agr2, Ern1 and Ern2 were significantly upregulated upon Xbp1s expression. Xbp1s recognizes the CCACG E-box motif in the promoters of its target genes, but analysis of the promoters of Agr2, Ern1 and Ern2 did not reveal a putative Xbp1s binding site suggesting

that overexpression of Xbp1s indirectly leads to upregulation of the expression of these genes in the absence of exogenous ER stress. To assess the ability of ectopic Xbp1s expression to rescue the sensitivity of Spdef KO organoids to ER stress, we compared the survival of Rosa (control), Spdef KO, Spdef KO-HA-Spdef and Spdef KO-Xbp1s organoids to varying concentrations of TG. At 29.6nM of TG, while only ~20% of the Spdef KO organoids survived, ectopic expression of either Spdef-HA or Xbp1s abrogated the sensitivity of Spdef KO organoids to the drug to levels similar to that of Rosa control organoids (Fig. 4.16D). Altogether, these results establish Spdef as a direct transcriptional regulator of genes involved in the unfolded protein response and explain the reduced capacity of Spdef KO organoids to form tumors *in vivo* due to impaired resolution of ER stress.

4.8 Discussion and future directions

Here we describe a previously unappreciated role for the ETS transcription factor Spdef in promoting pancreatic cancer in part by regulating Xbp1 activation in response to ER stress. Our results show that Spdef is induced in pancreatic cancer cells, and that it regulates the expression of Ern2 and other UPR-related genes to promote Xbp1 splicing and protect cancer cells from ER stress-induced cell death. We showed that expression of a constitutive active form of Xbp1 (Xbp1-s) is able to rescue the increased sensitivity of Spdef KO organoids to an ER stress agent. Collectively, these results establish a new oncogenic role for Spdef in pancreatic cancer and suggest that tumor cells hijack a developmental function of this transcription factor to promote ER homeostasis and tumorigenesis.

Our lab and others have previously shown that cancer cells promote mRNA translation and protein synthesis through hyperactivation of signal transduction pathways (Schwanhäusser et al. 2011; Gleimer and Parham 2003a; Chio et al. 2016). Therefore, they

require a robust unfolded protein response to protect their proteome from the increased load to the ER and the multiple endogenous and exogenous factors (e.g. ROS, protein synthesis, hypoxia and nutrient deprivation) that lead to ER stress. Previous studies have also shown that multiple genes involved in the ER stress response are overexpressed in cancer and are required for tumorigenesis (Romero-Ramirez et al. 2004). For example, hypoxia-induced Xbp1 expression and its activation through non-canonical splicing in a Hif1a-independent manner is essential for tumor formation in vivo and survival under hypoxic conditions (Romero-Ramirez et al. 2004). Additionally, the expression of the ER stress sensor BiP (Hspa5) is required for tumor growth and development in vivo (Jamora et al. 1996). Inhibition of the Ire1β paralogue, Ire1α, has also been shown to reduce inflammation-induced colonic tumorigenesis in mice (Li et al. 2017). Interestingly, however, in secretory goblet cells, Ire1β, but not Ire1α, promotes efficient protein folding and secretion into the ER, and Ire1β can induce Xbp1 splicing and activation (Tsuru et al. 2013; Martino et al. 2013). One explanation of our results *in vivo* is that in response to ER stress during tumorigenesis, Spdef positively regulates the expression of key UPR genes, including Ern2 and Agr2, which leads to Xbp1 activation and thus a robust induction of the unfolded protein response. Tumor cells lacking Spdef are unable to maintain ER homeostasis and undergo cell death.

Surprisingly, we found that *in vitro*, the levels of multiple UPR proteins (BiP, Atf6 and Chop) are elevated in Spdef KO organoids at baseline conditions. This suggests that these cells are already experiencing higher ER stress therefore reducing the potential amplitude for activation of the UPR. The mechanism of this upregulation seems to be post-transcriptional since we did not observe any changes by RT-qPCR.

Unresolved chronic ER stress leads to apoptosis, and we observed elevation in the expression of the apoptotic marker Puma in Spdef KO organoids treated with TG. However,

in vivo we did not observe any difference in the number of CC3-positive cells, suggesting cell death might occur at an earlier timepoint or through non-apoptotic mechanisms such as necroptosis. To address this question, we are planning to compare transplanted Spdef KO organoids to Rosa at earlier timepoints – e.g. 3 days, 7 days and 14 days post-surgery. In addition, the response to ER stress could be heterogenous and cells that are initially exposed to higher levels of hypoxia, ROS or nutrient deprivation could undergo apoptosis at an earlier time point. To this end, we also plan to perform IHC staining for apoptosis or a hypoxia/ROS marker (e.g. Hif1α) on those early timepoint transplants.

Importantly, despite the longer latency, the majority of Spdef KO mice do form tumors and eventually succumb to the disease, prompting further research into the compensatory mechanisms utilized by these surviving cells. To further elucidate the compensatory mechanisms employed by Spdef KO cancer cells *in vivo,* we are planning to conduct RNA-seq on endpoint tumors isolated from Rosa and Spdef KO transplants to identify upregulated or downregulated pathways. In addition, upregulation of Ire1α and/or its activated form, pIre1α, could be one mechanism by which cells adapt to the reduced levels of Ern2. To this end we also plan to stain tumor tissues from these experiments for Ire1α/pIre1β as well as compare the levels of Ire1α and pIre1α between Rosa and Spdef KO tumors by WB. Finally, to supplement these studies and evaluate the role of Spdef in pancreatic cancer initiation, we are developing a conditional Spdef KO mouse model by crossing $Spdef^{fl/fl}$ mice with the KC and KPC GEMM.

Although we showed that in Spdef KO tumor organoids, *in vitro,* splicing of Xbp1s is attenuated and its ectopic expression rescues the sensitivity of these organoids to TG, the exact mechanisms of our *in vivo* phenotype might differ from these *in vitro* observations. We were unable to obtain the previously published Xbp1s antibody (Biolegend) that has been

used for IHC due to supplier issues but an alternative to comparing the levels of spliced vs unspliced Xbp1 would be to use RNA *in situ* hybridization. To confirm that Xbp1 activation is sufficient for the observed Spdef KO phenotype *in vivo*, we are also assessing the ability of ectopically expressed, constitutively active Xbp1s to rescue the growth defect of Spdef KO tumor organoids *in vivo*. Although previous studies have shown that Ern2/Ire1β can induce splicing of the Xbp1 transcript in response to ER stress, our results show that Xbp1 splicing still occurs in Spdef KO organoids but its induction is attenuated. It is puzzling why Ire1α is unable to compensate for the reduced levels of Ire1β. Ire1α is ubiquitously expressed in mammalian cells, while the expression of Ire1β is confined to epithelial tissues within the GI tract (Bertolotti et al. 2001; Martino et al. 2013). Many of these epithelial cells have secretory functions and thus require a higher ER folding capacity which might explain the need for the supplementation of the UPR pathway by Ire1β. Moreover, the reduced levels of Agr2 in the Spdef KO organoids would lead to reduced ER folding capacity and explain the synergistic effects with reduced levels of Ern2. We are currently cloning shRNA hairpins against Ern2 to test whether Ern2 is necessary for Xbp1 activation *in vitro* and for the reduced tumor growth phenotype *in vivo*. Although we expect that loss of Ern2 should phenocopy the Spdef KO phenotype we observed *in vivo*, the impaired protein folding caused by the reduced levels of Agr2 in the Spdef KO tumor organoids might be necessary for the striking growth defect that we observed. Also of note is a recent report that described a delay in tumorigenesis when Agr2 was deleted in the KC GEMM model of PDAC (Dumartin et al. 2017). In addition, the multitude of other transcriptional targets of Spdef related to mucin production (Muc2, Muc6) and glycosylation (Gcnt3) might also play currently unappreciated synergistic roles with Ern2.

Although most of the experiments described in this study are focused on the cell-intrinsic function of Spdef in regulating PDAC progression, we do not disparage a non-cell-autonomous role for Spdef. The orthotopic mouse model host, that we utilized, has a spontaneous mutation in the Foxn1 gene that causes deterioration or absence of the thymus and an inability to produce T-cell. However, these mice have fully functional myeloid and natural killer (NK) cell compartments. Multiple mucins have been shown to inhibit NK cell-mediated tumor cell killing *in vitro* and *in vivo* (Zhang et al. 1997; Kaur et al. 2013). Therefore, the reduced mucin expression in the Spdef KO tumor cells might increase their susceptibility to clearance by NK cells *in vivo*. In addition, tumor-associated macrophages have been shown to interact with tumor epithelial cells in a cancer-promoting fashion via mucins such as Muc1, which could be another mechanism through which Spdef promotes tumorigenesis (Nath et al. 1999). Secreted mucins could also accumulate in the tumor periphery to form a physical barrier that restricts the infiltration of immune cells into the tumor (Kannagi 2002). Additionally, it is well recognized MHC Class I antigen presentation can act as a cell surface indicator of internal cellular stress responses such the UPR (Granados et al. 2009). Higher organisms have evolved different mechanisms employed by the innate immune system that help recognize and eliminate those damaged, infected or malignant cells in order to promote the survival of the organism (Gleimer and Parham 2003b). Persistent chronic ER stress has been shown to impair MHC class I surface expression and thus increase susceptibility to NK-mediated cytotoxicity (Ulianich et al. 2011). Therefore, the unresolved ER stress, characteristic of Spdef KO cells, might be another mechanism that increased their clearance by the innate immune system.

Inhibiting the UPR has become a coveted therapeutic avenue, and multiple pharmacological agents have been found to exhibit anti-tumor activity by targeting UPR

components (Ojha and Amaravadi 2017b). However, few of these compounds exhibit sufficient selectivity to achieve a clinically-useful therapeutic window. Xbp1 and Ire1α are essential genes in embryonic development, suggesting a limited clinical utility in their therapeutic targeting, whereas Spdef and Ern2 are both dispensable during development (Bertolotti et al. 2001; Marko et al. 2013). Although direct targeting of Spdef with a small molecule inhibitor might be difficult, the dual catalytic function and tissue-specific expression of Ire1β makes it an promising target for drug development.

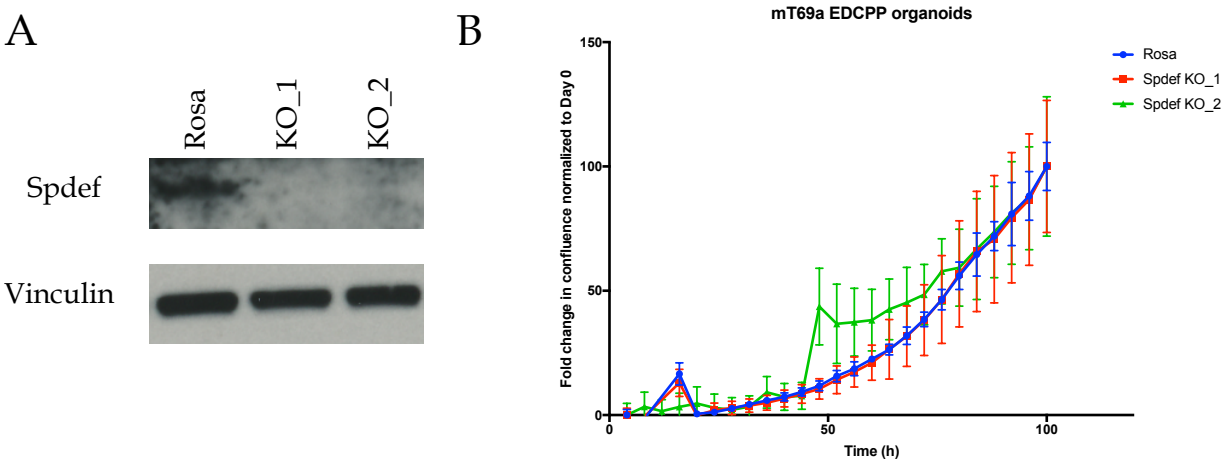

Figure 4.1 Spdef KO does not lead to a proliferation defect in tumor organoids
A) WB for Spdef confirmin CRISPR-Cas9-mediated knockout. Vinculin is a loading control
B) Incucyte proliferation of Rosa, Spdef_KO_1 and Spdef_KO_2 mT69a organoids over 100 hours

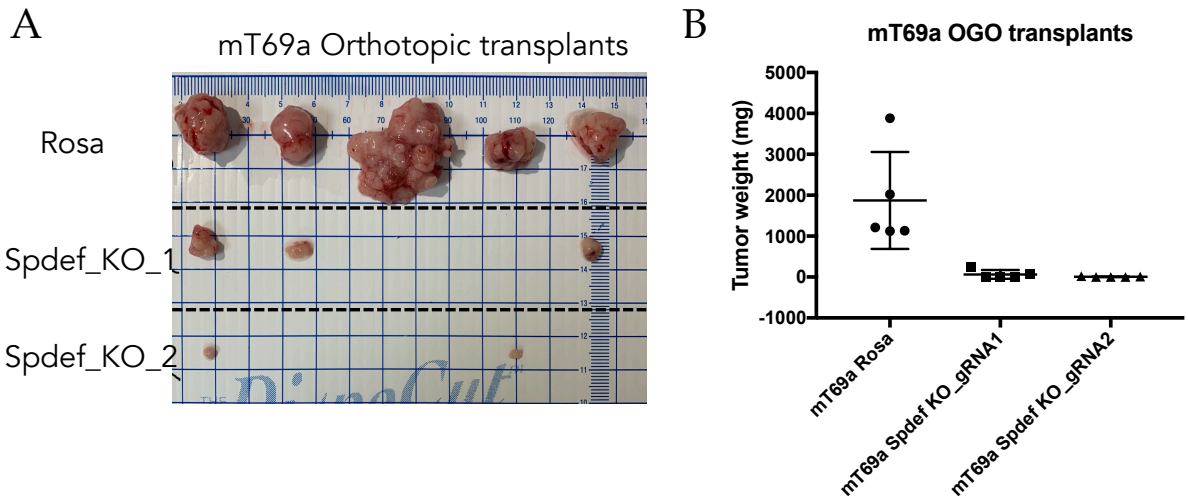

Figure 4.2 Spdef KO impairs orthotopic growth of tumor organoids in vivo.
A) Images of tumors formed 6 weeks following orthotopic transplantation of Rosa and 2 Spdef KO (n=5 for each genotype)
B) Quantification of tumor weight (mg) from A.

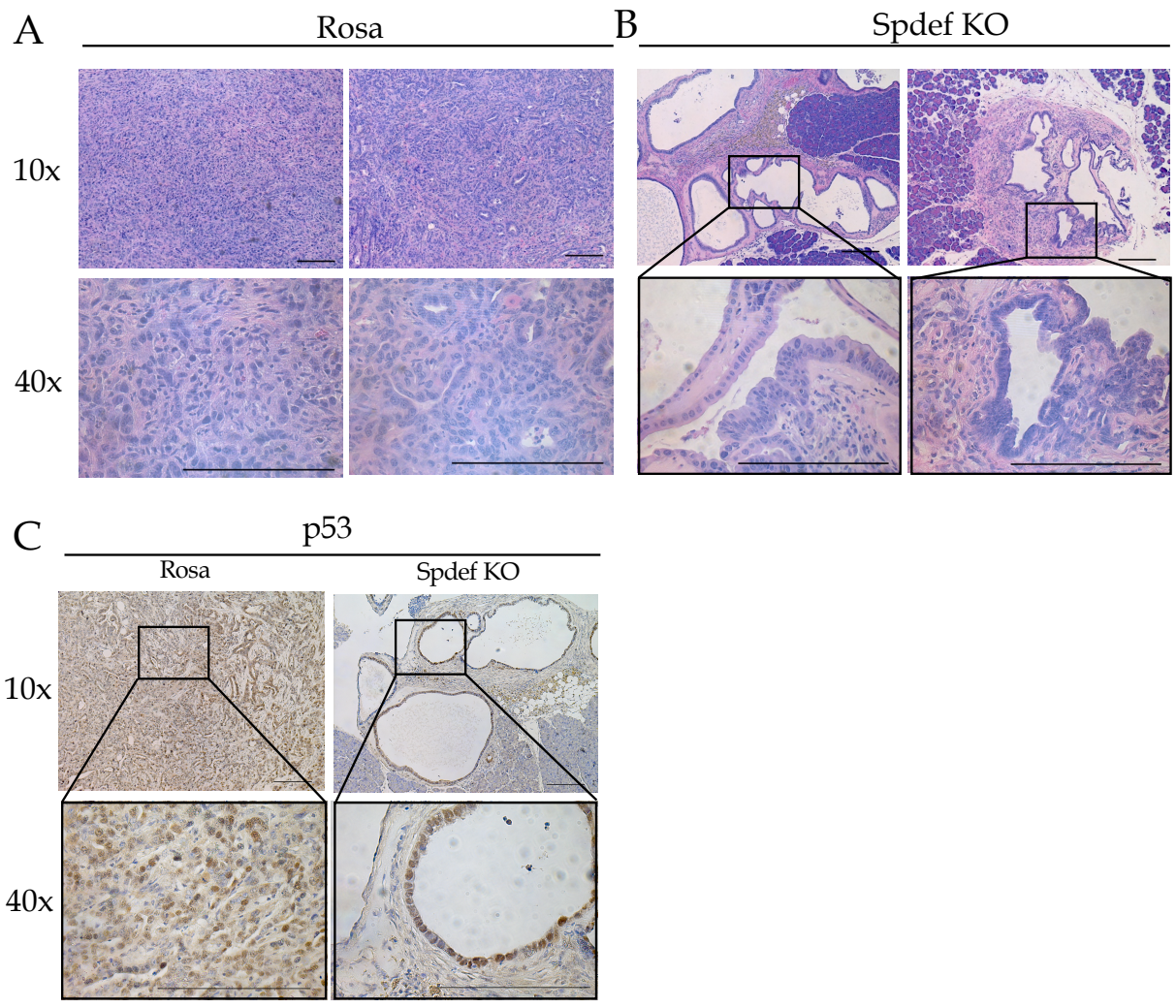

Figure 4.3 Spdef KO impairs orthotopic growth of tumor organoids in vivo.

A) Representative images of H&E staining of mT69a Rosa orthotopic organoid transplants 6 weeks post transplantation (scale bar: 200 μm)
B) Representative images of H&E staining of mT69a Spdef KO organoid transplants 6 weeks post transplantation (scale bar: 200 μm)
C) Representative images of IHC staining for p53 in mT69a Rosa and mT69a Spdef KO organoid transplants (scale bar: 200 μm)

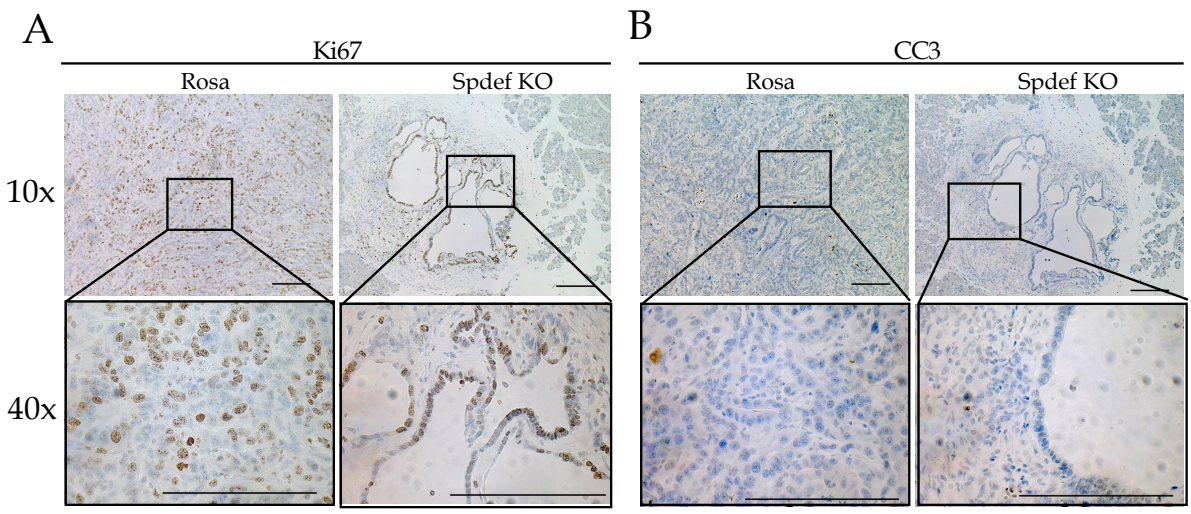

Figure 4.4 Spdef KO does not affect proliferation of apoptosis of orthotopically transplanted organoids.
A) Representative images of IHC staining for Ki67 in mT69a Rosa and mT69a Spdef KO organoid transplants (scale bar: 200 μm)
B) Representative images of IHC staining for cleaved caspase 3 in mT69a Rosa and mT69a Spdef KO organoid transplants (scale bar: 200 μm)

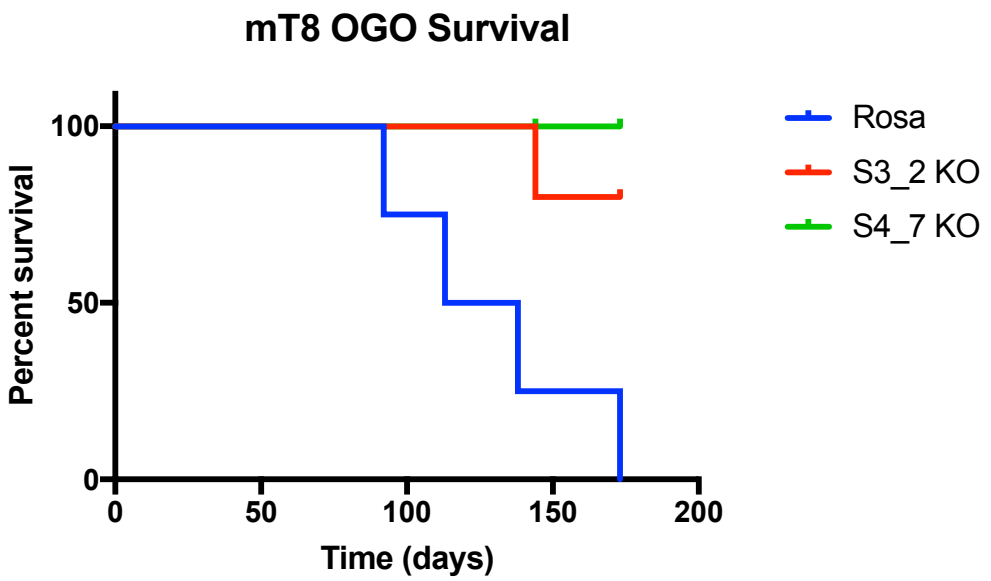

Figure 4.5 Spdef KO extends survival in an orthotopic transplantation model. Kaplan-Meier survival curve of mT8 organoids KO for Spdef or expressing a control Rosa gRNA (Rosa: n=4; S3_2 KO: n=5; S4_7 KO: n=5)

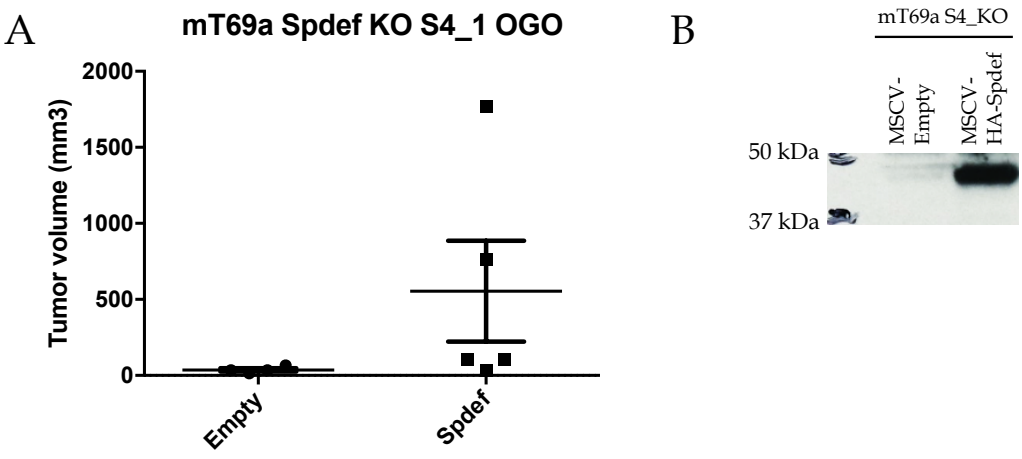

Figure 4.6 Re-expression of Spdef in Spdef KO organoids rescues tumor growth phenotype in vivo.
A) Quantification of orthotopically transplanted mT69a SpdefKO organoids expressing an MSCV empty vector and Spdef-HA cDNA.
B) WB for Spdef to confirm Spdef HA expression

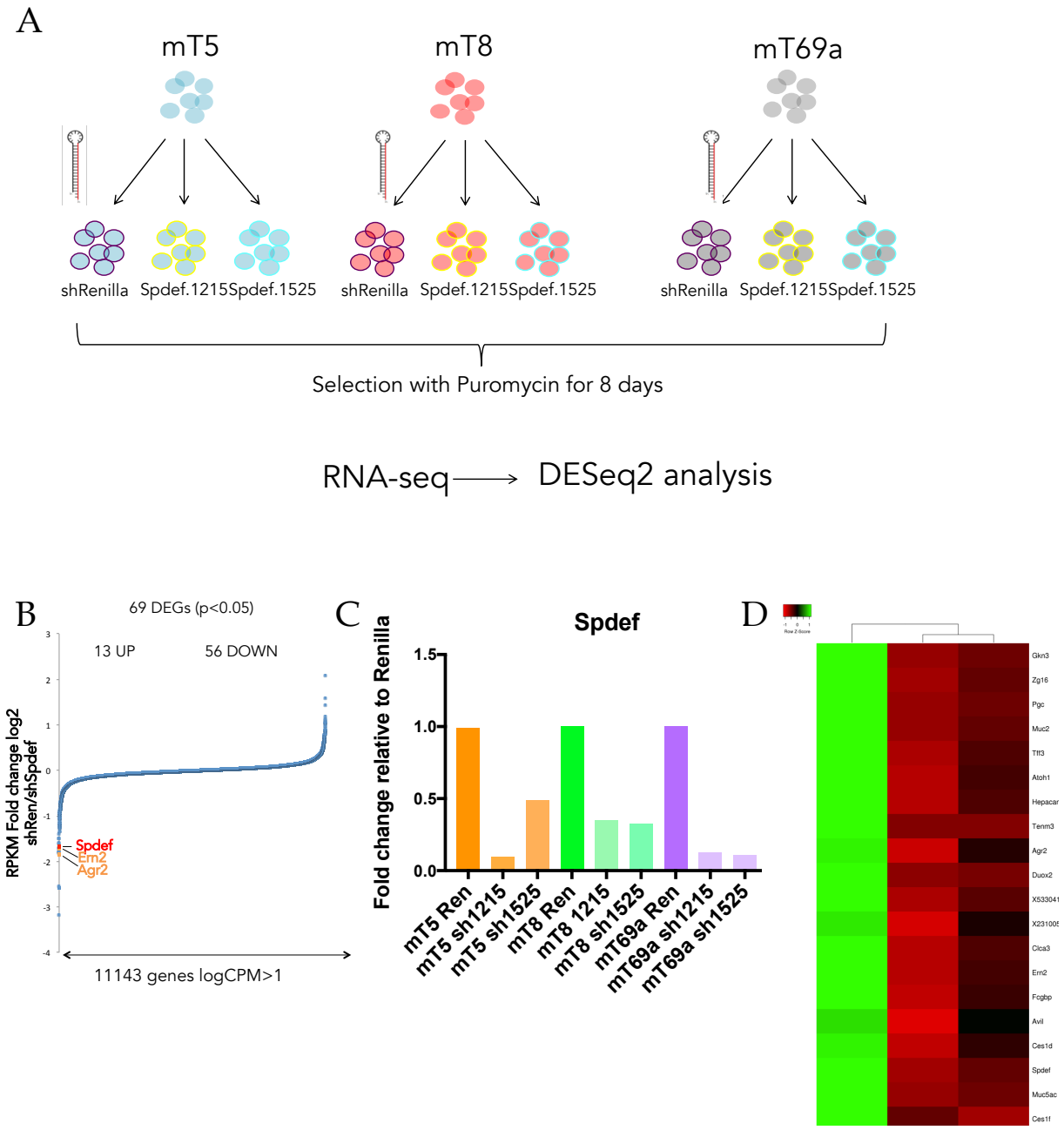

Figure 4.7 RNA-seq following Spdef KO in tumor organoids

A) Experimental design for RNA-seq experiment

B) RNA-seq analysis of gene expression changes in 3 tumor organoid lines expressing shRNAs against Spdef. Averaged RPKM values for 2 independent shRNAs were normalized to mRNA levels in control cells expressing shRen. Genes with RPKM<1 in the shRen sample were excluded. Genes are plotted from the most down-regulated genes on the left to the most upregulated genes on the right.

C) Normalized expression of Spdef in organoids used for RNA-seq in A.

D) Heatmap of top differentially expressed genes between Renilla control and Spdef shRNA-expressing organoid. Each row represents a gene and each column represents the averaged expression of each gene normalized within the biological replicates.

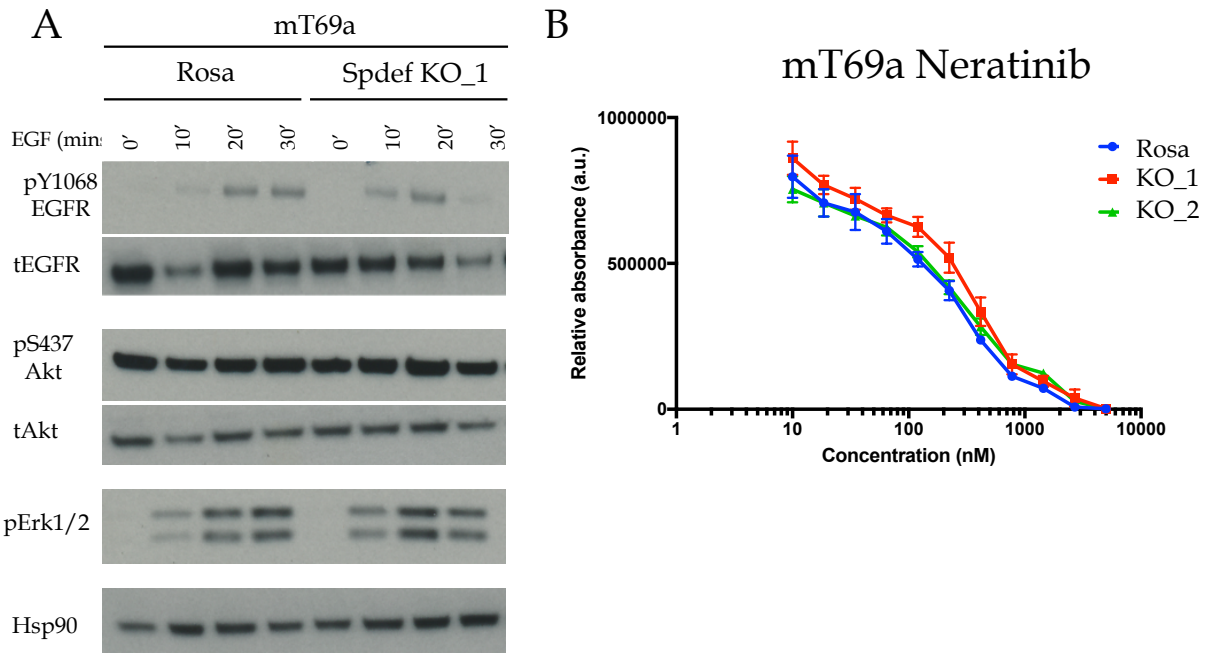

Figure 4.8 Spdef KO does not impair Erbb signalling

A) WB for pY1068 Egfr, total Egfr, pS437 Akt, total Akt, pErk1/2 and Hsp90 (loading control) in mT69a Rosa and Spdef KO organoids

B) EC survival of mT69a Rosa and Spdef KO organoids grown in the presence of Neratinib for 4 days measured by CellTiterGlo. Relative fold change in arbitrary luminescence unit normalized to Day 0 is plotted at different concentrations of Neratinib.

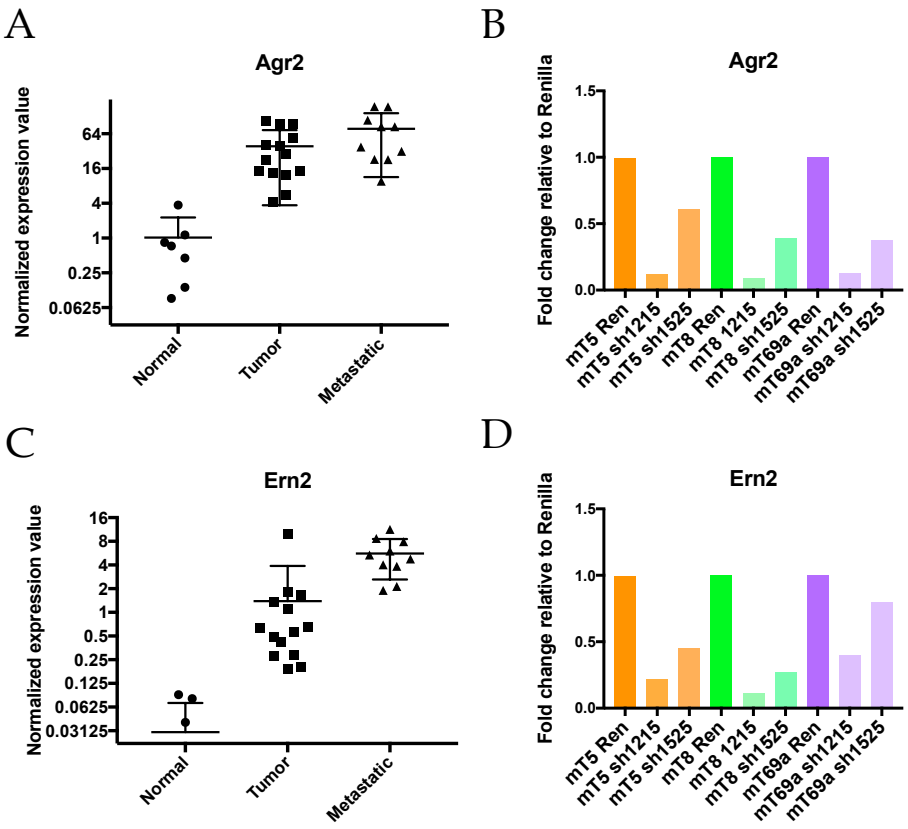

Figure 4.9 Spdef regulates the expression of Agr2 and Ern2 murine PDAC organoids.
A) Normalized expression values of Agr2 from RNAseq of normal, tumor and metastatic organoids.
B) Fold change of Agr2 expression normalized to Renilla-infected control organoids.
C) Normalized expression values of Ern2 from RNAseq of normal, tumor and metastatic organoids.
D) Fold change of Ern2 expression normalized to Renilla-infected control organoids.

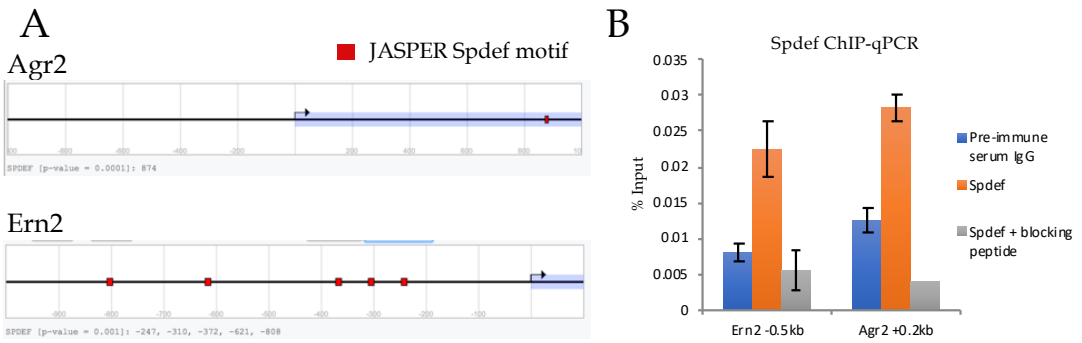

Figure 4.10. Spdef directly regulates the expression of the GI-specific gene Ern2 in murine PDAC organoids.

A) In silico motif analysis of Ern2 and Agr2 regulatory regions for Spdef binding motif ($p<0.01$)

B) ChIP-qPCR of Spdef for Ern2 +1.5kb . % input DNA is ploted for pre-immune serum IgG (control), Spdef IP and Spdef IP with a antibody blocking peptide

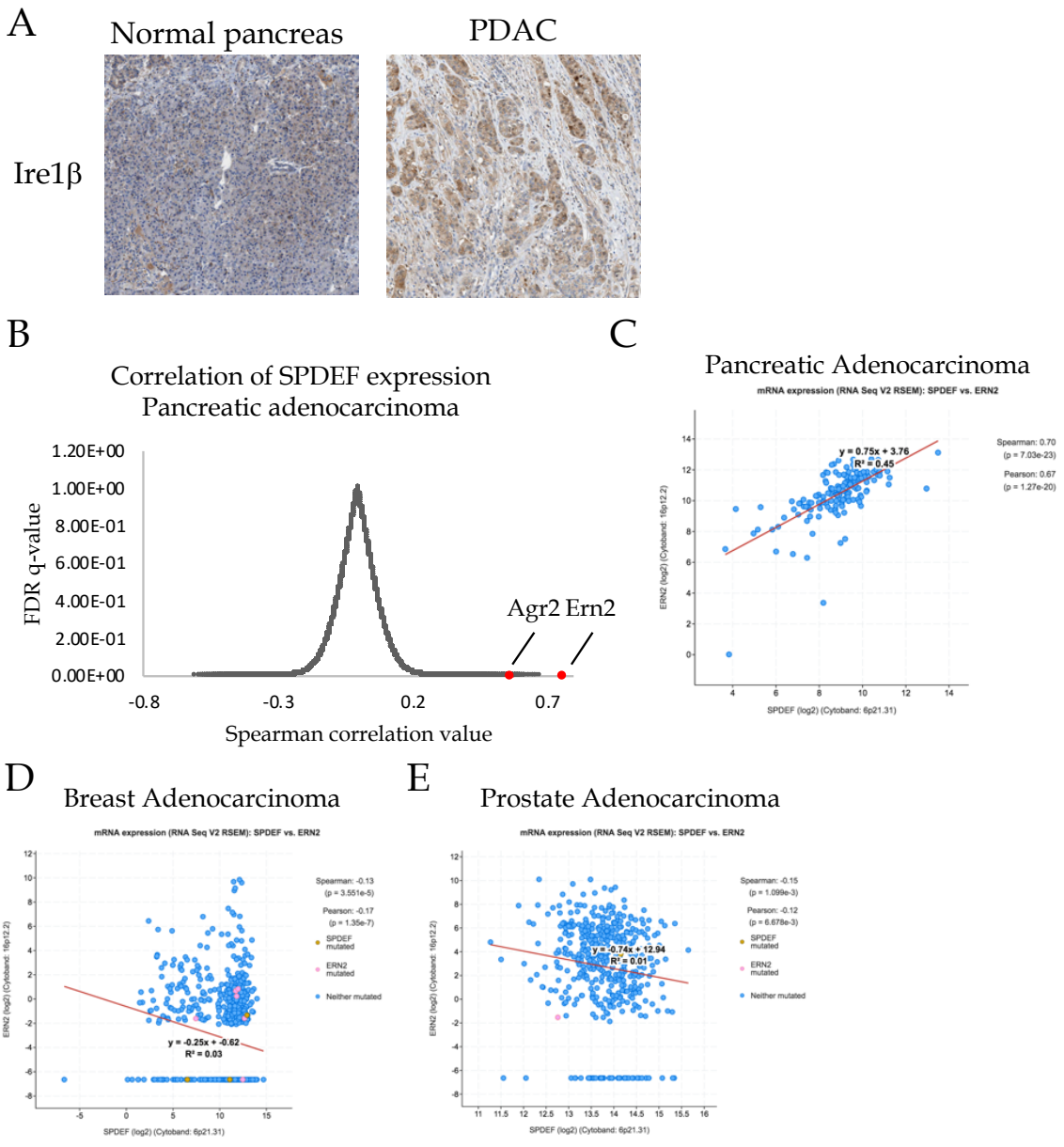

Figure 4.11 ERN2 is upregulated in human PDAC samples and its expression correlates with SPDEF in PDAC.

A) IHC staining for Ire1β from Human Protein Atlas database
B) Correlation of gene expression with SPDEF by RNA-seq in PDAC tumor samples from TCGA. Ern2 is the most highly correlated gene.
C) Correlation of ERN2 expression with Spdef in PDAC tumor samples from TCGA as measured by RNA-seq
D) Correlation of ERN2 expression with Spdef in breast adenocarcinoma tumor samples from TCGA as measured by RNA-seq
E) Correlation of ERN2 expression with Spdef in prostate adenocarcinoma tumor samples from TCGA as measured by RNA-seq

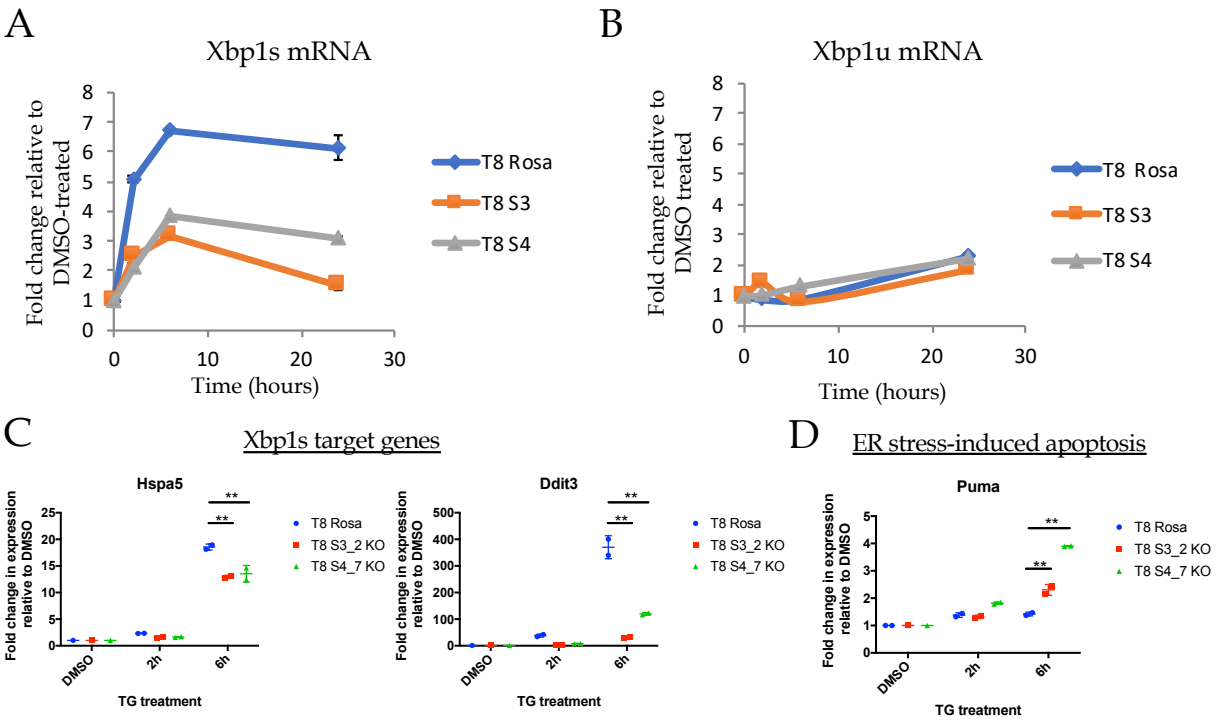

Figure 4.12. Xbp1 splicing in response to ER stress is attenuated in Spdef KO organoids

A) RT-qPCR for Xbp1s (spliced) following treatment with 50nM of thapsigargin at indicated time-points
B) RT-qPCR for Xbp1u (unspliced) following treatment with 50nM of thapsigargin at indicated time-points
C) RT-qPCR for Xbp1s target genes (Hspa5 and Ddit3) following treatment with 50nM of thapsigargin at indicated time-points
D) RT-qPCR for ER-stress induced apoptotic genes (Puma) following treatment with 50nM of thapsigargin at indicated time-points

A

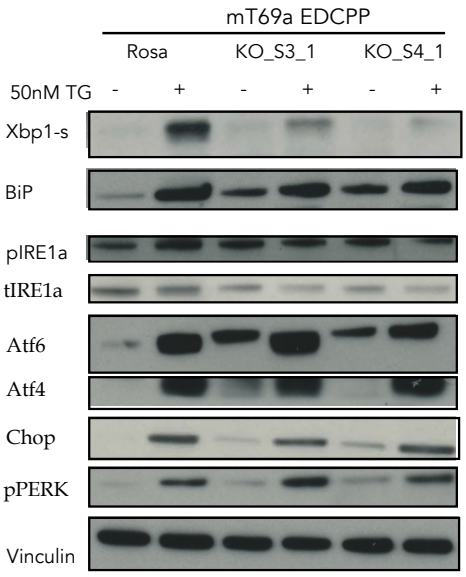

Figure 4.13. Activation status of UPR pathways in Spdef KO organoids by WB following 50nM TG treatment for 6 hours

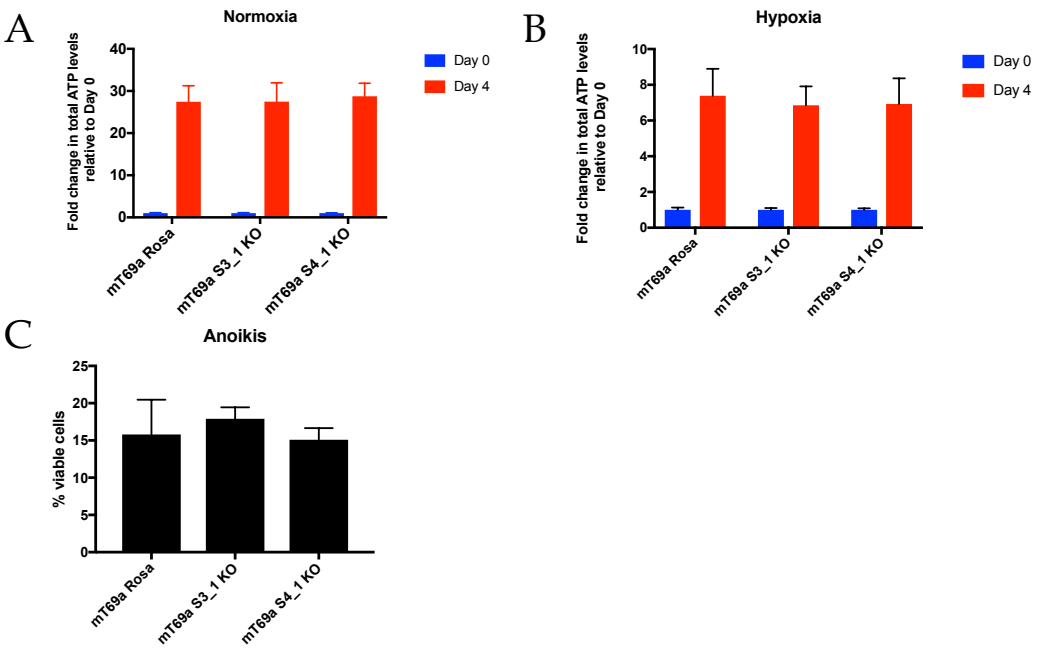

Figure 4.14 Survival of Spdef KO organoids in hypoxic and anoikis conditions.

A) Relative proliferation ratio (Day 4 / Day 0 counts) for Rosa and Spdef KO mT69a organoids in normoxia conditions (20% O2)

B) Relative proliferation ratio (Day 4 / Day 0 counts) for Rosa and Spdef KO mT69a organoids in hypoxia conditions (1% O2)

C) Percentage of viable anchorage-independent cells from organoids grown for 24 hours in non-adherent plates as measured by ratio of the number of Acridine orange cells (total number of cells) over propidium iodine positive cells (dead cells).

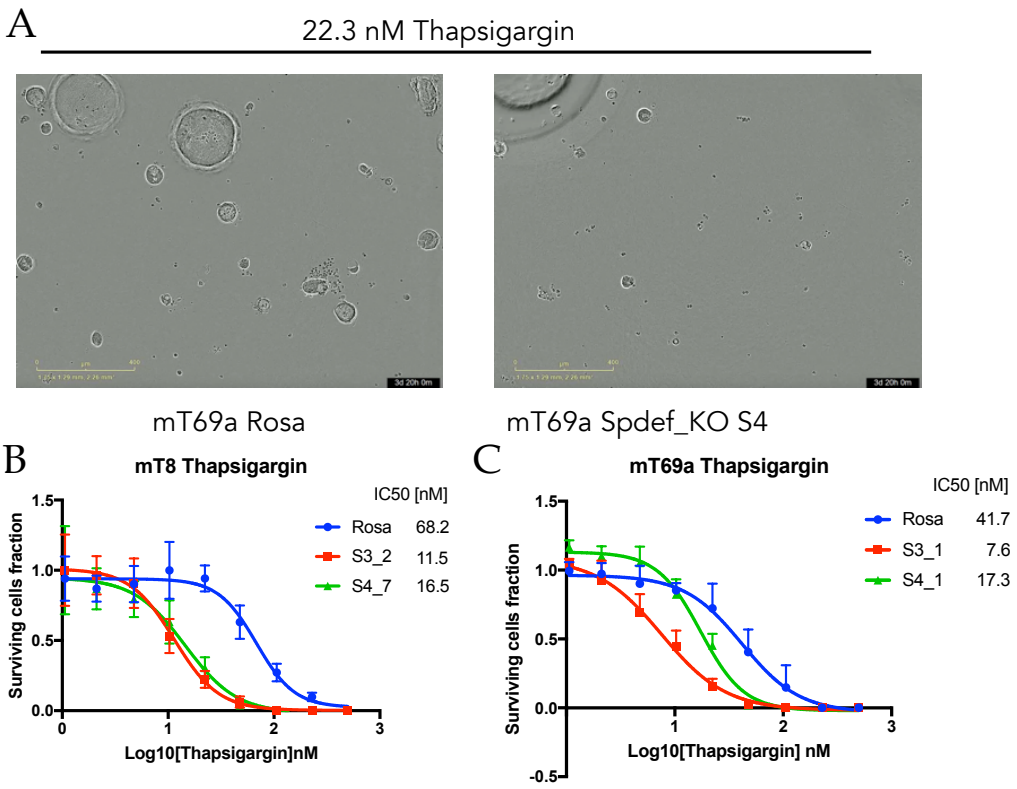

Figure 4.15 Spdef regulates ER homeostasis and protects PDAC organoids from ER-stress-induced cell death.
A) GI50 dose response curves of T8 tumor organoids treated with varying concentrations of Thapsigargin.
B) GI50 dose response curves of T69a tumor organoids treated with varying concentrations of Thapsigargin.
C) Representative images from Rosa and Spdef KO tumor organoids after 4 days of treatment with 22.3 nM of Thapsigargin.

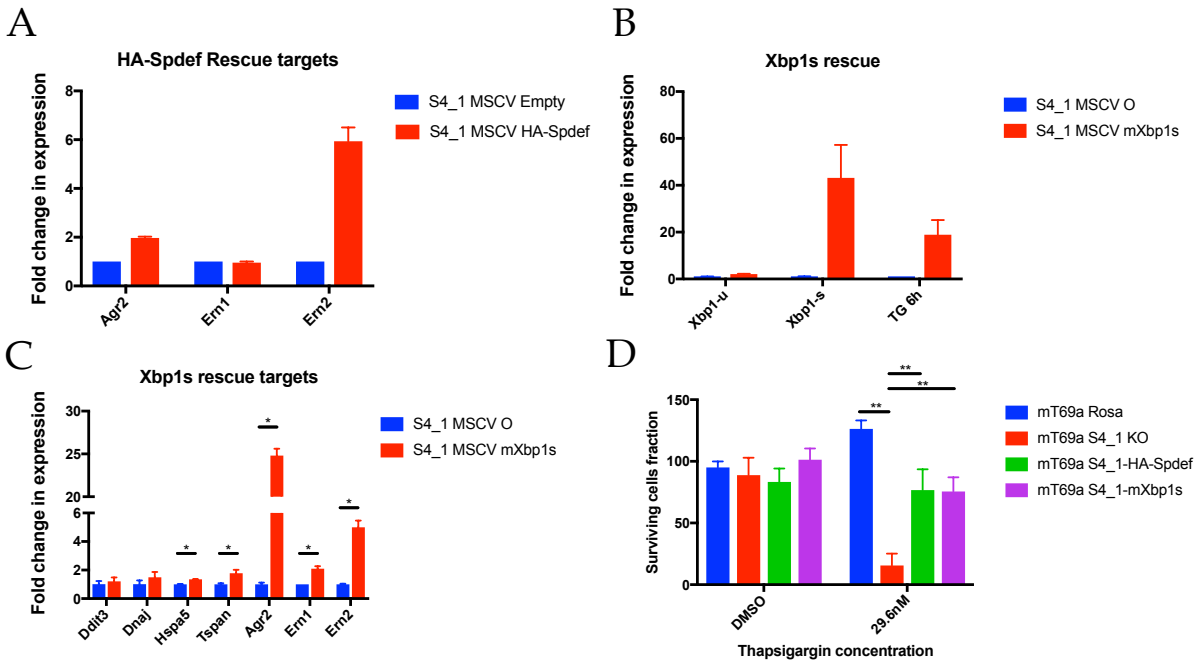

Figure 4.16 Spdef regulates ER homeostasis and protects PDAC organoids from ER-stress-induced cell death.

A) mRNA expression of Agr2, Ern1 and Ern2 in mT69a_Spdef KO organoids infected with an empty vector or MSCV-HA-Spdef normalized to Hprt levels within each sample and to empty vector values across samples.

B) mRNA expression of Xbp1-s and Xbp1-u in mT69a_Spdef KO organoids infected with an empty vector or MSCV-Xbp1s normalized to Actb levels within each sample and to empty vector values across samples.

C) mRNA expression of Xbp1-s in mT69a treated with TG for 6 hours normalized to Actb levels within each sample and to untreated control values across samples.

D) Cell viability measured by CellTiterGlo assay of Rosa, Spdef KO, Spdef KO HA-Spdef Rescue and Spdef KO mXbp1s Rescue organoids after 4 days of treatment with 22.3 nM of Thapsigargin.

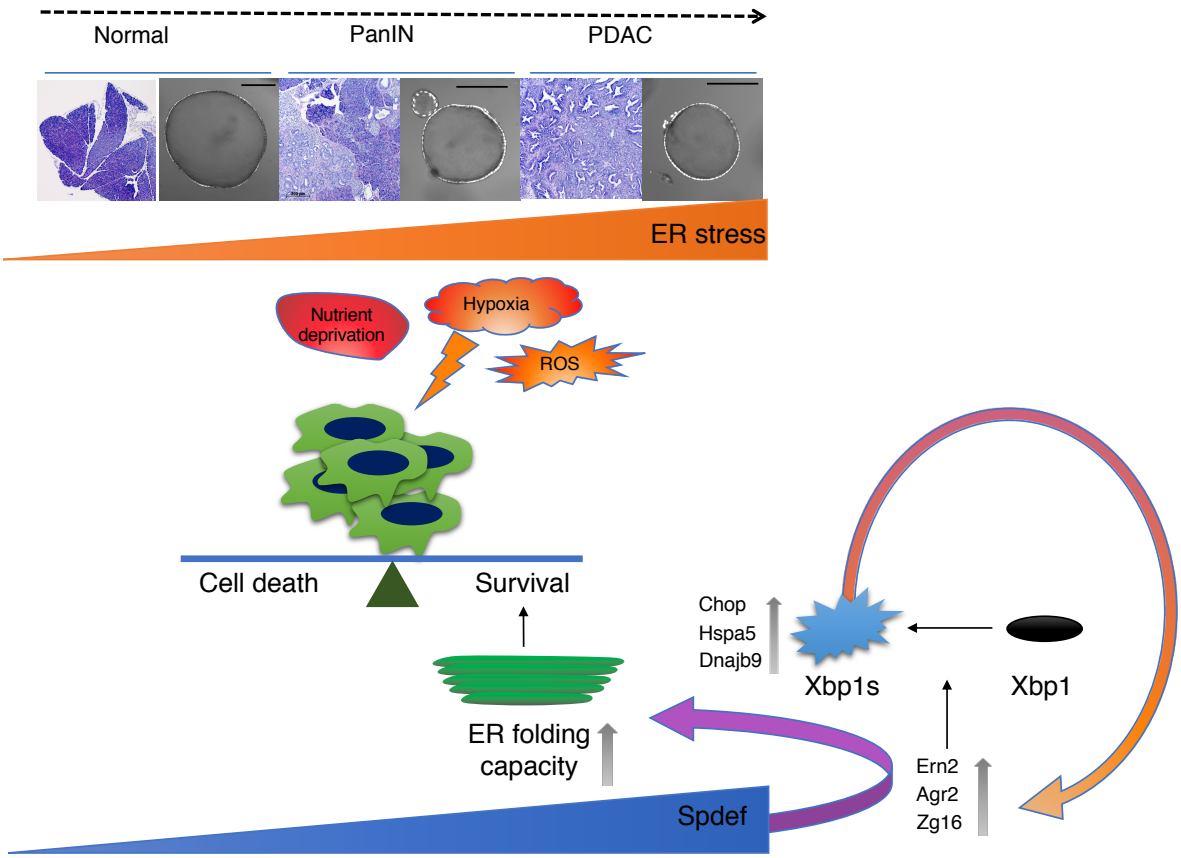

Figure 4.17. Model of Spdef acting as a survival factor by directly regulating the expression of UPR genes and protecting cancer cells from ER-stress-induced cell death. Nutrient deprivation, hypoxia and ROS expose tumor cells to high levels of ER stress. Spdef levels increase during PDAC tumorigenesis and lead to increased expression of multiple UPR genes (ern2, Agr2, Zg16). The protein product of Ern2, Ire1b, initiates the non-canonical splicing of the mRNA of Xbp1, producing Xbp1s – a highly active transcription factor . Xbp1s induces the expression of multiple UPR genes involved in increasing the protein folding capacity of the ER.

CHAPTER 6. CONCLUSIONS AND PERSPECTIVES

This study investigated the oncogenic roles of two transcription factors in pancreatic cancer: Myc and Spdef. Using a 3D organoid model of PDAC, we showed that Myc's activity changes with tumor progression, which was not reflected by its protein levels. This induction of its activity could be explained by the differential affinity of Myc for its target genes exhibited in tumor organoids. We hypothesize that Myc could cooperate with tumor-specific transcriptional regulators, including transcription factors, such as the ETS factor Spdef, to induce a tumor-specific transcriptional program that drives oncogenesis. We also identified a previously unappreciated dependency of pancreatic cancer on Spdef, seemingly independent of Myc. Spdef expression is induced during the early PanIN stages of pancreatic cancer, both *in vivo* and in *ex vivo* organoid cultures, and it is the most highly upregulated transcription factor in tumor organoids. We showed that by direct transcriptional activation of genes involved in the unfolded protein response, Spdef could protect tumor cells from ER-stress-induced cell death and thus promote tumorigenesis *in vivo*.

The multi-faceted functions of transcription factors as central nodes of converging cell signaling pathways that promote tumorigenesis make them coveted therapeutic targets. However, they remain notoriously hard to target directly by traditional small molecule inhibitors (Lambert et al. 2018). In the case of Myc the absence of a well-defined ligand binding pocket has stymied progress in developing targeted inhibitors. Efforts to inhibit its expression through general BET bromodomain inhibitors such as JQ1 and OTX015 have suffered from the lack of selectivity and quick tumor-adaptive responses (Shu et al. 2016; Kurimchak et al. 2016; Shi et al. 2016). More selective strategies to inhibit MYC have focused on small molecule inhibitors disrupting the interaction between MYC and its direct binding partner, the transcription factor MAX. However, inhibiting MYC-MAX interaction *in vivo* has been limited

by fast metabolism, poor potency, resistance mechanisms, and poor tumor penetrability of these small molecule inhibitors (Guo et al. 2009; Whitfield et al. 2017). A promising approach of using cell-penetrating Omomyc peptides to inhibit Myc's function was recently described by two groups, but the clinical pharmacokinetic/pharmacodynamic profiles of peptides remain to be investigated (Wang et al. 2019; Beaulieu et al. 2019). Despite these advances there have been no successful Myc inhibitors in the clinic. This work proposes two new approaches to target Myc – 1) by understanding the tumor-specific effector pathways of its function and 2) by targeting the tumor-specific co-operation between Myc and other transcription factors.

Our work also identified a new potential role for the ETS factor Spdef in promoting pancreatic cancer by directly regulating the expression of genes involved the response to ER stress. Spdef is not expressed in mouse or human 2D cultures, underscoring the importance of using physiologically relevant systems like the organoid model of PDAC. Previous studies have supported the utility of inhibiting the UPR as a monotherapy or, in combination with chemotherapy, as a therapeutic approach in pancreatic cancer (Nawrocki et al. 2005a, 2005b; Thakur et al. 2018). Although further experiments are needed to confirm that regulating the UPR is the sole effector of the tumor-promoting role of Spdef in PDAC, our data suggest that targeting this transcription factor might be a viable therapeutic option. To confirm that Spdef is required for the maintenance of PDAC tumors *in vivo,* we transplanted tumor organoids expressing an inducible ddCas9 protein and a gRNA targeting either a Rosa control genomic region or the Spdef gene. Unfortunately, this experiment did not lead to cleavage of the targeted Spdef region and thus had no effect on tumor size. We are now approaching this issue using RNAi by transplanting mice with tumor organoids expressing doxycycline-inducible shRNA hairpins against Spdef and inducing expression of the hairpin by

administering doxycycline via their drinking water *in vivo* after tumors formed. These experiments will further validate Spdef as a therapeutic target in PDAC.

A recent interest in the field of targeted protein degraders might offer a solution to the issues related to directly inhibiting transcription factors therapeutically (Mullard 2019). The idea behind this technology is that using functional ligands that can recruit E3 ubiquitin ligases could allow one to design targeted bifunctional molecules whereby one part of the molecule binds to a target protein while the other tags it for proteosomal degradation by an E3 ubiquitin ligase (Cromm and Crews 2017). The promise of using TPDs to target transcription factors lies in their mechanism of action. In contrast to typical small molecule inhibitors, TPDs could degrade proteins even if they do not have a well-defined catalytic domain. Moreover, a TPD can bind anywhere on the surface of the target protein thus expanding the probability of finding a good binder significantly. The first TPD has now entered the clinic targeting the androgen receptor and multiple groups have shown success in degrading 'undruggable' targets including EBB3, Tau, TACC3 (Lai and Crews 2017).

Within the next decade, pancreatic cancer is projected to become the second-leading cause of cancer related deaths in the USA, which reflects the inadequacy of the treatment options for this disease (Rahib et al. 2014). Surgery is currently the only long-term option for these patients but longer follow-up has shown that only 4% of patients live more than 10 years after surgery (Paniccia et al. 2015). Pancreatic cancer generally recurs within six months if no postoperative treatment is given. Even with adjuvant chemotherapy, most patients will survive less than three years. The dire statistics for this disease become even more devastating when we consider that only 20% of patients are candidates for surgical resection and the median survival for those who aren't is merely 8-9 months following diagnosis. Despite the transformative effects of the recent advances in immunotherapy and personalized medicine

in other solid tumors, the current first-line standard of care for patients with PDAC remains chemotherapy – gemcitabine or Folfirinox. Folfirinox is a combination chemotherapy consisting of four agents (oxaliplatin, irinotecan, fluorouracil, and leucovorin), and recent clinical trials have reported significant increase in both disease-free and overall survival in both adjuvant post-surgery and metastatic settings (Conroy et al. 2011, 2018). Recent advances in cataloguing the genetic drivers of the disease have revealed few new actionable mutations (Liu et al. 2016b). The breakthrough discovery of the synthetic lethal relationship between inactivating mutations in the BRCA1/2 proteins and PARP enzymes has led to the development of multiple PARP inhibitors, such as olaparib, that have shown significant efficacy in the clinic (Robson et al. 2017). In a recently conducted Phase 3 trial, maintenance therapy with olaparib in patients with metastatic pancreatic cancer with a germline mutation in BRCA1/2 doubled progression-free survival, making olaparib one of the few promising targeted therapies for a small subset of patients (3-5%) (Golan et al. 2019). Nevertheless, pancreatic cancer remains a significant medical challenge. We hope that this study opens up new avenues for developing targeted therapies against this devastating disease.

CHAPTER 7. MATERIALS AND METHODS

Organoids

Organoids were isolated and cultured as previously described (Boj et al. 2015). +++ media was used for all washes during organoid passaging and is defined as Advanced DMEM supplemented with 1% Penicilin/streptomycin, 10mM HEPES (Thermo), 20mM Glutamax (Thermo). Briefly, organoids were maintained in 100% Matrigel domes (Corning) and grown in Advanced DMEM +++ media supplemented with B27 (Invitrogen), 1.25 mM N-Acetylcysteine (Sigma), 10 nM gastrin (Sigma) and the growth factors: 50 ng/ml EGF (Peprotech), 10% RSPO1-conditioned media (kindly provided by Calvin Kuo), 100 ng/ml Noggin (Peprotech), 100 ng/ml FGF10 (Peprotech) and 10 mM Nicotinamide (Sigma). To prepare frozen stocks, organoid cultures were dissociated and mixed with Recovery cell culture freezing medium (Gibco) and froze following the standard procedures. When required, the cultures were thawed using standard thawing procedures, embedded in Matrigel and cultured as described above. For the first 3 days after thawing, the culture medium was supplemented with Y-27632 (10 µM, Sigma-Aldrich).

Animals

All animal experiments were reviewed and approved by the IACUC of Cold Spring Harbor Laboratory. 6-8-week-old Nu/Nu mice were used as recipients for orthotopic transplantation (Charles River). The number of animals in each experiment is stated in the figure legends.

Orthotopic transplantation of organoids

All transplanted cells were resuspended in 50 ul of 50% matrigel (diluted in sterile 1xPBS). Organoids were dissociated into single cells as described under "organoid culture". 20,000 mT69a cells and 350,000 mT8 organoids were transplanted per animal. All tools used for the surgery were sterilized and surgical site was cleaned with betadine prior to surgery. Mice were maintained under 2% inhalation Isofluorane for the duration of surgery. 5mg/kg Ketofen was give prior to surgery as prophylactic anesthesia. A 1-cm incision was made in the skin and peritoneum above the spleen. The pancreas was placed outside the abdominal cavity by gently lifting the spleen. Cells were injected into the tail of the pancreas. Silk sutures were used to close the peritoneal incision and wound clips were used for the skin incision. Mice were allowed to recover from anesthesia in a heated chamber before return to their cages.

Plasmids

For Spdef RNA-seq experiments MSCV-miRE-shRNA-PGK-PuroR-IRES-GFP retroviral vectors were used. cDNA constructs were expressed from an MSCV-based vector containg either a puromycin or neomycin resistance gene. CRISPR knockout experiments were used using a modified EDCPP lentiviral vector system.

Antibodies

Spdef antibodies were produced through a contract with Thermo Fisher. Briefly, Based on hydrophobicity, hydrophilicity and specificity scores generated from a proprietary Thermo Fisher algorithm and the NIH AbDesigner tool (https://hpcwebapps.cit.nih.gov/AbDesigner/), two peptides were selected (spanning amino acids 33-50 and 75-91) of the mouse Spdef protein to use as antigens. Each peptide was used to immunize two rabbits with 3 subsequent boosts (day 14, 42 and 56) and bleeds were

collected 72 days following initial immunization. The antibodies were affinity purified using the immunizing peptide.

Table 1. Antibodies

Antibody target	Vendor	Catalog No.	Host species	WB	IHC	IP	ChIP
Spdef 1161	Thermo	NA	Rabbit	1:1000	1:1000	1ug	-
Myc N262	Santa Cruz	Sc-764	Rabbit	-	-	-	5ug
Myc	Abcam	Ab32702	Rabbit	1:1000	-	-	-
Ki67	Thermo	MA5-14520	Rabbit	-	1:200	-	-
Cleaved Caspase 3	CST	9661S	Rabbit	-	1:200	-	-
P53			Rabbit	-		-	-
Vinculin	CST	13901S	Rabbit	1:5000	-	-	-
EGFR pY1068	CST	2234S	Rabbit	1:1000	-	-	-
EGFR	CST	4267S	Rabbit	1:1000	-	-	-
AKT pS437	CST	4060S	Rabbit	1:1000	-	-	-
AKT	CST	9272S	Rabbit	1:1000	-	-	-
pERK1/2	CST	9101S	Rabbit	1:1000	-	-	-
Hsp90	Millipore	05-594	Rabbit	1:1000	-	-	-
Xbp1-s	CST	12782S	Rabbit	1:1000	-	-	-
BiP	CST	3117S	Rabbit	1:1000	-	-	-
pIRE1a	Novus	NB100-2323	Rabbit	1:1000	-	-	-
IRE1a	CST	3294	Rabbit	1:1000	-	-	-
Atf6	Novus	70B1413.1	Rabbit	1:1000	-	-	-
Atf4	Proteintech	10835-1-AP	Rabbit	1:1000	-	-	-
Chop	Thermo	MA1-250	Rabbit	1:1000	-	-	-

pPERK	CST	3179	Rabbit	1:1000	-	-	-

Table 2. Oligonucletide sequences

Name	Sequence	Application
Spdef.1215 miRE	TGCTGTTGACAGTGAGCGCAGGAGAAAGGCAT CTTCAAAATAGTGAAGCCACAGATGTATTTTGA AGATGCCTTTCTCCTTTGCCTACTGCCTCGGA	shRNA
Spdef.1525 miRE	TGCTGTTGACAGTGAGCGAACAGCCACTGATCT AGGGATATAGTGAAGCCACAGATGTATATCCCT AGATCAGTGGCTGTCTGCCTACTGCCTCGGA	shRNA
Sh R.luciferase miRE	TGCTGTTGACAGTGAGCGCAGGAATTATAATGC TTATCTATAGTGAAGCCACAGATGTATAGATAA GCATTATAATTCCTATGCCTACTGCCTCGGA	shRNA
Spdef_2	CCGGTTGCCTGCTACTGTT	gRNA
Spdef_3	CCTGGACATCTGGAAGTCAG	gRNA
Rosa	TAGGAGCCATGGCCGCGTCCGG	gRNA
Xbp1s Fwd	CTGAGTCCGAATCAGGTGCAG	RT-qPCR
Xbp1s Rev	GTCCATGGGAAGATGTTCTGG	RT-qPCR
Xbp1u Fwd	CAGCACTCAGACTATGTGCA	RT-qPCR
Xbp1s Rev	GTCCATGGGAAGATGTTCTGG	RT-qPCR
Spdef Fwd	GTGCAATCGATGGTTGTGGG	RT-qPCR
Spdef Rev	CCAGGGTCTGCTGTGATGTT	RT-qPCR
Actb Fwd	TTGCTGACAGGATGCAGAAG	RT-qPCR
Actb Rev	ACATCTGCTGGAAGGTGGAC	RT-qPCR

Retroviral production and infection

Transient transfection was performed using XtremeGene 9 (Sigma). For retroviral packaging, Phoenix cells stably expressing ecotropic envelope proteins were used. Phoenix cells were transfected with 20ug of plasmid of interest and virus was collected 48-72 hrs post

transfection. For lentiviruses, 293T cells were co-transfected with 1:2:2 molar ratio of plasmid of interest and pMD.2 and psPAX plasmids. For infection, dissociated organoids were resuspended in +++ media containing retrovirus and polybrene and centrifuged for 1-2 hours at 800g. Antibiotic selection of retrovirally-infected organoids (puromycin 2ug/mL) or neomycin (1mg/mL) was performed for at least 48 hours beginning 24 hours after infection.

Co-immunoprecipitation

Cells were grown in 15cm plates were washed three times with ice-cold PBS. 1mL of ice cold lysis buffer (1mM Tris pH 8, 150nM NaCl, 1% Triton-X, 2mM EDTA) supplemented with protease and phosphatase inhibitor cocktail tablets (Roche) was added directly onto the plates. Cells were collected using a cell lifter and incubated on ice for 15 minutes with intermittent vortexing every 5 minutes. Lysed cells were cleared of any insoluble cell debri by centrifugation (12,000 g for 5 mins at 4C). Supernatant was used to determine protein concentration by DC protein assay. 1 mg of protein was used for each immunoprecipitation and 25ug of each lysate was saved as input. Antibodies or pre-conjugated antibody-bead complexes were added according to Table and incubated with constant agitation overnight at 4C. To remove any non-specific binders, the beads were washed three times with Lysis buffer followed by a final wash with PBS. To elute antigens, a 2X LDS Loading buffer in lysis buffer was used. Samples were boiled at 90C for 5 minutes and magnetic beads were removed using a magnet. Samples were then processed for Western blotting.

Western blotting

Standard techniques were employed for immunoblotting of mouse organoids. Organoids were quickly harvested using cold PBS on ice. Organoids were then lysed with 25

mM HEPES, pH 7.5; 150 mM NaCl; 1% NP-40; 10 mM MgCl2; 1 mM EDTA; 2% Glycerol. Protein lysates were separated in 4-12% Bis-Tris NuPage gels (Life Technologies). Western blots were probed with the antibodies in Table.

Antibody bead conjugation

Except for the commercially available anti-Flag M2 (Sigma, M8823) and anti-HA (Thermo, 10003D) magnetic beads, all other antibodies used for co-immunoprecipitation experiments were cross-linked to Protein A/G Dynabeads beads (Thermo, 88802). 1ug of antibody was coupled to 30uL of Protein A/G magnetic beads for 30 minutes at room temperature. Bead-antibody complexes were then resuspended in 250uL of 5mM BS3 (bis(sulfosuccinimidyl)suberate) and incubated at room temperateure for 30 minutes. Bead-antibody complexes were then resuspended in 0.125M of PBS/Glycine and incubated for 5 mins. Cross-linked beads were washed in TBS/0.1% Tween and used for immunoprecipitation experiments.

Chromatin immunoprecipitaton:

For organoid cultures:

Organoids were maintained in complete organoid media until subconfluent. To dissociate organoids from the matrigel, complete media was replaced with a 2ug/mL dispase dissolved in Advanced DMEM +++ media and incubated for 20 minutes in a 37 C incubator. Organoids were washed with Advanced DMEM +++ media and pelleted at 300g for 5 mins at 4 C. To dissociate organoids to single cells, organoid pellets was resuspended in 1mL of TryplE and incubated at 37C for 12 minutes with constant agitation (650rpm). Cells were washed with Advanced DMEM +++ and pelleted at 300g for 5 mins at 4 C. Final pellet was

resuspended in 500 uL and cells were counted using a life/dead Acridine Orange/Propidium Iodine stain. 5x10^6 cells were resuspended in 2 mL of 1% Forlmaldehyde in Advanced DMEM +++ media and incubated for 12 minutes rocking at room temperature. To quench formaldehyde, glycine was added to 0.125M concentration and the cell solution was incubated for 5 minutes. Cells were pelleted by centrifugation at 300g for 5 minutes at 4C. Cell pellet was washed 1x with ice-cold PBS and pelleted at 300g for 5 minutes at 4C. Pellets were snap-frozen on dry ice and stored at -80C until ready for further processing.

For adherent 2D cultures:

1% formaldehyde was added to 2D media and cells were incubated for 10 minutes at room temperature. Formaldehyde was quenched with 0.125M glycine for 5 minutes. Plates were washed 3x with PBS and cells were scraped and resuspended in 1mL of PBS using a cell lifter. Cells were pelleted at 300g for 5 minutes at 4C and pellets were snap-frozen on dry ice and stored at -80C until ready for further processing.

Immunoprecipitation:

To isolate intact nuclei, 5x10^6 Fixed cells were resuspended in cell lysis buffer and incubated on ice for 15 minutes. Nuclei were pelleted by centrifugation () and resupsended in nuclear lysis buffer. Chromatin was sheared by sonication using a Bioruptor with 30s on/off cycles at low instensity. Chromatin shearing was empirically tested by reverse-crosslinking the DNA at 65C for 2 hours followed by DNA extraction using a PCR purification kit (Invitrogen). Purified DNA was run on a 2% agarose gel at 100V for 25 minutes. For a successful ChIP experiment, chromatin was expected to be between 200 and 500 bp. Sheared chromatin was cleared by centrifugation at 15000g for 10 minutes at 4C. The supernatant was diluted with IP dilution buffer to 1mL and 50uL were saved for input control (1:200). Antibodies (amounts/volumes are specified in Table) were added and the solution was

incubated at 4C on a rocker overnight. Protein A/G magnetic beads were blocked in 5% BSA/TBST and washed 3x with TBST. Antibody-chromatin complexes were centrifuged at 12,000g for 10 minutes to remove antibody aggregates and 30uL of blocked beads were added and incubated at 4C on a rocker for 3 hours. Using a magnetic stand, beads were washed 2x with Mixed Micelle Wash buffer, 2x Biffer 500, 3x with Li/Cl detergent buffer and 2x with TE buffer. Beads were then resuspended in 150uL 2%SDS/TE buffer and 150uL 2%SDS/TE buffer was added to input controls. DNA was reverse crosslinked by incubating the samples at 65C overnight and DNA was purified using Invitrogen PCR purification kit.

ChIP-seq

Library preparation and Illumina sequencing

50-100 million cells were corsslinked for ChIP-seq experiments. 1-10ng of purified DNA was used to create ChIP-seq libraries using the TruSeq ChIP Sample Prep Kit (Illumina) following the manufacturer's instructions. The quality of each library was determined using a Bioanalyzer and a High Sensitivity chip (Agilent). Library DNA sizes ranged from 250-300 bp. Barcoded libraries were multiplexed at equal molar ratio and sequenced using an Illumina Next Seq platform as single end reads of 76 bp.

Data analysis

Reads were mapped to the murine genome assebly mm9 using Bowtie. The MACS2 peak finding algorhitm was used to identify ChIP-Seq peaks.

Density map generation

In the generation of density plots, all Myc peaks with an FDR<0.05% and a minimal fold enrichment of 5 over input were used. Myc peaks were considered as promoter peaks if the peak showed at least 1 bp overlap with a 2kb window surrounding RefSeq gene

transcription start sites (TSSs), else they were considered distal peaks. Heatmap matrices were created by counting tags using the indicated window size with 50bp bins. The DeepSeq package was used to generate plots.

Immunohistochemistry

Tissues were fixed in 10% Neutral Buffered Formalin for 24 hours before paraffin embedding and sectioning. Human tissue microarrays were purchased from Biomax (#P1000a). Slides cut from paraffin blocks were de-paraffinized and rehydrated. Antigen retrieval was performed in 10 mM citrate buffer (pH 6) for 6 minutes in a pressure cooker. For immunohistochemical staining, endogenous peroxidase activity was quenched by incubation in 3% hydrogen peroxide for 15 minutes followed by rinsing in water and blocking in 2.5% normal horse serum. Slides were incubated with primary antibody diluted in blocking solution overnight at 4°C. Secondary antibody (Vector Immpress) was used according to manufacturer's instructions followed by development using DAB (Vector). Slides were dehydrated and mounted with coverslips and imaged using a Zeiss microscope. Antibodies used are described in Table.

GI50 assays

A single cell suspension of organoids was prepared as described above. Live cell concentration was determined by counting Acridine Orange/Propidium Iodide (AO/PI) (#CS2-0106; Nexcelom Science) stained cells using Cellometer Auto 2000 Cell Viability Counter. 500 cells were resuspended in 30uL of 10% matrigel/complete media and were plated in non-adherent 384-well plates. Single-cell organoids were allowed to recover overnight (16 hours) before the addition of the drug. Thapsigargin was resuspended to 1mM

in DMSO and was dispensed at varying concentrations using a Tecan HP D3000e digital dispenser. Cell growth was monitored by phase-contrast imaging using Incucyte over 4 days. To determine final cell viability, organoids were incubated with equal amount of CellTiterGlo luminescent reagent (#G7570, Promega) for 10 mins at room temperature. Luminescence was recorded using MiniMax spectrophotometer and relative luminescence was compared to a DMSO control treated organoids. GI50 values were calculated using a four parameter non-linear regression model.

RNA isolation

Total RNA was extracted from cells using TRIzol (Invitrogen) according to manufacturer's instructions using the PureLink RNA isolation kit (Invitrogen). RNA was treated with DNase I to eliminate contaminating genomic DNA.

Quantitative reverse transcription polymerase chain reaction (qRT-PCR)

RNA was extracted from cell cultures or freshly isolated tissues using TRIzol reagent (Invitrogen), followed by column-based purification with the PureLink RNA Mini Kit (Ambion). cDNA was synthesized using 1 μg of total RNA and TaqMan Reverse Transcription Reagents (Applied Biosystems). All targets were amplified (40 cycles) using gene-specific Taqman primers and probe sets (Applied Biosystems) on a 7900HT Real time-PCR instrument (Applied Biosystems). Relative gene expression quantification was performed using the ΔΔCt method with the Sequence Detection Systems Software, Version 1.9.1 (Applied Biosystems). Expression levels were normalized by *Hprt.*

Library preparation and RNA-sequencing

For each organoid line, 4-6 wells of organoids from a 24 well plate were harvested in 1 mL of TRIzol reagent and flash-frozen. All lines were at passage 3 or 4 post-isolation. RNA was extracted using the TRIzol Plus RNA Purification Kit (LifeTechnologies) per manufacturer's instructions. RNA samples were treated on column with PureLink DNase (Life Technologies). The quality of purified RNA samples was determined using a Bioanlyzer 2100 (Agilent) with an RNA 6000 Nano Kit. RNAs with RNA Integrity Number (RIN) values greater than 9.0 were used to generate sequencing libraries. Libraries were generated from 1 μg of total RNA using a TruSeq Stranded Total RNA Kit with Ribo-zero human/mouse/rat (Illumina # RS-122-2201) per manufacturer's instructions. For the final amplification, 11 cycles of PCR were used. Libraries were quality checked and quantified using a Bioanalyzer 2100 (Agilent) with a DNA 1000 Kit. Equimolar amounts of libraries were pooled and subjected to paired-end, 101 base-pair sequencing at the Cold Spring Harbor DNA Sequencing Next Generation Shared Resource using an Illumina NextSeq. Pathway enrichment analysis was performed on a set of curated canonical pathways from KEGG, Reactome and Biocarta available in the molecular signatures database (MSigDB) by using the GseaPreranked tool available in GSEA software.

Data plotting and statistical analysis

Data plotting and statistical analysis was performed using Prism 7 (Graphpad) or Excel. Figures were prepared using Powerpoint (Microsoft) and Illustrator (Adobe). All data are represented as means and standard deviation (error bars) unless otherwise indicated. Asterisks denote p-value as follows: *p<.05, **p<.01, ***p<.001, ****p<.0001.

References

Acosta-Alvear D, Zhou Y, Blais A, Tsikitis M, Lents NH, Arias C, Lennon CJ, Kluger Y, Dynlacht BD. 2007. XBP1 Controls Diverse Cell Type- and Condition-Specific Transcriptional Regulatory Networks. *Mol Cell* **27**: 53–66. https://linkinghub.elsevier.com/retrieve/pii/S1097276507004005.

Aguirre AJ. 2003. Activated Kras and Ink4a/Arf deficiency cooperate to produce metastatic pancreatic ductal adenocarcinoma. *Genes Dev* **17**: 3112–3126. http://www.genesdev.org/cgi/doi/10.1101/gad.1158703.

Allen BL, Taatjes DJ. 2015. The Mediator complex: a central integrator of transcription. *Nat Rev Mol Cell Biol* **16**: 155–166. http://www.ncbi.nlm.nih.gov/pubmed/25693131 (Accessed June 5, 2019).

Amati B, Dalton S, Brooks MW, Littlewood TD, Evan GI, Land H. 1992a. Transcriptional activation by the human c-Myc oncoprotein in yeast requires interaction with Max. *Nature* **359**: 423–426. http://www.nature.com/articles/359423a0.

Amati B, Dalton S, Brooks MW, Littlewood TD, Evan GI, Land H. 1992b. Transcriptional activation by the human c-Myc oncoprotein in yeast requires interaction with Max. *Nature* **359**: 423–426. http://www.nature.com/articles/359423a0.

Amati B, Littlewood TD, Evan GI, Land H. 1993. The c-Myc protein induces cell cycle progression and apoptosis through dimerization with Max. *EMBO J* **12**: 5083–7. http://www.ncbi.nlm.nih.gov/pubmed/8262051.

Arsura M, Deshpande A, Hann SR, Sonenshein GE. 1995. Variant Max protein, derived by alternative splicing, associates with c-Myc in vivo and inhibits transactivation. *Mol Cell Biol* **15**: 6702–6709. http://mcb.asm.org/lookup/doi/10.1128/MCB.15.12.6702.

Ayer DE, Kretzner L, Eisenman RN. 1993. Mad: A heterodimeric partner for Max that antagonizes Myc transcriptional activity. *Cell* **72**: 211–222. https://linkinghub.elsevier.com/retrieve/pii/0092867493906619.

Barbieri CE, Baca SC, Lawrence MS, Demichelis F, Blattner M, Theurillat J-P, White TA, Stojanov P, Van Allen E, Stransky N, et al. 2012. Exome sequencing identifies recurrent SPOP, FOXA1 and MED12 mutations in prostate cancer. *Nat Genet* **44**: 685–689. http://www.ncbi.nlm.nih.gov/pubmed/22610119 (Accessed June 5, 2019).

Beaulieu M-E, Jauset T, Massó-Vallés D, Martínez-Martín S, Rahl P, Maltais L, Zacarias-Fluck MF, Casacuberta-Serra S, Serrano del Pozo E, Fiore C, et al. 2019. Intrinsic cell-penetrating activity propels Omomyc from proof of concept to viable anti-MYC therapy. *Sci Transl Med* **11**: eaar5012. http://stm.sciencemag.org/lookup/doi/10.1126/scitranslmed.aar5012.

Berger SL. 2002. Histone modifications in transcriptional regulation. *Curr Opin Genet Dev* **12**: 142–148. https://linkinghub.elsevier.com/retrieve/pii/S0959437X02002794.

Berger SL, Kouzarides T, Shiekhattar R, Shilatifard A. 2009a. An operational definition of epigenetics. *Genes Dev* **23**: 781–783. http://www.ncbi.nlm.nih.gov/pubmed/19339683 (Accessed June 4, 2019).

Berger SL, Kouzarides T, Shiekhattar R, Shilatifard A. 2009b. An operational definition of epigenetics. *Genes Dev* **23**: 781–783. http://genesdev.cshlp.org/cgi/doi/10.1101/gad.1787609.

Bertolotti A, Wang X, Novoa I, Jungreis R, Schlessinger K, Cho JH, West AB, Ron D. 2001. Increased sensitivity to dextran sodium sulfate colitis in IRE1β-deficient mice. *J Clin Invest* **107**: 585–593. http://www.jci.org/articles/view/11476.

Bertolotti A, Zhang Y, Hendershot LM, Harding HP, Ron D. 2000. Dynamic interaction of BiP and ER stress transducers in the unfolded-protein response. *Nat Cell Biol* **2**: 326–332. http://www.nature.com/articles/ncb0600_326.

Biffi G, Oni TE, Spielman B, Hao Y, Elyada E, Park Y, Preall J, Tuveson DA. 2019. IL1-Induced JAK/STAT Signaling Is Antagonized by TGFβ to Shape CAF Heterogeneity in Pancreatic Ductal Adenocarcinoma. *Cancer Discov* **9**: 282–301. http://cancerdiscovery.aacrjournals.org/lookup/doi/10.1158/2159-8290.CD-18-0710.

Boj SF, Hwang C-I, Baker LA, Chio IIC, Engle DD, Corbo V, Jager M, Ponz-Sarvise M, Tiriac H, Spector MS, et al. 2015. Organoid Models of Human and Mouse Ductal Pancreatic Cancer. *Cell* **160**: 324–338. https://linkinghub.elsevier.com/retrieve/pii/S009286741401592X.

Bradner JE, Hnisz D, Young RA. 2017. Transcriptional Addiction in Cancer. *Cell* **168**: 629–643. http://dx.doi.org/10.1016/j.cell.2016.12.013.

Bray F, Ferlay J, Soerjomataram I, Siegel RL, Torre LA, Jemal A. 2018. Global cancer statistics 2018: GLOBOCAN estimates of incidence and mortality worldwide for 36 cancers in 185 countries. *CA Cancer J Clin* **68**: 394–424. http://doi.wiley.com/10.3322/caac.21492.

Bruenderman EH, Martin RCG. 2015. High-risk population in sporadic pancreatic adenocarcinoma: guidelines for screening. *J Surg Res* **194**: 212–219. https://linkinghub.elsevier.com/retrieve/pii/S0022480414006246.

Buchwalter G, Hickey MM, Cromer A, Selfors LM, Gunawardane RN, Frishman J, Jeselsohn R, Lim E, Chi D, Fu X, et al. 2013. PDEF Promotes Luminal Differentiation and Acts as a Survival Factor for ER-Positive Breast Cancer Cells. *Cancer Cell* **23**: 753–767. https://linkinghub.elsevier.com/retrieve/pii/S1535610813001906.

Candido JB, Morton JP, Bailey P, Campbell AD, Karim SA, Jamieson T, Lapienyte L, Gopinathan A, Clark W, McGhee EJ, et al. 2018. CSF1R+ Macrophages Sustain Pancreatic Tumor Growth through T Cell Suppression and Maintenance of Key Gene Programs that Define the Squamous Subtype. *Cell Rep* **23**: 1448–1460. https://doi.org/10.1016/j.celrep.2018.03.131 (Accessed June 5, 2019).

Carroll JS, Meyer CA, Song J, Li W, Geistlinger TR, Eeckhoute J, Brodsky AS, Keeton EK,

Fertuck KC, Hall GF, et al. 2006. Genome-wide analysis of estrogen receptor binding sites. *Nat Genet* **38**: 1289–1297. http://www.nature.com/articles/ng1901 (Accessed June 5, 2019).

Castor CW, Wilson SM, Heiss PR, Seidman JC. 1979. Activation of lung connective tissue cells in vitro. *Am Rev Respir Dis* **120**: 101–6. http://www.ncbi.nlm.nih.gov/pubmed/464373 (Accessed June 5, 2019).

Chen J, Zhang Z, Li L, Chen B-C, Revyakin A, Hajj B, Legant W, Dahan M, Lionnet T, Betzig E, et al. 2014. Single-Molecule Dynamics of Enhanceosome Assembly in Embryonic Stem Cells. *Cell* **156**: 1274–1285. http://www.ncbi.nlm.nih.gov/pubmed/24630727 (Accessed June 5, 2019).

Chen X. 2002. Overexpression of glucose-regulated protein 94 (Grp94) in esophageal adenocarcinomas of a rat surgical model and humans. *Carcinogenesis* **23**: 123–130. https://academic.oup.com/carcin/article-lookup/doi/10.1093/carcin/23.1.123.

Ciechanover A, DiGiuseppe JA, Bercovich B, Orian A, Richter JD, Schwartz AL, Brodeur GM. 1991. Degradation of nuclear oncoproteins by the ubiquitin system in vitro. *Proc Natl Acad Sci* **88**: 139–143. http://www.pnas.org/cgi/doi/10.1073/pnas.88.1.139.

Cirillo LA, Zaret KS. 1999a. An Early Developmental Transcription Factor Complex that Is More Stable on Nucleosome Core Particles Than on Free DNA. *Mol Cell* **4**: 961–969. https://www.sciencedirect.com/science/article/pii/S1097276500802257?via%3Dihub (Accessed June 5, 2019).

Cirillo LA, Zaret KS. 1999b. An Early Developmental Transcription Factor Complex that Is More Stable on Nucleosome Core Particles Than on Free DNA. *Mol Cell* **4**: 961–969. http://www.ncbi.nlm.nih.gov/pubmed/23761328 (Accessed May 28, 2019).

Collisson EA, Sadanandam A, Olson P, Gibb WJ, Truitt M, Gu S, Cooc J, Weinkle J, Kim GE, Jakkula L, et al. 2011. Subtypes of pancreatic ductal adenocarcinoma and their differing responses to therapy. *Nat Med* **17**: 500–503. http://www.nature.com/articles/nm.2344.

Coniglio SJ, Eugenin E, Dobrenis K, Stanley ER, West BL, Symons MH, Segall JE. 2012. Microglial Stimulation of Glioblastoma Invasion Involves Epidermal Growth Factor Receptor (EGFR) and Colony Stimulating Factor 1 Receptor (CSF-1R) Signaling. *Mol Med* **18**: 519–527. http://www.ncbi.nlm.nih.gov/pubmed/22294205 (Accessed June 5, 2019).

Connor AA, Denroche RE, Jang GH, Timms L, Kalimuthu SN, Selander I, McPherson T, Wilson GW, Chan-Seng-Yue MA, Borozan I, et al. 2017. Association of Distinct Mutational Signatures With Correlates of Increased Immune Activity in Pancreatic Ductal Adenocarcinoma. *JAMA Oncol* **3**: 774. http://oncology.jamanetwork.com/article.aspx?doi=10.1001/jamaoncol.2016.3916.

Conroy T, Desseigne F, Ychou M, Bouché O, Guimbaud R, Bécouarn Y, Adenis A, Raoul J-L, Gourgou-Bourgade S, de la Fouchardière C, et al. 2011. FOLFIRINOX versus Gemcitabine for Metastatic Pancreatic Cancer. *N Engl J Med* **364**: 1817–1825.

http://www.nejm.org/doi/10.1056/NEJMoa1011923.

Conroy T, Hammel P, Hebbar M, Ben Abdelghani M, Wei AC, Raoul J-L, Choné L, Francois E, Artru P, Biagi JJ, et al. 2018. FOLFIRINOX or Gemcitabine as Adjuvant Therapy for Pancreatic Cancer. *N Engl J Med* **379**: 2395–2406. http://www.nejm.org/doi/10.1056/NEJMoa1809775.

Coppola JA, Cole MD. 1986. Constitutive c-myc oncogene expression blocks mouse erythroleukaemia cell differentiation but not commitment. *Nature* **320**: 760–763. http://www.nature.com/articles/320760a0.

Crippa S, Salvia R, Warshaw AL, Domínguez I, Bassi C, Falconi M, Thayer SP, Zamboni G, Lauwers GY, Mino-Kenudson M, et al. 2008. Mucinous Cystic Neoplasm of the Pancreas is Not an Aggressive Entity. *Ann Surg* **247**: 571–579. https://insights.ovid.com/crossref?an=00000658-200804000-00003.

Cromm PM, Crews CM. 2017. Targeted Protein Degradation: from Chemical Biology to Drug Discovery. *Cell Chem Biol* **24**: 1181–1190.

Cubilla AL, Fitzgerald PJ. 1976. Morphological Lesions Associated with Human Primary Invasive Nonendocrine Pancreas Cancer. *Cancer Res*.

Cubilla AL, Fitzgerald PJ. 1975. Morphological Patterns of Primary Nonendocrine Human Pancreas Carcinoma. *Cancer Res*.

Cunningham JT, Moreno M V., Lodi A, Ronen SM, Ruggero D. 2014. Protein and Nucleotide Biosynthesis Are Coupled by a Single Rate-Limiting Enzyme, PRPS2, to Drive Cancer. *Cell* **157**: 1088–1103. https://linkinghub.elsevier.com/retrieve/pii/S0092867414004826.

Dang C V. 2012. MYC on the Path to Cancer. *Cell* **149**: 22–35. https://linkinghub.elsevier.com/retrieve/pii/S0092867412002966.

Dang C V., Kim J, Gao P, Yustein J. 2008. The interplay between MYC and HIF in cancer. *Nat Rev Cancer* **8**: 51–56. http://www.nature.com/articles/nrc2274.

Darzynkiewicz Z, Traganos F, Melamed MR. 1980a. New cell cycle compartments identified by multiparameter flow cytometry. *Cytometry* **1**: 98–108. http://doi.wiley.com/10.1002/cyto.990010203.

Darzynkiewicz Z, Traganos F, Melamed MR. 1980b. New cell cycle compartments identified by multiparameter flow cytometry. *Cytometry* **1**: 98–108. http://doi.wiley.com/10.1002/cyto.990010203.

Davis AC, Wims M, Spotts GD, Hann SR, Bradley A. 1993. A null c-myc mutation causes lethality before 10.5 days of gestation in homozygotes and reduced fertility in heterozygous female mice. *Genes Dev* **7**: 671–682. http://www.genesdev.org/cgi/doi/10.1101/gad.7.4.671.

de Gramont A, Faivre S, Raymond E. 2017. Novel TGF- β inhibitors ready for prime time in onco-immunology. *Oncoimmunology* **6**: e1257453.

https://www.tandfonline.com/doi/full/10.1080/2162402X.2016.1257453.

De La O J-P, Emerson LL, Goodman JL, Froebe SC, Illum BE, Curtis AB, Murtaugh LC. 2008. Notch and Kras reprogram pancreatic acinar cells to ductal intraepithelial neoplasia. *Proc Natl Acad Sci* **105**: 18907–18912. http://www.pnas.org/cgi/doi/10.1073/pnas.0810111105.

Degnan BM, Degnan SM, Naganuma T, Morse DE. 1993. The ets multigene family is conserved throughout the Metazoa. *Nucleic Acids Res* **21**: 3479–3484. https://academic.oup.com/nar/article-lookup/doi/10.1093/nar/21.15.3479.

Delmore JE, Issa GC, Lemieux ME, Rahl PB, Shi J, Jacobs HM, Kastritis E, Gilpatrick T, Paranal RM, Qi J, et al. 2011. BET Bromodomain Inhibition as a Therapeutic Strategy to Target c-Myc. *Cell* **146**: 904–917. https://linkinghub.elsevier.com/retrieve/pii/S0092867411009433.

Dumartin L, Alrawashdeh W, Trabulo SM, Radon TP, Steiger K, Feakins RM, di Magliano MP, Heeschen C, Esposito I, Lemoine NR, et al. 2017. ER stress protein AGR2 precedes and is involved in the regulation of pancreatic cancer initiation. *Oncogene* **36**: 3094–3103. http://www.nature.com/articles/onc2016459.

Eser S, Schnieke A, Schneider G, Saur D. 2014. Oncogenic KRAS signalling in pancreatic cancer. *Br J Cancer* **111**: 817–822. http://www.nature.com/articles/bjc2014215.

Evan GI, Wyllie AH, Gilbert CS, Littlewood TD, Land H, Brooks M, Waters CM, Penn LZ, Hancock DC. 1992. Induction of apoptosis in fibroblasts by c-myc protein. *Cell* **69**: 119–128. https://linkinghub.elsevier.com/retrieve/pii/009286749290123T.

Fernandez PM, Tabbara SO, Jacobs LK, Manning FCR, Tsangaris TN, Schwartz AM, Kennedy KA, Patierno SR. 2000. Overexpression of the glucose-regulated stress gene GRP78 in malignant but not benign human breast lesions. *Breast Cancer Res Treat* **59**: 15–26. http://link.springer.com/10.1023/A:1006332011207.

Finkel RS, Mercuri E, Darras BT, Connolly AM, Kuntz NL, Kirschner J, Chiriboga CA, Saito K, Servais L, Tizzano E, et al. 2017. Nusinersen versus Sham Control in Infantile-Onset Spinal Muscular Atrophy. *N Engl J Med* **377**: 1723–1732. http://www.nejm.org/doi/10.1056/NEJMoa1702752.

Fusakio ME, Willy JA, Wang Y, Mirek ET, Al Baghdadi RJT, Adams CM, Anthony TG, Wek RC. 2016. Transcription factor ATF4 directs basal and stress-induced gene expression in the unfolded protein response and cholesterol metabolism in the liver ed. S. Wolin. *Mol Biol Cell* **27**: 1536–1551. https://www.molbiolcell.org/doi/10.1091/mbc.E16-01-0039.

Gazit G, Lu J, Lee AS. 1999. De-regulation of GRP stress protein expression in human breast cancer cell lines. *Breast Cancer Res Treat* **54**: 135–146. http://link.springer.com/10.1023/A:1006102411439.

Gebhardt A, Frye M, Herold S, Benitah SA, Braun K, Samans B, Watt FM, Elsässer H-P, Eilers M. 2006. Myc regulates keratinocyte adhesion and differentiation via complex

formation with Miz1. *J Cell Biol* **172**: 139–149. http://www.jcb.org/lookup/doi/10.1083/jcb.200506057.

Gebhardt JCM, Suter DM, Roy R, Zhao ZW, Chapman AR, Basu S, Maniatis T, Xie XS. 2013. Single-molecule imaging of transcription factor binding to DNA in live mammalian cells. *Nat Methods* **10**: 421–426. http://www.nature.com/articles/nmeth.2411 (Accessed June 5, 2019).

Ghosh R, Lipson KL, Sargent KE, Mercurio AM, Hunt JS, Ron D, Urano F. 2010. Transcriptional Regulation of VEGF-A by the Unfolded Protein Response Pathway ed. M. V. Blagosklonny. *PLoS One* **5**: e9575. https://dx.plos.org/10.1371/journal.pone.0009575.

Gleimer M, Parham P. 2003a. Stress Management. *Immunity* **19**: 469–477. http://www.ncbi.nlm.nih.gov/pubmed/17522715 (Accessed June 5, 2019).

Gleimer M, Parham P. 2003b. Stress Management. *Immunity* **19**: 469–477. https://linkinghub.elsevier.com/retrieve/pii/S1074761303002723.

Golan T, Hammel P, Reni M, Van Cutsem E, Macarulla T, Hall MJ, Park J-O, Hochhauser D, Arnold D, Oh D-Y, et al. 2019. Maintenance Olaparib for Germline *BRCA* -Mutated Metastatic Pancreatic Cancer. *N Engl J Med* NEJMoa1903387. http://www.nejm.org/doi/10.1056/NEJMoa1903387 (Accessed June 19, 2019).

Granados DP, Tanguay P-L, Hardy M-P, Caron É, de Verteuil D, Meloche S, Perreault C. 2009. ER stress affects processing of MHC class I-associated peptides. *BMC Immunol* **10**: 10. http://bmcimmunol.biomedcentral.com/articles/10.1186/1471-2172-10-10.

Grant AG, Duke D, Hermon-Taylor J. 1979. Establishment and characterization of primary human pancreatic carcinoma in continuous cell culture and in nude mice. *Br J Cancer* **39**: 143–151. http://www.ncbi.nlm.nih.gov/pubmed/435363 (Accessed June 17, 2019).

Gregorieff A, Stange DE, Kujala P, Begthel H, van den Born M, Korving J, Peters PJ, Clevers H. 2009. The Ets-Domain Transcription Factor Spdef Promotes Maturation of Goblet and Paneth Cells in the Intestinal Epithelium. *Gastroenterology* **137**.

Guccione E, Martinato F, Finocchiaro G, Luzi L, Tizzoni L, Dall' Olio V, Zardo G, Nervi C, Bernard L, Amati B. 2006. Myc-binding-site recognition in the human genome is determined by chromatin context. *Nat Cell Biol* **8**: 764–770. http://www.nature.com/articles/ncb1434.

Gunawardane RN, Sgroi DC, Wrobel CN, Koh E, Daley GQ, Brugge JS. 2005. Novel Role for PDEF in Epithelial Cell Migration and Invasion. *Cancer Res* **65**: 11572–11580. http://cancerres.aacrjournals.org/lookup/doi/10.1158/0008-5472.CAN-05-1196.

Guo J, Parise RA, Joseph E, Egorin MJ, Lazo JS, Prochownik E V., Eiseman JL. 2009. Efficacy, pharmacokinetics, tisssue distribution, and metabolism of the Myc–Max disruptor, 10058-F4 [Z,E]-5-[4-ethylbenzylidine]-2-thioxothiazolidin-4-one, in mice. *Cancer Chemother Pharmacol* **63**: 615–625. http://link.springer.com/10.1007/s00280-008-0774-y.

Guo M, Tomoshige K, Meister M, Muley T, Fukazawa T, Tsuchiya T, Karns R, Warth A, Fink-Baldauf IM, Nagayasu T, et al. 2017. Gene signature driving invasive mucinous adenocarcinoma of the lung. *EMBO Mol Med* **9**: 462–481. http://embomolmed.embopress.org/lookup/doi/10.15252/emmm.201606711.

Gutiérrez ML, Corchete L, Teodosio C, Sarasquete ME, Abad M del M, Iglesias M, Esteban C, Sayagues JM, Orfao A, Muñoz-Bellvis L. 2015. Identification and characterization of the gene expression profiles for protein coding and non-coding RNAs of pancreatic ductal adenocarcinomas. *Oncotarget* **6**: 19070–86. http://www.ncbi.nlm.nih.gov/pubmed/26053098 (Accessed June 4, 2019).

Habbe N, Shi G, Meguid RA, Fendrich V, Esni F, Chen H, Feldmann G, Stoffers DA, Konieczny SF, Leach SD, et al. 2008. Spontaneous induction of murine pancreatic intraepithelial neoplasia (mPanIN) by acinar cell targeting of oncogenic Kras in adult mice. *Proc Natl Acad Sci* **105**: 18913–18918. http://www.pnas.org/cgi/doi/10.1073/pnas.0810097105.

Han T, Jiao F, Hu H, Yuan C, Wang L, Jin Z-L, Song W, Wang L-W. 2016. EZH2 promotes cell migration and invasion but not alters cell proliferation by suppressing E-cadherin, partly through association with MALAT-1 in pancreatic cancer. *Oncotarget* **7**: 11194–207. http://www.ncbi.nlm.nih.gov/pubmed/26848980 (Accessed June 4, 2019).

Hann SR. 2006. Role of post-translational modifications in regulating c-Myc proteolysis, transcriptional activity and biological function. *Semin Cancer Biol* **16**: 288–302. https://linkinghub.elsevier.com/retrieve/pii/S1044579X06000708.

Hann SR, Eisenman RN. 1984. Proteins encoded by the human c-myc oncogene: differential expression in neoplastic cells. *Mol Cell Biol* **4**: 2486–2497. http://www.ncbi.nlm.nih.gov/pubmed/6513926.

Harbison CT, Gordon DB, Lee TI, Rinaldi NJ, Macisaac KD, Danford TW, Hannett NM, Tagne J-B, Reynolds DB, Yoo J, et al. 2004. Transcriptional regulatory code of a eukaryotic genome. *Nature* **431**: 99–104. http://www.nature.com/articles/nature02800.

Harding HP, Zhang Y, Bertolotti A, Zeng H, Ron D. 2000. Perk Is Essential for Translational Regulation and Cell Survival during the Unfolded Protein Response. *Mol Cell* **5**: 897–904. https://linkinghub.elsevier.com/retrieve/pii/S1097276500803305.

He C, Jiang H, Geng S, Sheng H, Shen X, Zhang X, Zhu S, Chen X, Yang C, Gao H. 2012. Analysis of whole genomic expression profiles and screening of the key signaling pathways associated with pancreatic cancer. *Int J Clin Exp Pathol* **5**: 537–46. http://www.ncbi.nlm.nih.gov/pubmed/22949936 (Accessed June 4, 2019).

Heeg S, Das KK, Reichert M, Bakir B, Takano S, Caspers J, Aiello NM, Wu K, Neesse A, Maitra A, et al. 2016a. ETS-Transcription Factor ETV1 Regulates Stromal Expansion and Metastasis in Pancreatic Cancer. *Gastroenterology* **151**: 540-553.e14. http://www.ncbi.nlm.nih.gov/pubmed/15958574 (Accessed June 5, 2019).

Heeg S, Das KK, Reichert M, Bakir B, Takano S, Caspers J, Aiello NM, Wu K, Neesse A,

Maitra A, et al. 2016b. ETS-Transcription Factor ETV1 Regulates Stromal Expansion and Metastasis in Pancreatic Cancer. *Gastroenterology* **151**: 540-553.e14. https://linkinghub.elsevier.com/retrieve/pii/S0016508516346194.

Henriksson ML, Edin S, Dahlin AM, Oldenborg P-A, Öberg Å, Van Guelpen B, Rutegård J, Stenling R, Palmqvist R. 2011. Colorectal Cancer Cells Activate Adjacent Fibroblasts Resulting in FGF1/FGFR3 Signaling and Increased Invasion. *Am J Pathol* **178**: 1387–1394. http://www.ncbi.nlm.nih.gov/pubmed/21356388 (Accessed June 5, 2019).

Herold S, Wanzel M, Beuger V, Frohme C, Beul D, Hillukkala T, Syvaoja J, Saluz H-P, Haenel F, Eilers M. 2002. Negative Regulation of the Mammalian UV Response by Myc through Association with Miz-1. *Mol Cell* **10**: 509–521. https://linkinghub.elsevier.com/retrieve/pii/S1097276502006330.

Hingorani SR, Petricoin EF, Maitra A, Rajapakse V, King C, Jacobetz MA, Ross S, Conrads TP, Veenstra TD, Hitt BA, et al. 2003. Preinvasive and invasive ductal pancreatic cancer and its early detection in the mouse. *Cancer Cell* **4**: 437–50. http://www.ncbi.nlm.nih.gov/pubmed/14706336.

Hingorani SR, Wang L, Multani AS, Combs C, Deramaudt TB, Hruban RH, Rustgi AK, Chang S, Tuveson DA. 2005a. Trp53R172H and KrasG12D cooperate to promote chromosomal instability and widely metastatic pancreatic ductal adenocarcinoma in mice. *Cancer Cell* **7**: 469–483. https://linkinghub.elsevier.com/retrieve/pii/S1535610805001285.

Hingorani SR, Wang L, Multani AS, Combs C, Deramaudt TB, Hruban RH, Rustgi AK, Chang S, Tuveson DA. 2005b. Trp53R172H and KrasG12D cooperate to promote chromosomal instability and widely metastatic pancreatic ductal adenocarcinoma in mice. *Cancer Cell* **7**: 469–483. https://linkinghub.elsevier.com/retrieve/pii/S1535610805001285.

Hollenhorst PC, Ferris MW, Hull MA, Chae H, Kim S, Graves BJ. 2011a. Oncogenic ETS proteins mimic activated RAS/MAPK signaling in prostate cells. *Genes Dev* **25**: 2147–2157. http://genesdev.cshlp.org/cgi/doi/10.1101/gad.17546311.

Hollenhorst PC, McIntosh LP, Graves BJ. 2011b. Genomic and Biochemical Insights into the Specificity of ETS Transcription Factors. *Annu Rev Biochem* **80**: 437–471. http://www.annualreviews.org/doi/10.1146/annurev.biochem.79.081507.103945.

Hollien J, Weissman JS. 2006. Decay of Endoplasmic Reticulum-Localized mRNAs During the Unfolded Protein Response. *Science (80-)* **313**: 104–107. http://www.sciencemag.org/lookup/doi/10.1126/science.1129631.

Hollingsworth MA, Swanson BJ. 2004. Mucins in cancer: protection and control of the cell surface. *Nat Rev Cancer* **4**: 45–60. http://www.nature.com/articles/nrc1251.

Hruban RH, Goggins M, Parsons J, Kern SE. 2000. Progression model for pancreatic cancer. *Clin Cancer Res* **6**: 2969–72. http://www.ncbi.nlm.nih.gov/pubmed/10955772.

Ijichi H, Chytil A, Gorska AE, Aakre ME, Fujitani Y, Fujitani S, Wright CVE, Moses HL. 2006. Aggressive pancreatic ductal adenocarcinoma in mice caused by pancreas-specific blockade of transforming growth factor-beta signaling in cooperation with active Kras expression. *Genes Dev* **20**: 3147–3160. http://www.genesdev.org/cgi/doi/10.1101/gad.1475506.

Ikeda J, Kaneda S, Kuwabara K, Ogawa S, Kobayashi T, Matsumoto M, Yura T, Yanagi H. 1997. Cloning and Expression of cDNA Encoding the Human 150 kDa Oxygen-Regulated Protein, ORP150. *Biochem Biophys Res Commun* **230**: 94–99. https://linkinghub.elsevier.com/retrieve/pii/S0006291X96958908.

Imler JL, Schatz C, Wasylyk C, Chatton B, Wasylyk B. 1988. A Harvey-ras responsive transcription element is also responsive to a tumour-promoter and to serum. *Nature* **332**: 275–278. http://www.nature.com/articles/332275a0.

In I, Chio C, Jafarnejad SM, Ponz-Sarvise M, Pappin DJ, Sonenberg N, Tuveson Correspondence DA. 2016. NRF2 Promotes Tumor Maintenance by Modulating mRNA Translation in Pancreatic Cancer. *Cell* **166**: 963–976. http://dx.doi.org/10.1016/j.cell.2016.06.056 (Accessed May 29, 2019).

Iwawaki T, Akai R, Yamanaka S, Kohno K. 2009. Function of IRE1 alpha in the placenta is essential for placental development and embryonic viability. *Proc Natl Acad Sci* **106**: 16657–16662. http://www.pnas.org/cgi/doi/10.1073/pnas.0903775106.

Izeradjene K, Combs C, Best M, Gopinathan A, Wagner A, Grady WM, Deng C-X, Hruban RH, Adsay NV, Tuveson DA, et al. 2007. KrasG12D and Smad4/Dpc4 Haploinsufficiency Cooperate to Induce Mucinous Cystic Neoplasms and Invasive Adenocarcinoma of the Pancreas. *Cancer Cell* **11**: 229–243. https://linkinghub.elsevier.com/retrieve/pii/S1535610807000578.

Jamora C, Dennert G, Lee AS. 1996. Inhibition of tumor progression by suppression of stress protein GRP78/BiP induction in fibrosarcoma B/C10ME. *Proc Natl Acad Sci* **93**: 7690–7694. http://www.ncbi.nlm.nih.gov/pubmed/8755537 (Accessed May 31, 2019).

Ji B, Tsou L, Wang H, Gaiser S, Chang DZ, Daniluk J, Bi Y, Grote T, Longnecker DS, Logsdon CD. 2009. Ras Activity Levels Control the Development of Pancreatic Diseases. *Gastroenterology* **137**: 1072-1082.e6. https://linkinghub.elsevier.com/retrieve/pii/S0016508509009007.

Jobe NP, Rösel D, Dvořánková B, Kodet O, Lacina L, Mateu R, Smetana K, Brábek J. 2016. Simultaneous blocking of IL-6 and IL-8 is sufficient to fully inhibit CAF-induced human melanoma cell invasiveness. *Histochem Cell Biol* **146**: 205–217. http://www.ncbi.nlm.nih.gov/pubmed/27102177 (Accessed June 5, 2019).

Kannagi R. 2002. Regulatory roles of carbohydrate ligands for selectins in the homing of lymphocytes. *Curr Opin Struct Biol* **12**: 599–608. http://www.ncbi.nlm.nih.gov/pubmed/12464311.

Karagöz GE, Acosta-Alvear D, Nguyen HT, Lee CP, Chu F, Walter P. 2017. An unfolded

protein-induced conformational switch activates mammalian IRE1. *Elife* **6**. https://elifesciences.org/articles/30700.

Karin M. 1994. Signal transduction from the cell surface to the nucleus through the phosphorylation of transcription factors. *Curr Opin Cell Biol* **6**: 415–424. https://linkinghub.elsevier.com/retrieve/pii/0955067494900353.

Kato M, Shimada Y, Tanaka H, Hosotani R, Ohshio G, Ishizaki K, Imamura M. 1999. Characterization of six cell lines established from human pancreatic adenocarcinomas. *Cancer* **85**: 832–40. http://www.ncbi.nlm.nih.gov/pubmed/10091760 (Accessed June 17, 2019).

Katoh M, Igarashi M, Fukuda H, Nakagama H, Katoh M. 2013. Cancer genetics and genomics of human FOX family genes. *Cancer Lett* **328**: 198–206. https://www.sciencedirect.com/science/article/pii/S0304383512005666?via%3Dihub (Accessed June 5, 2019).

Kaur S, Kumar S, Momi N, Sasson AR, Batra SK. 2013. Mucins in pancreatic cancer and its microenvironment. *Nat Rev Gastroenterol Hepatol* **10**: 607–620. http://www.nature.com/articles/nrgastro.2013.120.

Kobberup S, Nyeng P, Juhl K, Hutton J, Jensen J. 2007. ETS-family genes in pancreatic development. *Dev Dyn* **236**: 3100–3110. http://doi.wiley.com/10.1002/dvdy.21292 (Accessed May 27, 2019).

Kojima K, Vickers SM, Adsay NV, Jhala NC, Kim H-G, Schoeb TR, Grizzle WE, Klug CA. 2007. Inactivation of Smad4 Accelerates Kras G12D -Mediated Pancreatic Neoplasia. *Cancer Res* **67**: 8121–8130. http://cancerres.aacrjournals.org/lookup/doi/10.1158/0008-5472.CAN-06-4167.

Kole R, Krainer AR, Altman S. 2012. RNA therapeutics: beyond RNA interference and antisense oligonucleotides. *Nat Rev Drug Discov* **11**: 125–140. http://www.nature.com/articles/nrd3625.

Komatsu M, Yee L, Carraway KL. 1999. Overexpression of sialomucin complex, a rat homologue of MUC4, inhibits tumor killing by lymphokine-activated killer cells. *Cancer Res*.

Kopp JL, von Figura G, Mayes E, Liu F-F, Dubois CL, Morris JP, Pan FC, Akiyama H, Wright CVE, Jensen K, et al. 2012. Identification of Sox9-Dependent Acinar-to-Ductal Reprogramming as the Principal Mechanism for Initiation of Pancreatic Ductal Adenocarcinoma. *Cancer Cell* **22**: 737–750. https://linkinghub.elsevier.com/retrieve/pii/S1535610812004497.

Korennykh A V., Egea PF, Korostelev AA, Finer-Moore J, Zhang C, Shokat KM, Stroud RM, Walter P. 2009. The unfolded protein response signals through high-order assembly of Ire1. *Nature* **457**: 687–693. http://www.nature.com/articles/nature07661.

Kortlever RM, Sodir NM, Wilson CH, Burkhart DL, Pellegrinet L, Brown Swigart L,

Littlewood TD, Evan GI. 2017. Myc Cooperates with Ras by Programming Inflammation and Immune Suppression. *Cell* **171**: 1301-1315.e14. https://linkinghub.elsevier.com/retrieve/pii/S0092867417313223.

Kurimchak AM, Shelton C, Duncan KE, Johnson KJ, Brown J, O'Brien S, Gabbasov R, Fink LS, Li Y, Lounsbury N, et al. 2016. Resistance to BET Bromodomain Inhibitors Is Mediated by Kinome Reprogramming in Ovarian Cancer. *Cell Rep* **16**: 1273–1286. https://linkinghub.elsevier.com/retrieve/pii/S2211124716308609.

Lai AC, Crews CM. 2017. Induced protein degradation: an emerging drug discovery paradigm. *Nat Rev Drug Discov* **16**: 101–114. http://www.nature.com/articles/nrd.2016.211.

Lambert M, Jambon S, Depauw S, David-Cordonnier M-H. 2018. Targeting Transcription Factors for Cancer Treatment. *Molecules* **23**: 1479. http://www.mdpi.com/1420-3049/23/6/1479.

Land H, Parada LF, Weinberg RA. 1983. Tumorigenic conversion of primary embryo fibroblasts requires at least two cooperating oncogenes. *Nature* **304**: 596–602. http://www.nature.com/articles/304596a0.

Lee AYL, Dubois CL, Sarai K, Zarei S, Schaeffer DF, Sander M, Kopp JL. 2019. Cell of origin affects tumour development and phenotype in pancreatic ductal adenocarcinoma. *Gut* **68**: 487–498. http://gut.bmj.com/lookup/doi/10.1136/gutjnl-2017-314426.

Li F, Wang Y, Zeller KI, Potter JJ, Wonsey DR, O'Donnell KA, Kim J -w., Yustein JT, Lee LA, Dang C V. 2005a. Myc Stimulates Nuclearly Encoded Mitochondrial Genes and Mitochondrial Biogenesis. *Mol Cell Biol* **25**: 6225–6234. http://mcb.asm.org/cgi/doi/10.1128/MCB.25.14.6225-6234.2005.

Li F, Wang Y, Zeller KI, Potter JJ, Wonsey DR, O'Donnell KA, Kim J -w., Yustein JT, Lee LA, Dang C V. 2005b. Myc Stimulates Nuclearly Encoded Mitochondrial Genes and Mitochondrial Biogenesis. *Mol Cell Biol* **25**: 6225–6234. http://www.ncbi.nlm.nih.gov/pubmed/19864427 (Accessed May 28, 2019).

Li H, Korennykh A V., Behrman SL, Walter P. 2010. Mammalian endoplasmic reticulum stress sensor IRE1 signals by dynamic clustering. *Proc Natl Acad Sci* **107**: 16113–16118. http://www.pnas.org/cgi/doi/10.1073/pnas.1010580107.

Li X-X, Zhang H-S, Xu Y-M, Zhang R-J, Chen Y, Fan L, Qin Y-Q, Liu Y, Li M, Fang J. 2017. Knockdown of IRE1α inhibits colonic tumorigenesis through decreasing β-catenin and IRE1α targeting suppresses colon cancer cells. *Oncogene* **36**: 6738–6746. http://www.ncbi.nlm.nih.gov/pubmed/28825721 (Accessed May 31, 2019).

Li X, Wang L, Nunes DP, Troxler RF, Offner GD. 2005c. Suppression of MUC1 synthesis downregulates expression of the epidermal growth factor receptor. *Cancer Biol Ther* **4**: 968–973. http://www.tandfonline.com/doi/abs/10.4161/cbt.4.9.1913.

Li X, Wang W, Xi Y, Gao M, Tran M, Aziz KE, Qin J, Li W, Chen J. 2016. FOXR2 Interacts

with MYC to Promote Its Transcriptional Activities and Tumorigenesis. *Cell Rep* **16**: 487–497. https://linkinghub.elsevier.com/retrieve/pii/S2211124716307239.

Lin CYY, Lovén J, Rahl PBB, Paranal RMM, Burge CBB, Bradner JEE, Lee TII, Young RAA. 2012. Transcriptional amplification in tumor cells with elevated c-Myc. *Cell* **151**: 56–67. http://www.ncbi.nlm.nih.gov/pubmed/23021215 (Accessed June 5, 2019).

Littlewood TD, Amati B, Land H, Evan GI. 1992. Max and C-Myc Max DNA-Binding Activities in Cell-Extracts. *Oncogene*.

Liu J, Chen S, Wang W, Ning B-F, Chen F, Shen W, Ding J, Chen W, Xie W-F, Zhang X. 2016a. Cancer-associated fibroblasts promote hepatocellular carcinoma metastasis through chemokine-activated hedgehog and TGF-β pathways. *Cancer Lett* **379**: 49–59. http://www.ncbi.nlm.nih.gov/pubmed/27216982 (Accessed June 5, 2019).

Liu J, Chen S, Wang W, Ning B-F, Chen F, Shen W, Ding J, Chen W, Xie W-F, Zhang X. 2016b. Cancer-associated fibroblasts promote hepatocellular carcinoma metastasis through chemokine-activated hedgehog and TGF-β pathways. *Cancer Lett* **379**: 49–59. https://linkinghub.elsevier.com/retrieve/pii/S0304383516303354.

Lo Y-H, Chung E, Li Z, Wan Y-W, Mahe MM, Chen M-S, Noah TK, Bell KN, Yalamanchili HK, Klisch TJ, et al. 2017. Transcriptional Regulation by ATOH1 and its Target SPDEF in the Intestine. *Cell Mol Gastroenterol Hepatol* **3**: 51–71. http://www.ncbi.nlm.nih.gov/pubmed/28174757 (Accessed May 28, 2019).

Ma Y, Hendershot LM. 2004. The role of the unfolded protein response in tumour development: friend or foe? *Nat Rev Cancer* **4**: 966–977. http://www.nature.com/articles/nrc1505.

Makinen N, Mehine M, Tolvanen J, Kaasinen E, Li Y, Lehtonen HJ, Gentile M, Yan J, Enge M, Taipale M, et al. 2011. MED12, the Mediator Complex Subunit 12 Gene, Is Mutated at High Frequency in Uterine Leiomyomas. *Science (80-)* **334**: 252–255. http://www.ncbi.nlm.nih.gov/pubmed/21868628 (Accessed June 5, 2019).

Marko CK, Menon BB, Chen G, Whitsett JA, Clevers H, Gipson IK. 2013. Spdef null mice lack conjunctival goblet cells and provide a model of dry eye. *Am J Pathol* **183**: 35–48. http://www.ncbi.nlm.nih.gov/pubmed/23665202 (Accessed May 28, 2019).

Maroulakou IG, Bowe DB. 2000. Expression and function of Ets transcription factors in mammalian development: a regulatory network. *Oncogene* **19**: 6432–6442. http://www.nature.com/articles/1204039.

Martino MB, Jones L, Brighton B, Ehre C, Abdulah L, Davis CW, Ron D, O'Neal WK, Ribeiro CMP. 2013. The ER stress transducer IRE1β is required for airway epithelial mucin production. *Mucosal Immunol* **6**: 639–654. http://www.ncbi.nlm.nih.gov/pubmed/23168839 (Accessed May 31, 2019).

Mayran A, Drouin J. 2018. Pioneer transcription factors shape the epigenetic landscape. *J Biol Chem* **293**: 13795–13804. http://www.ncbi.nlm.nih.gov/pubmed/29507097

(Accessed June 5, 2019).

McCauley HA, Liu C-YC-Y, Attia AC, Wikenheiser-Brokamp KA, Zhang Y, Whitsett JA, Guasch G. 2014. TGF signaling inhibits goblet cell differentiation via SPDEF in conjunctival epithelium. *Development* **141**: 4628–4639. http://www.ncbi.nlm.nih.gov/pubmed/25377551 (Accessed May 28, 2019).

Meissl K, Macho-Maschler S, Müller M, Strobl B. 2017. The good and the bad faces of STAT1 in solid tumours. *Cytokine* **89**: 12–20. https://linkinghub.elsevier.com/retrieve/pii/S1043466615300995.

Mercer TR, Dinger ME, Mattick JS. 2009. Long non-coding RNAs: insights into functions. *Nat Rev Genet* **10**: 155–159. http://www.nature.com/articles/nrg2521.

Min A, Zhu C, Wang J, Peng S, Shuai C, Gao S, Tang Z, Su T. 2015. Focal Adhesion Kinase Knockdown in Carcinoma-Associated Fibroblasts Inhibits Oral Squamous Cell Carcinoma Metastasis via Downregulating MCP-1/CCL2 Expression. *J Biochem Mol Toxicol* **29**: 70–76. http://www.ncbi.nlm.nih.gov/pubmed/25199511 (Accessed June 5, 2019).

Moffitt RA, Marayati R, Flate EL, Volmar KE, Loeza SGH, Hoadley KA, Rashid NU, Williams LA, Eaton SC, Chung AH, et al. 2015a. Virtual microdissection identifies distinct tumor- and stroma-specific subtypes of pancreatic ductal adenocarcinoma. *Nat Genet*.

Moffitt RA, Marayati R, Flate EL, Volmar KE, Loeza SGH, Hoadley KA, Rashid NU, Williams LA, Eaton SC, Chung AH, et al. 2015b. Virtual microdissection identifies distinct tumor- and stroma-specific subtypes of pancreatic ductal adenocarcinoma. *Nat Genet* **47**: 1168–1178. http://www.nature.com/articles/ng.3398.

Morgunova E, Taipale J. 2017. Structural perspective of cooperative transcription factor binding. *Curr Opin Struct Biol* **47**: 1–8. http://www.ncbi.nlm.nih.gov/pubmed/28349863 (Accessed June 5, 2019).

Mueller S, Engleitner T, Maresch R, Zukowska M, Lange S, Kaltenbacher T, Konukiewitz B, Öllinger R, Zwiebel M, Strong A, et al. 2018. Evolutionary routes and KRAS dosage define pancreatic cancer phenotypes. *Nature* **554**: 62–68. http://www.nature.com/articles/nature25459.

Mullard A. 2019. First targeted protein degrader hits the clinic. *Nat Rev Drug Discov 2019 184*.

Murchison EP, Hannon GJ. 2004. miRNAs on the move: miRNA biogenesis and the RNAi machinery. *Curr Opin Cell Biol* **16**: 223–229. https://linkinghub.elsevier.com/retrieve/pii/S0955067404000547.

Mutations K, Ductal P, Klimstra DS, Longnecker DS. 1994. K-ras Mutations Pancreatic Ductal Proliferative Lesions. *Am J Pathol* **145**: 1547–1548.

Nath, Hartnell*, Happerfield, Miles, Burchell, Taylor-Papadimitriou, Crocker*s. 1999.

Macrophage-tumour cell interactions: identification of MUC1 on breast cancer cells as a potential counter-receptor for the macrophage-restricted receptor, sialoadhesin. *Immunology* **98**: 213–219. http://doi.wiley.com/10.1046/j.1365-2567.1999.00827.x.

Nawrocki ST, Carew JS, Dunner K, Boise LH, Chiao PJ, Huang P, Abbruzzese JL, McConkey DJ. 2005a. Bortezomib Inhibits PKR-Like Endoplasmic Reticulum (ER) Kinase and Induces Apoptosis via ER Stress in Human Pancreatic Cancer Cells. *Cancer Res* **65**: 11510–11519. http://cancerres.aacrjournals.org/lookup/doi/10.1158/0008-5472.CAN-05-2394.

Nawrocki ST, Carew JS, Pino MS, Highshaw RA, Dunner K, Huang P, Abbruzzese JL, McConkey DJ. 2005b. Bortezomib Sensitizes Pancreatic Cancer Cells to Endoplasmic Reticulum Stress-Mediated Apoptosis. *Cancer Res* **65**: 11658–11666. http://cancerres.aacrjournals.org/lookup/doi/10.1158/0008-5472.CAN-05-2370.

Nie Z, Hu G, Wei G, Cui K, Yamane A, Resch W, Wang R, Green DR, Tessarollo L, Casellas R, et al. 2012. c-Myc Is a Universal Amplifier of Expressed Genes in Lymphocytes and Embryonic Stem Cells. *Cell* **151**: 68–79. https://linkinghub.elsevier.com/retrieve/pii/S0092867412011014.

Nishitoh H. 2012. CHOP is a multifunctional transcription factor in the ER stress response. *J Biochem* **151**: 217–219. https://academic.oup.com/jb/article-lookup/doi/10.1093/jb/mvr143.

Nones K, Waddell N, Song S, Patch A-M, Miller D, Johns A, Wu J, Kassahn KS, Wood D, Bailey P, et al. 2014. Genome-wide DNA methylation patterns in pancreatic ductal adenocarcinoma reveal epigenetic deregulation of SLIT-ROBO, ITGA2 and MET signaling. *Int J Cancer* **135**: 1110–1118. http://doi.wiley.com/10.1002/ijc.28765.

O&apos BC, Connell, Cheung AF, Simkevich CP, Tam W, Ren X, Mateyak MK, Sedivy JM. 2003. A Large Scale Genetic Analysis of c-Myc-regulated Gene Expression Patterns. *J Biol Chem* **278**: 12563–12573. http://www.jbc.org/lookup/doi/10.1074/jbc.M210462200.

Oettgen P, Finger E, Sun Z, Akbarali Y, Thamrongsak U, Boltax J, Grall F, Dube A, Weiss A, Brown L, et al. 2000. PDEF, a Novel Prostate Epithelium-specific Ets Transcription Factor, Interacts with the Androgen Receptor and Activates Prostate-specific Antigen Gene Expression. *J Biol Chem* **275**: 1216–1225. http://www.jbc.org/cgi/doi/10.1074/jbc.275.2.1216.

Ojha R, Amaravadi RK. 2017a. Targeting the unfolded protein response in cancer. *Pharmacol Res* **120**: 258–266. https://linkinghub.elsevier.com/retrieve/pii/S104366181631413X.

Ojha R, Amaravadi RK. 2017b. Targeting the unfolded protein response in cancer. *Pharmacol Res* **120**: 258–266. http://www.ncbi.nlm.nih.gov/pubmed/28396092 (Accessed May 29, 2019).

Okamura K, Kimata Y, Higashio H, Tsuru A, Kohno K. 2000. Dissociation of Kar2p/BiP from an ER Sensory Molecule, Ire1p, Triggers the Unfolded Protein Response in Yeast.

Biochem Biophys Res Commun **279**: 445–450. https://linkinghub.elsevier.com/retrieve/pii/S0006291X00939871.

Olive KP, Tuveson DA, Ruhe ZC, Yin B, Willis NA, Bronson RT, Crowley D, Jacks T. 2004. Mutant p53 Gain of Function in Two Mouse Models of Li-Fraumeni Syndrome. *Cell* **119**: 847–860. https://linkinghub.elsevier.com/retrieve/pii/S0092867404010463.

Orimo A, Gupta PB, Sgroi DC, Arenzana-Seisdedos F, Delaunay T, Naeem R, Carey VJ, Richardson AL, Weinberg RA. 2005. Stromal Fibroblasts Present in Invasive Human Breast Carcinomas Promote Tumor Growth and Angiogenesis through Elevated SDF-1/CXCL12 Secretion. *Cell* **121**: 335–348. http://www.ncbi.nlm.nih.gov/pubmed/15882617 (Accessed June 5, 2019).

Oslowski CM, Urano F. 2011. Measuring ER Stress and the Unfolded Protein Response Using Mammalian Tissue Culture System. In *Genes and Development*, pp. 71–92 https://linkinghub.elsevier.com/retrieve/pii/B9780123851147000040.

Padovan-Merhar O, Nair GP, Biaesch AG, Mayer A, Scarfone S, Foley SW, Wu AR, Churchman LS, Singh A, Raj A. 2015. Single Mammalian Cells Compensate for Differences in Cellular Volume and DNA Copy Number through Independent Global Transcriptional Mechanisms. *Mol Cell* **58**: 339–352. https://linkinghub.elsevier.com/retrieve/pii/S1097276515001707.

Paniccia A, Hosokawa P, Henderson W, Schulick RD, Edil BH, McCarter MD, Gajdos C. 2015. Characteristics of 10-Year Survivors of Pancreatic Ductal Adenocarcinoma. *JAMA Surg* **150**: 701. http://archsurg.jamanetwork.com/article.aspx?doi=10.1001/jamasurg.2015.0668.

Panne D. 2008. The enhanceosome. *Curr Opin Struct Biol* **18**: 236–242. http://www.ncbi.nlm.nih.gov/pubmed/18206362 (Accessed June 5, 2019).

Park KS, Korfhagen TR, Bruno MD, Kitzmiller JA, Wan H, Wert SE, Khurana Hershey GK, Chen G, Whitsett JA. 2007. SPDEF regulates goblet cell hyperplasia in the airway epithelium. *J Clin Invest* **117**: 978–988.

Parsa I, Longnecker DS, Scarpelli DG, Pour P, Lefkowitz M. 1985. Ductal Metaplasia of Human Exocrine Pancreas and Its Association with Carcinoma. *Cancer Res*.

Petersen GM. 2016. Familial Pancreatic Cancer. *Semin Oncol* **43**: 548. http://www.ncbi.nlm.nih.gov/pubmed/27899186 (Accessed June 17, 2019).

Pincus D, Chevalier MW, Aragón T, van Anken E, Vidal SE, El-Samad H, Walter P. 2010. BiP Binding to the ER-Stress Sensor Ire1 Tunes the Homeostatic Behavior of the Unfolded Protein Response ed. J.W. Kelly. *PLoS Biol* **8**: e1000415. http://dx.plos.org/10.1371/journal.pbio.1000415.

Pochampalli MR, Bejjani RM el, Schroeder JA. 2007a. MUC1 is a novel regulator of ErbB1 receptor trafficking. *Oncogene* **26**: 1693–1701. http://www.nature.com/articles/1209976.

Pochampalli MR, Bitler BG, Schroeder JA. 2007b. Transforming Growth Factor α–Dependent Cancer Progression Is Modulated by Muc1. *Cancer Res* **67**: 6591–6598. http://cancerres.aacrjournals.org/lookup/doi/10.1158/0008-5472.CAN-06-4518.

Pochampalli MR, Bitler BG, Schroeder JA. 2007c. Transforming Growth Factor α–Dependent Cancer Progression Is Modulated by Muc1. *Cancer Res* **67**: 6591–6598. http://cancerres.aacrjournals.org/lookup/doi/10.1158/0008-5472.CAN-06-4518.

Podsypanina K, Politi K, Beverly LJ, Varmus HE. 2008. Oncogene cooperation in tumor maintenance and tumor recurrence in mouse mammary tumors induced by Myc and mutant Kras. *Proc Natl Acad Sci* **105**: 5242–5247. http://www.pnas.org/lookup/doi/10.1073/pnas.0801197105.

Pommier A, Anaparthy N, Memos N, Kelley ZL, Gouronnec A, Yan R, Auffray C, Albrengues J, Egeblad M, Iacobuzio-Donahue CA, et al. 2018. Unresolved endoplasmic reticulum stress engenders immune-resistant, latent pancreatic cancer metastases. *Science (80-)* **360**: eaao4908. http://www.ncbi.nlm.nih.gov/pubmed/12464311.

Pour P, Althoff J, Takahashi M. 1977. Early lesions of pancreatic ductal carcinoma in the hamster model. *Am J Pathol* **88**: 291–308. http://www.ncbi.nlm.nih.gov/pubmed/195472 (Accessed April 3, 2019).

Quail DF, Joyce JA. 2013a. Microenvironmental regulation of tumor progression and metastasis. *Nat Med* **19**: 1423–1437. http://www.nature.com/articles/nm.3394 (Accessed June 5, 2019).

Quail DF, Joyce JA. 2013b. Microenvironmental regulation of tumor progression and metastasis. *Nat Med* **19**: 1423–1437. http://www.nature.com/articles/nm.3394.

Quail DF, Joyce JA. 2013c. Microenvironmental regulation of tumor progression and metastasis. *Nat Med* **19**: 1423–1437. http://www.nature.com/articles/nm.3394.

Rada-Iglesias A, Bajpai R, Prescott S, Brugmann SA, Swigut T, Wysocka J. 2012. Epigenomic Annotation of Enhancers Predicts Transcriptional Regulators of Human Neural Crest. *Cell Stem Cell* **11**: 633–648. https://linkinghub.elsevier.com/retrieve/pii/S1934590912004213.

Rahib L, Smith BD, Aizenberg R, Rosenzweig AB, Fleshman JM, Matrisian LM. 2014. Projecting Cancer Incidence and Deaths to 2030: The Unexpected Burden of Thyroid, Liver, and Pancreas Cancers in the United States. *Cancer Res* **74**: 2913–2921. http://cancerres.aacrjournals.org/cgi/doi/10.1158/0008-5472.CAN-14-0155.

Raphael BJ, Hruban RH, Aguirre AJ, Moffitt RA, Yeh JJ, Stewart C, Robertson AG, Cherniack AD, Gupta M, Getz G, et al. 2017a. Integrated Genomic Characterization of Pancreatic Ductal Adenocarcinoma. *Cancer Cell* **32**: 185-203.e13. http://www.ncbi.nlm.nih.gov/pubmed/28810144 (Accessed June 4, 2019).

Raphael BJ, Hruban RH, Aguirre AJ, Moffitt RA, Yeh JJ, Stewart C, Robertson AG, Cherniack AD, Gupta M, Getz G, et al. 2017b. Integrated Genomic Characterization of

Pancreatic Ductal Adenocarcinoma. *Cancer Cell* **32**: 185-203.e13. https://linkinghub.elsevier.com/retrieve/pii/S1535610817302994.

Rau A, Flister M, Rui H, Auer PL. 2018. Exploring drivers of gene expression in the Cancer Genome Atlas ed. J. Kelso. *Bioinformatics*. https://academic.oup.com/bioinformatics/advance-article/doi/10.1093/bioinformatics/bty551/5047764.

Robson M, Im S-A, Senkus E, Xu B, Domchek SM, Masuda N, Delaloge S, Li W, Tung N, Armstrong A, et al. 2017. Olaparib for Metastatic Breast Cancer in Patients with a Germline BRCA Mutation. *N Engl J Med* **377**: 523–533. http://www.nejm.org/doi/10.1056/NEJMoa1706450 (Accessed June 15, 2019).

Roe J-S, Hwang C-I, Somerville TDD, Milazzo JP, Lee EJ, Da Silva B, Maiorino L, Tiriac H, Young CM, Miyabayashi K, et al. 2017. Enhancer Reprogramming Promotes Pancreatic Cancer Metastasis. *Cell* **170**: 875-888.e20. http://www.ncbi.nlm.nih.gov/pubmed/28757253 (Accessed June 5, 2019).

Romero-Ramirez L, Cao H, Nelson D, Hammond E, Lee A-H, Yoshida H, Mori K, Glimcher LH, Denko NC, Giaccia AJ, et al. 2004. XBP1 Is Essential for Survival under Hypoxic Conditions and Is Required for Tumor Growth. *Cancer Res* **64**: 5943–5947. http://www.ncbi.nlm.nih.gov/pubmed/15342372 (Accessed May 29, 2019).

Roybal CN, Yang S, Sun C-W, Hurtado D, Vander Jagt DL, Townes TM, Abcouwer SF. 2004. Homocysteine Increases the Expression of Vascular Endothelial Growth Factor by a Mechanism Involving Endoplasmic Reticulum Stress and Transcription Factor ATF4. *J Biol Chem* **279**: 14844–14852. http://www.jbc.org/lookup/doi/10.1074/jbc.M312948200.

Rückert F, Aust D, Böhme I, Werner K, Brandt A, Diamandis EP, Krautz C, Hering S, Saeger H-D, Grützmann R, et al. 2012. Five Primary Human Pancreatic Adenocarcinoma Cell Lines Established by the Outgrowth Method. *J Surg Res* **172**: 29–39. https://linkinghub.elsevier.com/retrieve/pii/S0022480411003714.

Sabò A, Kress TR, Pelizzola M, de Pretis S, Gorski MM, Tesi A, Morelli MJ, Bora P, Doni M, Verrecchia A, et al. 2014. Selective transcriptional regulation by Myc in cellular growth control and lymphomagenesis. *Nature* **511**: 488–492. http://www.nature.com/articles/nature13537.

Saborowski M, Saborowski A, Morris JP, Bosbach B, Dow LE, Pelletier J, Klimstra DS, Lowe SW. 2014. A modular and flexible ESC-based mouse model of pancreatic cancer. *Genes Dev* **28**: 85–97. http://genesdev.cshlp.org/cgi/doi/10.1101/gad.232082.113.

Saha D, Datta PK, Beauchamp RD. 2001. Oncogenic ras represses transforming growth factor-beta /Smad signaling by degrading tumor suppressor Smad4. *J Biol Chem* **276**: 29531–7. http://www.ncbi.nlm.nih.gov/pubmed/11371552 (Accessed May 28, 2019).

Sanda T, Lawton LN, Barrasa MI, Fan ZP, Kohlhammer H, Gutierrez A, Ma W, Tatarek J, Ahn Y, Kelliher MA, et al. 2012. Core Transcriptional Regulatory Circuit Controlled by

the TAL1 Complex in Human T Cell Acute Lymphoblastic Leukemia. *Cancer Cell* **22**: 209–221. http://www.ncbi.nlm.nih.gov/pubmed/22897851 (Accessed June 5, 2019).

Sander JD, Joung JK. 2014. CRISPR-Cas systems for editing, regulating and targeting genomes. *Nat Biotechnol* **32**: 347–355. http://www.nature.com/articles/nbt.2842.

Sandgren EP, Luetteke NC, Palmiter RD, Brinster RL, Lee DC. 1990. Overexpression of TGFα in transgenic mice: Induction of epithelial hyperplasia, pancreatic metaplasia, and carcinoma of the breast. *Cell* **61**: 1121–1135. https://www.sciencedirect.com/science/article/pii/009286749090075P?via%3Dihub (Accessed April 3, 2019).

Schlosser I, Hölzel M, Hoffmann R, Burtscher H, Kohlhuber F, Schuhmacher M, Chapman R, Weidle UH, Eick D. 2005. Dissection of transcriptional programmes in response to serum and c-Myc in a human B-cell line. *Oncogene* **24**: 520–524. http://www.nature.com/articles/1208198.

Scholzen T, Gerdes J. 2000. The Ki-67 protein: From the known and the unknown. *J Cell Physiol* **182**: 311–322. http://doi.wiley.com/10.1002/%28SICI%291097-4652%28200003%29182%3A3%3C311%3A%3AAID-JCP1%3E3.0.CO%3B2-9.

Schutte M, Hruban RH, Geradts J, Maynard R, Hilgers W, Rabindran SK, Moskaluk CA, Hahn SA, Schwarte-Waldhoff I, Schmiegel W, et al. 1997. Abrogation of the Rb/p16 tumor-suppressive pathway in virtually all pancreatic carcinomas. *Cancer Res*.

Schwanhäusser B, Busse D, Li N, Dittmar G, Schuchhardt J, Wolf J, Chen W, Selbach M. 2011. Global quantification of mammalian gene expression control. *Nature* **473**: 337–342. http://www.nature.com/articles/nature10098 (Accessed May 29, 2019).

Sears R. 2000. Multiple Ras-dependent phosphorylation pathways regulate Myc protein stability. *Genes Dev* **14**: 2501–2514. http://www.genesdev.org/cgi/doi/10.1101/gad.836800.

Sears R, Leone G, DeGregori J, Nevins JR. 1999. Ras Enhances Myc Protein Stability. *Mol Cell* **3**: 169–179. https://linkinghub.elsevier.com/retrieve/pii/S1097276500803081.

Seidel JJ. 2002. An ERK2 docking site in the Pointed domain distinguishes a subset of ETS transcription factors. *Genes Dev* **16**: 127–137. http://www.genesdev.org/cgi/doi/10.1101/gad.950902.

Senapati S, Chaturvedi P, Chaney WG, Chakraborty S, Gnanapragassam VS, Sasson AR, Batra SK. 2011a. Novel Interaction of MUC4 and Galectin: Potential Pathobiological Implications for Metastasis in Lethal Pancreatic Cancer. *Clin Cancer Res* **17**: 267–274. http://clincancerres.aacrjournals.org/cgi/doi/10.1158/1078-0432.CCR-10-1937.

Senapati S, Chaturvedi P, Chaney WG, Chakraborty S, Gnanapragassam VS, Sasson AR, Batra SK. 2011b. Novel Interaction of MUC4 and Galectin: Potential Pathobiological Implications for Metastasis in Lethal Pancreatic Cancer. *Clin Cancer Res* **17**: 267–274. http://clincancerres.aacrjournals.org/cgi/doi/10.1158/1078-0432.CCR-10-1937.

Senturk S, Shirole NH, Nowak DG, Corbo V, Pal D, Vaughan A, Tuveson DA, Trotman LC, Kinney JB, Sordella R. 2017. Rapid and tunable method to temporally control gene editing based on conditional Cas9 stabilization. *Nat Commun* **8**: 14370. http://www.nature.com/articles/ncomms14370.

Shen J, Chen X, Hendershot L, Prywes R. 2002. ER stress regulation of ATF6 localization by dissociation of BiP/GRP78 binding and unmasking of Golgi localization signals. *Dev Cell* **3**: 99–111. http://www.ncbi.nlm.nih.gov/pubmed/12110171.

Sherman MH, Yu RT, Engle DD, Ding N, Atkins AR, Tiriac H, Collisson EA, Connor F, Van Dyke T, Kozlov S, et al. 2014. Vitamin D Receptor-Mediated Stromal Reprogramming Suppresses Pancreatitis and Enhances Pancreatic Cancer Therapy. *Cell* **159**: 80–93. http://www.ncbi.nlm.nih.gov/pubmed/25259922 (Accessed June 5, 2019).

Sherman MH, Yu RT, Tseng TW, Sousa CM, Liu S, Truitt ML, He N, Ding N, Liddle C, Atkins AR, et al. 2017. Stromal cues regulate the pancreatic cancer epigenome and metabolome. *Proc Natl Acad Sci* **114**: 1129–1134. www.pnas.org/cgi/doi/10.1073/pnas.1620164114 (Accessed June 5, 2019).

Shi X, Mihaylova VT, Kuruvilla L, Chen F, Viviano S, Baldassarre M, Sperandio D, Martinez R, Yue P, Bates JG, et al. 2016. Loss of TRIM33 causes resistance to BET bromodomain inhibitors through MYC- and TGF-β–dependent mechanisms. *Proc Natl Acad Sci* **113**: E4558–E4566. http://www.pnas.org/lookup/doi/10.1073/pnas.1608319113.

Shu S, Lin CY, He HH, Witwicki RM, Tabassum DP, Roberts JM, Janiszewska M, Jin Huh S, Liang Y, Ryan J, et al. 2016. Response and resistance to BET bromodomain inhibitors in triple-negative breast cancer. *Nature* **529**: 413–417. http://www.nature.com/articles/nature16508.

Shuda M, Kondoh N, Imazeki N, Tanaka K, Okada T, Mori K, Hada A, Arai M, Wakatsuki T, Matsubara O, et al. 2003. Activation of the ATF6, XBP1 and grp78 genes in human hepatocellular carcinoma: a possible involvement of the ER stress pathway in hepatocarcinogenesis. *J Hepatol* **38**: 605–614. https://linkinghub.elsevier.com/retrieve/pii/S0168827803000291.

Singh PK, Hollingsworth MA. 2006. Cell surface-associated mucins in signal transduction. *Trends Cell Biol* **16**: 467–476. https://linkinghub.elsevier.com/retrieve/pii/S0962892406001954.

Sodir NM, Kortlever RM, Barthet VJ, Pellegrinet L, Campos T, Kupczak S, Swigart LB, Soucek L, Arends MJ, Littlewood TD, et al. 2019. Myc instructs and maintains pancreatic adenocarcinoma phenotype. *bioRxiv* 556399. https://www.biorxiv.org/content/10.1101/556399v1 (Accessed June 13, 2019).

Sodir NM, Swigart LB, Karnezis AN, Hanahan D, Evan GI, Soucek L. 2011. Endogenous Myc maintains the tumor microenvironment. *Genes Dev* **25**: 907–916. http://genesdev.cshlp.org/cgi/doi/10.1101/gad.2038411.

Song MS, Park YK, Lee JH, Park K. 2001. Induction of glucose-regulated protein 78 by

chronic hypoxia in human gastric tumor cells through a protein kinase C-ε/ERK/AP-1 signaling cascade. *Cancer Res*.

Sood AK, Saxena R, Groth J, Desouki MM, Cheewakriangkrai C, Rodabaugh KJ, Kasyapa CS, Geradts J. 2007. Expression characteristics of prostate-derived Ets factor support a role in breast and prostate cancer progression. *Hum Pathol* **38**: 1628–1638. https://linkinghub.elsevier.com/retrieve/pii/S0046817707001566.

Soucek L, Whitfield J, Martins CP, Finch AJ, Murphy DJ, Sodir NM, Karnezis AN, Swigart LB, Nasi S, Evan GI. 2008. Modelling Myc inhibition as a cancer therapy. *Nature* **455**: 679–683. http://www.nature.com/articles/nature07260.

Soucek L, Whitfield JR, Sodir NM, Masso-Valles D, Serrano E, Karnezis AN, Swigart LB, Evan GI. 2013. Inhibition of Myc family proteins eradicates KRas-driven lung cancer in mice. *Genes Dev* **27**: 504–513. http://genesdev.cshlp.org/cgi/doi/10.1101/gad.205542.112.

Staller P, Peukert K, Kiermaier A, Seoane J, Lukas J, Karsunky H, Möröy T, Bartek J, Massagué J, Hänel F, et al. 2001a. Repression of p15INK4b expression by Myc through association with Miz-1. *Nat Cell Biol* **3**: 392–399. http://www.nature.com/articles/ncb0401_392.

Staller P, Peukert K, Kiermaier A, Seoane J, Lukas J, Karsunky H, Möröy T, Bartek J, Massagué J, Hänel F, et al. 2001b. Repression of p15INK4b expression by Myc through association with Miz-1. *Nat Cell Biol* **3**: 392–399. http://www.nature.com/articles/ncb0401_392.

Steffan JJ, Koul S, Meacham RB, Koul HK. 2012. The Transcription Factor SPDEF Suppresses Prostate Tumor Metastasis. *J Biol Chem* **287**: 29968–29978. http://www.jbc.org/lookup/doi/10.1074/jbc.M112.379396.

Stinson J. 2003. Regulation of TCF ETS-domain transcription factors by helix-loop-helix motifs. *Nucleic Acids Res* **31**: 4717–4728. https://academic.oup.com/nar/article-lookup/doi/10.1093/nar/gkg689.

Thakur PC, Miller-Ocuin JL, Nguyen K, Matsuda R, Singhi AD, Zeh HJ, Bahary N. 2018. Inhibition of endoplasmic-reticulum-stress-mediated autophagy enhances the effectiveness of chemotherapeutics on pancreatic cancer. *J Transl Med* **16**: 190. http://www.ncbi.nlm.nih.gov/pubmed/29986726 (Accessed June 15, 2019).

Tiriac H, Belleau P, Engle DD, Plenker D, Deschênes A, Somerville TDD, Froeling FEM, Burkhart RA, Denroche RE, Jang G-H, et al. 2018. Organoid Profiling Identifies Common Responders to Chemotherapy in Pancreatic Cancer. *Cancer Discov* **8**: 1112–1129. http://cancerdiscovery.aacrjournals.org/lookup/doi/10.1158/2159-8290.CD-18-0349.

Tomasek JJ, Gabbiani G, Hinz B, Chaponnier C, Brown RA. 2002. Myofibroblasts and mechano-regulation of connective tissue remodelling. *Nat Rev Mol Cell Biol* **3**: 349–363. http://www.ncbi.nlm.nih.gov/pubmed/11988769 (Accessed June 5, 2019).

Tsuru A, Fujimoto N, Takahashi S, Saito M, Nakamura D, Iwano M, Iwawaki T, Kadokura H, Ron D, Kohno K. 2013. Negative feedback by IRE1 optimizes mucin production in goblet cells. *Proc Natl Acad Sci* **110**: 2864–2869. http://www.ncbi.nlm.nih.gov/pubmed/23386727 (Accessed May 31, 2019).

Uhlen M, Fagerberg L, Hallstrom BM, Lindskog C, Oksvold P, Mardinoglu A, Sivertsson A, Kampf C, Sjostedt E, Asplund A, et al. 2015. Tissue-based map of the human proteome. *Science (80-)* **347**: 1260419–1260419. http://www.sciencemag.org/cgi/doi/10.1126/science.1260419.

Ulianich L, Terrazzano G, Annunziatella M, Ruggiero G, Beguinot F, Di Jeso B. 2011. ER stress impairs MHC Class I surface expression and increases susceptibility of thyroid cells to NK-mediated cytotoxicity. *Biochim Biophys Acta - Mol Basis Dis* **1812**: 431–438. http://www.ncbi.nlm.nih.gov/pubmed/8262051.

Valsesia-Wittmann S, Magdeleine M, Dupasquier S, Garin E, Jallas A-C, Combaret V, Krause A, Leissner P, Puisieux A. 2004. Oncogenic cooperation between H-Twist and N-Myc overrides failsafe programs in cancer cells. *Cancer Cell* **6**: 625–630. https://linkinghub.elsevier.com/retrieve/pii/S1535610804003083.

Visel A. 2004. GenePaint.org: an atlas of gene expression patterns in the mouse embryo. *Nucleic Acids Res* **32**: 552D – 556. https://academic.oup.com/nar/article-lookup/doi/10.1093/nar/gkh029.

von Eyss B, Eilers M. 2011. Addicted to Myc--but why? *Genes Dev* **25**: 895–7. http://www.ncbi.nlm.nih.gov/pubmed/21536730 (Accessed June 12, 2019).

Walz S, Lorenzin F, Morton J, Wiese KE, von Eyss B, Herold S, Rycak L, Dumay-Odelot H, Karim S, Bartkuhn M, et al. 2014. Activation and repression by oncogenic MYC shape tumour-specific gene expression profiles. *Nature* **511**: 483–487. http://www.nature.com/articles/nature13473.

Wang E, Sorolla A, Cunningham PT, Bogdawa HM, Beck S, Golden E, Dewhurst RE, Florez L, Cruickshank MN, Hoffmann K, et al. 2019. Tumor penetrating peptides inhibiting MYC as a potent targeted therapeutic strategy for triple-negative breast cancers. *Oncogene* **38**: 140–150. http://www.nature.com/articles/s41388-018-0421-y.

Wasylyk B, Hagman J, Gutierrez-Hartmann A. 1998. Ets transcription factors: Nuclear effectors of the Ras-MAP-kinase signaling pathway. *Trends Biochem Sci*.

Wasylyk C, Bradford AP, Gutierrez-Hartmann A, Wasylyk B. 1997. Conserved mechanisms of Ras regulation of evolutionary related transcription factors, Ets1 and Pointed P2. *Oncogene* **14**: 899–913. http://www.nature.com/articles/1200914.

Wei GH, Badis G, Berger MF, Kivioja T, Palin K, Enge M, Bonke M, Jolma A, Varjosalo M, Gehrke AR, et al. 2010. Genome-wide analysis of ETS-family DNA-binding in vitro and in vivo. *Cell* **61**: 1121–1135. https://linkinghub.elsevier.com/retrieve/pii/009286749090075P.

Weinstein IB. 2002. CANCER: Enhanced: Addiction to Oncogenes--the Achilles Heal of Cancer. *Science (80-)* **297**: 63–64. http://www.sciencemag.org/cgi/doi/10.1126/science.1073096.

Whitfield JR, Beaulieu M-E, Soucek L. 2017. Strategies to Inhibit Myc and Their Clinical Applicability. *Front Cell Dev Biol* **5**. http://journal.frontiersin.org/article/10.3389/fcell.2017.00010/full.

Wilson BG, Roberts CWM. 2011. SWI/SNF nucleosome remodellers and cancer. *Nat Rev Cancer* **11**: 481–492. http://www.nature.com/articles/nrc3068.

Wilson JS, Pirola RC, Apte M V. 2014. Stars and stripes in pancreatic cancer: role of stellate cells and stroma in cancer progression. *Front Physiol* **5**: 52. http://www.ncbi.nlm.nih.gov/pubmed/24592240 (Accessed June 5, 2019).

Xu Q, Li P, Chen X, Zong L, Jiang Z, Nan L, Lei J, Duan W, Zhang D, Li X, et al. 2015. miR-221/222 induces pancreatic cancer progression through the regulation of matrix metalloproteinases. *Oncotarget* **6**: 14153–64. http://www.ncbi.nlm.nih.gov/pubmed/25883224 (Accessed June 4, 2019).

Yamamoto K, Sato T, Matsui T, Sato M, Okada T, Yoshida H, Harada A, Mori K. 2007. Transcriptional Induction of Mammalian ER Quality Control Proteins Is Mediated by Single or Combined Action of ATF6α and XBP1. *Dev Cell* **13**: 365–376. https://linkinghub.elsevier.com/retrieve/pii/S1534580707003000.

Yancopoulos GD, Nisen PD, Tesfaye A, Kohl NE, Goldfarb MP, Alt FW. 1985a. N-myc can cooperate with ras to transform normal cells in culture. *Proc Natl Acad Sci* **82**: 5455–5459. http://www.pnas.org/cgi/doi/10.1073/pnas.82.16.5455.

Yancopoulos GD, Nisen PD, Tesfaye A, Kohl NE, Goldfarb MP, Alt FW. 1985b. N-myc can cooperate with ras to transform normal cells in culture. *Proc Natl Acad Sci* **82**: 5455–5459. http://www.jbc.org/lookup/doi/10.1074/jbc.M110636200.

Yang BS, Hauser CA, Henkel G, Colman MS, Van Beveren C, Stacey KJ, Hume DA, Maki RA, Ostrowski MC. 1996. Ras-mediated phosphorylation of a conserved threonine residue enhances the transactivation activities of c-Ets1 and c-Ets2. *Mol Cell Biol* **16**: 538–547. http://mcb.asm.org/lookup/doi/10.1128/MCB.16.2.538.

Ying H, Kimmelman AC, Lyssiotis CA, Hua S, Chu GC, Fletcher-Sananikone E, Locasale JW, Son J, Zhang H, Coloff JL, et al. 2012. Oncogenic Kras Maintains Pancreatic Tumors through Regulation of Anabolic Glucose Metabolism. *Cell* **149**: 656–670. https://linkinghub.elsevier.com/retrieve/pii/S0092867412003522.

Zaret KS, Carroll JS. 2011. Pioneer transcription factors: establishing competence for gene expression. *Genes Dev* **25**: 2227–2241. http://www.ncbi.nlm.nih.gov/pubmed/22056668 (Accessed June 5, 2019).

Zhang K, Sikut R, Hansson GC. 1997. A MUC1 Mucin Secreted from a Colon Carcinoma Cell Line Inhibits Target Cell Lysis by Natural Killer Cells. *Cell Immunol* **176**: 158–165.

https://linkinghub.elsevier.com/retrieve/pii/S0008874997910856.